JOURNAL OF THE AERONAUTICAL SCIENCES

VOLUME 21 FEBRUARY, 1954 NUMBER 2

The First Half-Century of Flight in America

The Seventeenth Wright Brothers Lecture

GLENN L. MARTIN

Introduction

I AM DEEPLY HONORED to have been chosen to deliver this Seventeenth Wright Brothers Lecture before the Institute of the Aeronautical Sciences on this Fiftieth Anniversary of Powered Flight. It was my privilege to present the Wilbur Wright Memorial Lecture before The Royal Aeronautical Society in London in 1931, and I am indeed proud to be numbered among those few men who have been twice honored in this series.

It is a humbling experience to face the task of reviewing, however briefly, the incredible story of the first half century of flight in America.

I am happy to assay this task, however, because of the deep sense of obligation I feel toward aviation in America. It has been the central theme of my life for a half century, and it has been the most demanding yet the most rewarding of any field of work I could possibly have chosen. It has enriched my life immeasurably in friendships, in honors and awards, and in that priceless feeling of successive jobs well done. Certainly no man can ask more of his chosen profession.

I hope that I have made some contribution to it, no matter how small, out of the depths of that obligation. If I have, however, it has been only as a member of a continuing team of enthusiastic and loyal coworkers who have shared with me the triumphs and the failures of these interesting years. It is my hope, too, to make contributions to it in the future, for I have no intention of ceasing my labors in aviation in America.

The Wright Brothers

It has been said that nothing in this first half of the Twentieth Century—not even the atomic bomb—transcends in importance the magnificent accomplishment of the Wright brothers at Kitty Hawk a half century ago. Having had some experience with airplanes and none with the atomic bomb, I am not prepared to dispute this high tribute to these famous brothers.

The death of Wilbur Wright in 1912 robbed our industry of its greatest pioneer, and I have no question that we have been the poorer for it. Fortunately, Orville Wright survived his brother by 35 years, and it was he who discharged the very great responsibility of holding the Wright name aloft through periods of severe trial and who preserved its dignity and integrity in the world's esteem.

I was closely acquainted with Orville Wright, for many years, first as friend and later as business associate and I can say that he was the most honest man I ever met. I am convinced that it was this devotion to truth—in all things—that lay at the root of the Wright brothers' success in creating the airplane. It has been honest men who have built our great industry and who will guide its sound growth in the future.

The quality of honesty in daily dealings is an infallible guide to a man's capabilities in the engineering and scientific fields. Structures and machines are unforgiving of the cheater and inevitably indict those who toy with the facts. It was their indomitable faith in truth that guided the Wright brothers through all their investigations and that ultimately—and, perhaps, inevitably—brought them to success at Kitty Hawk 50 years ago.

It would be a vain man, indeed, who would attempt to add to the stature of the Wright brothers and the technical magnificence of their 1903 Flyer. You are all familiar with the fact that this first airplane weighed 750 lbs. fully loaded yet was lifted into the air by an engine developing only 12 hp. This phenomenal power loading meant that each horsepower was lifting $62\frac{1}{2}$ lbs. of weight.

Presented before the Institute of the Aeronautical Sciences in the U.S. Chamber of Commerce Auditorium, Washington, D.C., December 17, 1953.

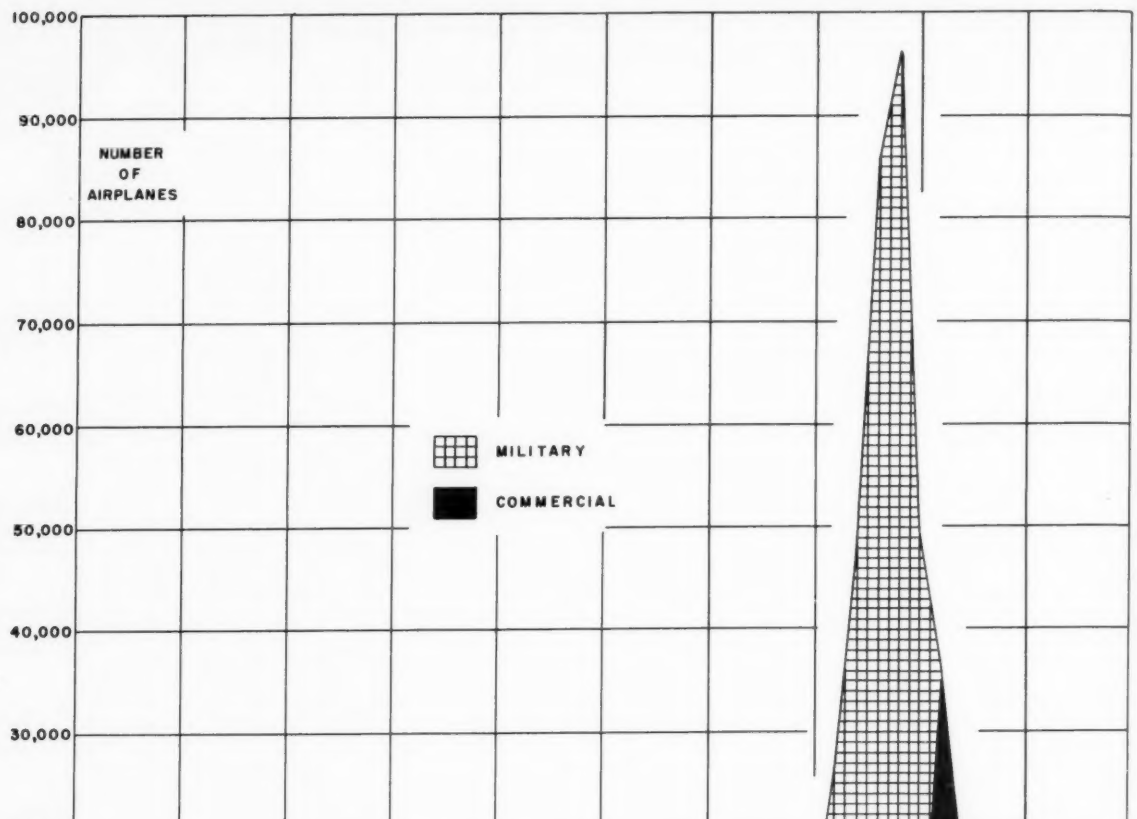

FIG. 1. Production history of the U.S. aircraft manufacturing industry during its first 50 years.

Their achievement was more than merely lifting themselves from the ground, for as we study their writings and records we have learned what truly scientific workers they were. You are familiar, I am sure, with their search for suitable testing methods during which they developed a number of ingenious devices for getting at the scientific truths of flight. Their wind tunnel, for exampie, used a honeycomb grid for straightening the airflow, and in its 27-m.p.h. throat they tested model wings that varied over a wide range of aspect ratio, camber, and taper. They made more than 1,000 glider flights at Kitty Hawk prior to their first powered machine. Unquestionably they read all of the written records of aeronautical thought available to them. Thus, they gave us not only the first airplane but an entire scientific method for work in the field of aeronautics.

But the Wrights did not work in a scientific wilderness. They stood on the foundation erected by their predecessors in science. Yet all of these pearls did not make a necklace until the inspired jewelers came along.

The Wrights brought to aviation the scientific approach to invention in which intuition and logic are used as a leavening for the diverse technical facts at hand. This method, of course, had prevailed for a century prior to the Wrights, but it was their course of action following a conclusion that made them immortals and their predecessors only dreamers and vain experimenters. Once having fashioned an idea, the Wrights proceeded to test it in scale form, either in their wind tunnel at Dayton or in a kite or glider at Kitty Hawk. This was their genius—no matter how sound or complete the idea, they were prepared from the start to

modify it, to improve it, or to abandon it. For them there was no perfection.

The real legacy of the Wright brothers to their contemporaries was the single truth that flight had been achieved. With this fact in hand, the rest of us were able to sweep all difficulties before us and rush to our individual successes. It is the haunting fear that what he is trying to do is impossible that corrodes the will of the inventor. Once this fear is removed, the spirit overrides all problems and moves quickly to the fruition of the dream.

All of us who followed the Wrights lived beyond such fears. Our only problem was how best to do the job. Freed of this worry, Glenn Curtiss on the East Coast sped on to success with an advanced design and I on the West Coast, designed, built, and taught myself to fly my first airplane without the benefit of ever having seen one. When I started, I did not know how to do the job; I only knew that the job could be done. But it was this single bit of information that dwarfed in importance all the other knowledge at my disposal in its contribution to my success.

I have had many years in which to recall my first flight and to attempt to express the experience in words, but I have always failed. Leaving the ground for the first time in a machine of your own design, which you have built with your own hands, is simply an indescribable experience. One of my genuine regrets, in the face of the miraculous progress we have made in aviation in the past half century, is that the exhiliration, pride, humility, fear, and triumph of such an experience now seems forever barred from human experience.

The Wrights unleashed a torrent of thought which even today shows no signs of abating. Once we had solved the initial problem of simply getting ourselves into the air, we turned to the great debate on the form of the airplane. I have often felt that aviation's most inventive period was its first. It was the period of the grand idea as the airplane quickly evolved from its original form in the 1903 Wright Flyer to the basic form in use today.

Before World War I

The 1911–1912 period is described in the history books as the age of the death-defying exhibition pilot, and in those two brief years such names as Lincoln Beachey, Arch Hoxsey, Ralph Johnstone, Phil Parmalee, Frank Coffin, Howard Gill, J. C. "Bud" Mars, "Becky" Havens, Charles Willard, and a host of others became immortal. But while their exhibitions provided thrills for the crowds and a fabulous revenue for the Wright and Curtiss Exhibition companies, these pioneer pilots were daily creating flight-test data on their machines and amassing important performance stability, and control experience for the designers. During every exhibition flight I ever made, I was alert to the performance and handling characteristics of my airplane and was making mental notes on its shortcomings and the possibilities of their improvement. Aeronautical science was being rapidly evolved, even while "ladies fainted and strong men quelled."

Until World War I aircraft manufacture consisted of building one airplane and, after that one was completed, transferring the personnel to start construction on the second, and so on. When I received a large order for the Model TT airplanes from the Signal Corps, it was perfectly clear that our way of doing things would have to change. We therefore adopted the new principle of making all of the parts first and assembling the airplanes as they moved along an assembly line. This led, of course, to the assignment of workmen to specific tasks, such as rib-making or engine mount fabrication, with no other duties. Our factory floor had to be laid out into separate departments and the work performed on a predetermined schedule. We prepared and used rudimentary flow charts for the first time and were able to pinpoint delays by determining the department in difficulty and ascertaining the preceding department from the chart, which spotted the trouble quickly.

Materials

Wood, of course, was our staple material in those days and I will certainly not defend it as a material of aircraft construction. Its principal difficulty was its variation in quality, almost from one board to the next. This naturally made it impossible to establish firm allowables for design or manufacture. Its strength characteristics literally changed with the weather, but we always believed it to be in excess of the required strength.

However, we soon learned many effective ways of treating, storing, and handling woods and veneers, and a visit to any major museum today will reveal wooden airplanes 30 or 40 years old still in good states of preservation.

The introduction of sheet metal into aircraft construction in the late twenties turned a great adventure into a science and revolutionized not only aircraft manufacture but design as well. We had been building metal airplanes for some years, of course, in the form of welded steel tubing fuselages introduced during World War I. The first high-strength aluminum alloy, 17S, was made and tested early in 1917, and it was first produced commercially in the U.S. for construction of the airship "Shenandoah" at the Naval Aircraft Factory during 1920–1921. Our first use of it in aircraft construction was in the fabrication of formed ribs and spars, which, when combined with the welded steel tubing fuselage, produced an all-metal airplane structure fabric-covered.

The Goodyear Tire & Rubber Company conducted an extensive research program on the forming and heat-treating of 17S in preparation for construction of the RS-1 dirigible, and I engaged their services for the

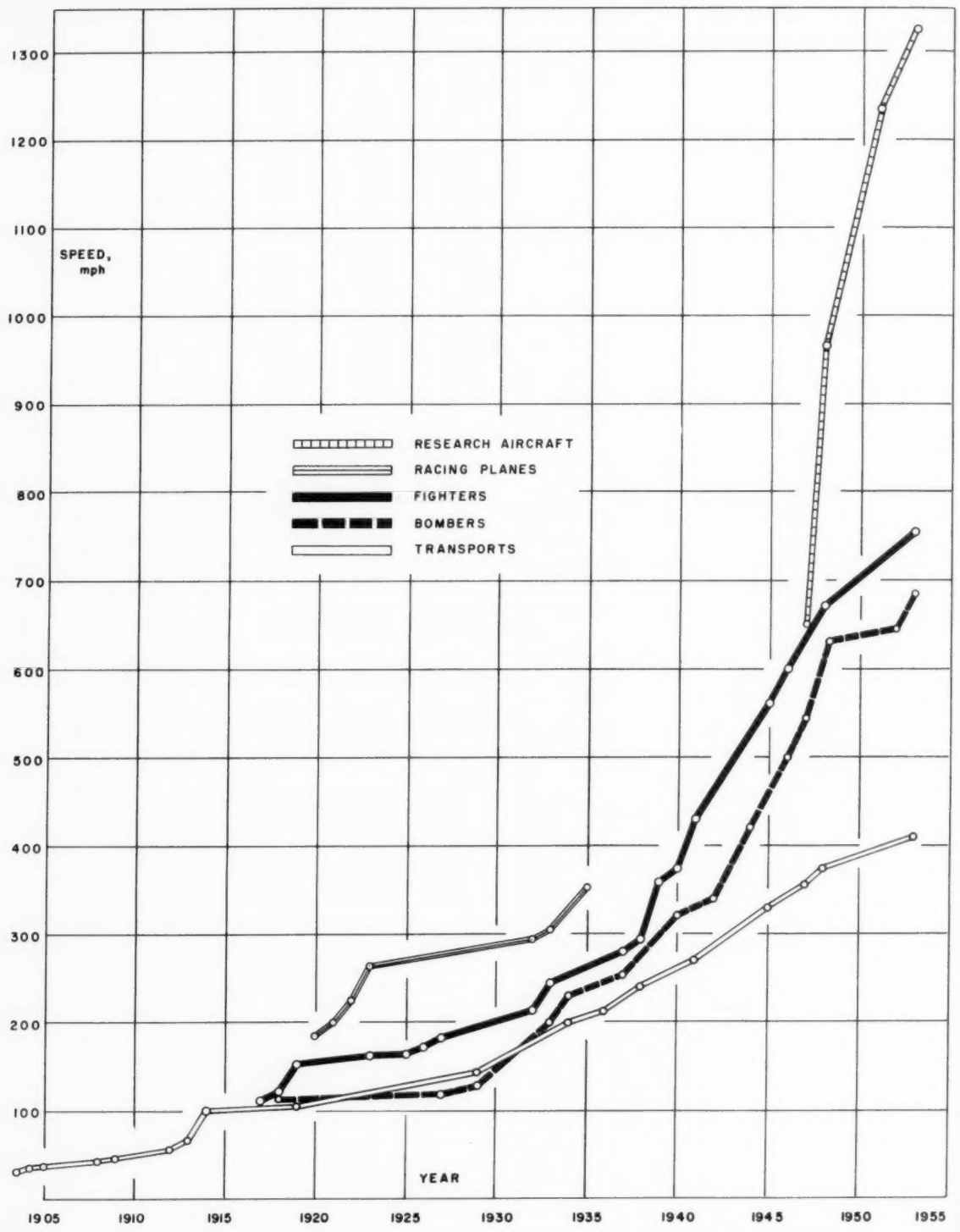

FIG. 2. Increase in maximum speed of basic types of U.S. aircraft during the first half century of flight.

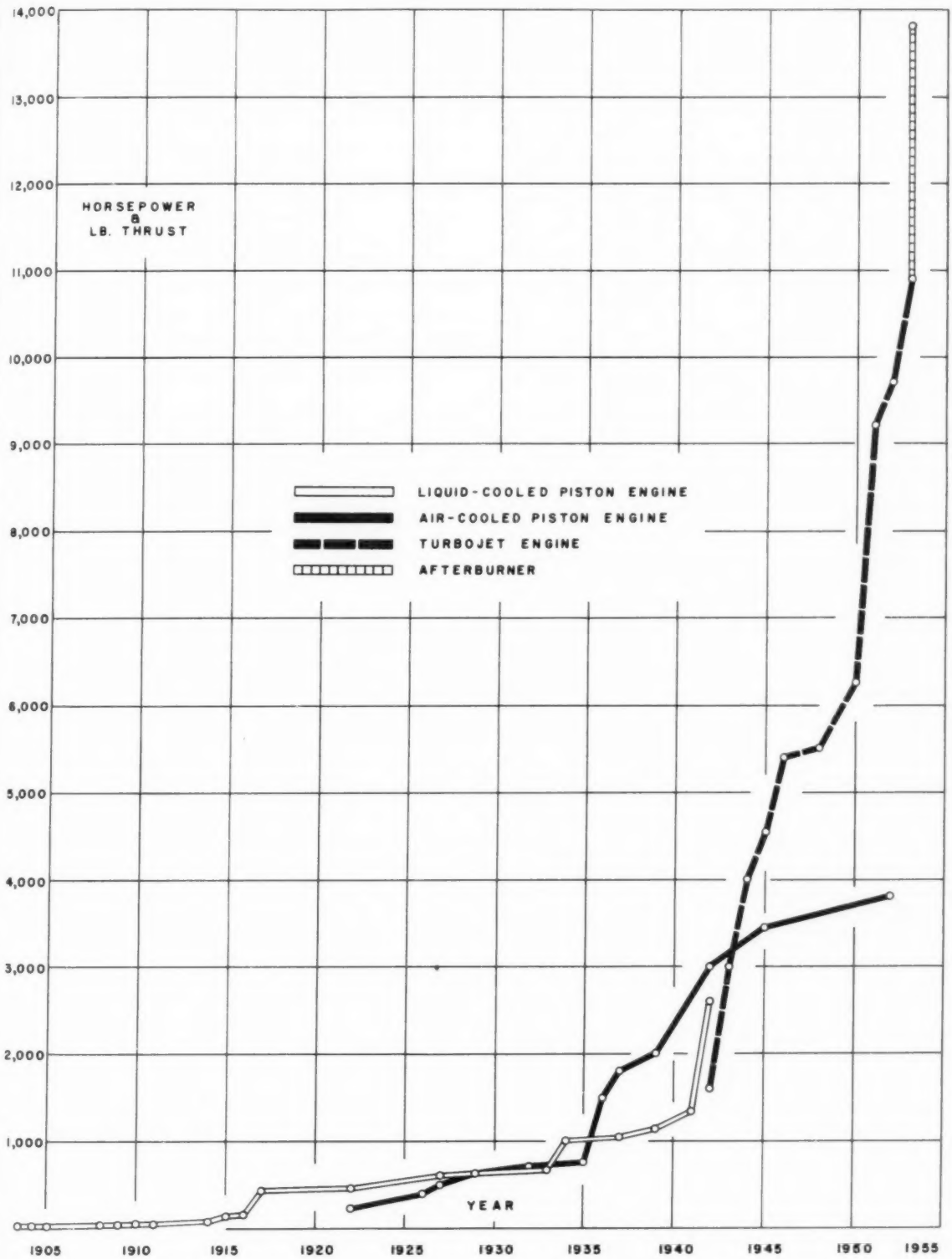

FIG. 3. Increase in output of U.S. aircraft power plants from 1903 through 1953.

fabrication of parts for the Martin MS-1, the first all-metal airplane in America.

Metal Aircraft

The cantilever wing marked another great revolution in aircraft design and manufacture. This problem had long been one simply of choice rather than possibility. A wing had to be thick in order to permit sufficient structure for internal bracing, and thick wings, of course, were high-drag wings. However, through wind-tunnel research we finally developed a profile thick enough to permit internal bracing, yet with acceptable drag characteristics. With these profiles available in the late twenties, we faced the problem of fabricating stress-skin structures in production.

It required development of a whole new science in manufacture. Heat-treating equipment, metal forming and cutting machines, and the entire new science of tooling had to be developed before mass production of metal aircraft was possible. So revolutionary was this new development that I solved the problem only by the layout and construction of an entirely new factory especially designed and equipped for metal aircraft fabrication.

With the all-metal cantilever monoplane and the semimonocoque fuselage, designers were able to make their calculations with great precision and aircraft performance moved ahead rapidly. I think it was at this period, in the early thirties, that science assumed the leadership over experiment and permitted aircraft design, for the first time in its history, to move forward to its full potentialities.

Aerodynamics

The man that founded our whole modern body of aerodynamic theory was Dr. Ludwig Prandtl, whose classic mind was lost to us only a few months ago. Prandtl presented his concept of the boundary layer in 1904, which clarified the puzzling relation between the classical hydrodynamics of perfect fluids and real airflows. The application of perfect fluid theory to many important practical aerodynamic problems resulted from this clarification of the role of viscosity. Continued research on the boundary layer by Prandtl and his associates at Göttingen resulted by 1920 in a qualitative understanding of skin friction, form drag, and stalling.

However, Prandtl's works did not become available in America until after World War I, and our authority in the early days was Frederick W. Lanchester, one of the great geniuses of aviation. His classic textbook, *Aeronautics*, appeared in 1907 and presented his concept of "circulation" and the existence of vortices at the tips of wings. I must admit that all of us found Lanchester very hard going, since he used very little mathematics in his work and relied largely on page after page of laborious discussion.

Succeeding papers by Prandtl and Lanchester between 1907 and 1919 developed the theory of the finite wing, the thing we were all interested in, and explained scientifically what we all had known from experience—that the best lift-drag characteristics are obtained from a high aspect ratio wing. The Lanchester-Prandtl theory, as some call it, provided the first rational basis for the aerodynamic design of wings and also gave loading information needed for structural design. It also clarified the aerodynamics of biplanes and explained the existence of interference between the two wings, which we had begun to suspect and which led, eventually, to the monoplane. One of the important results of this theory was the fact that it broke wing design down into two separate parts: the effect of air foil section and the separate effect of wing geometry.

Aircraft Construction Problems

The choice of materials for aircraft construction has never been a simple one because it lies at the root of nearly everything that is done in the manufacture of aircraft. The stress analysts, usually enthusiastically supported by the aerodynamics people, have always rushed to embrace a new and always promising aircraft material, and the fervor of their arguments has often severely tested the prudence of management. I have always admired this enthusiasm and this constant eagerness for progress, but the introduction of a new material in aircraft construction is a long and extremely costly business that must be considered from every possible angle. Usually, such materials require entirely new machinery, complex handling and processing, and invariably a substantial increase in costs in the early stages. Titanium, of course, is a current example of these promises and problems.

But progress must never be denied, and experience has shown the long-range economy of developing and using the very highest quality materials and fabrication techniques available. This is because of the unique structural requirements of the airplane in which its materials must be loaded just as near their limits as seasoned judgment will permit in order that structural efficiency be raised as high as possible.

It has always been wise to bear in mind that the actual costs of the materials in an aircraft structure is only 10–20 per cent of its total cost, the balance being in labor. Therefore, it has always been essential to choose a material that could be worked easily and rapidly, and it is good economy to pay twice as much for a new material if it reduces fabrication time by one-half or more. Unfortunately, this has rarely been the case, and, instead, we have attacked the problem of fabrication time by the more difficult approach of developing special tools and procedures.

Again, however, this approach requires assessment of the probable number of aircraft to be built of a new model, the extent of tooling complexity and cost vary-

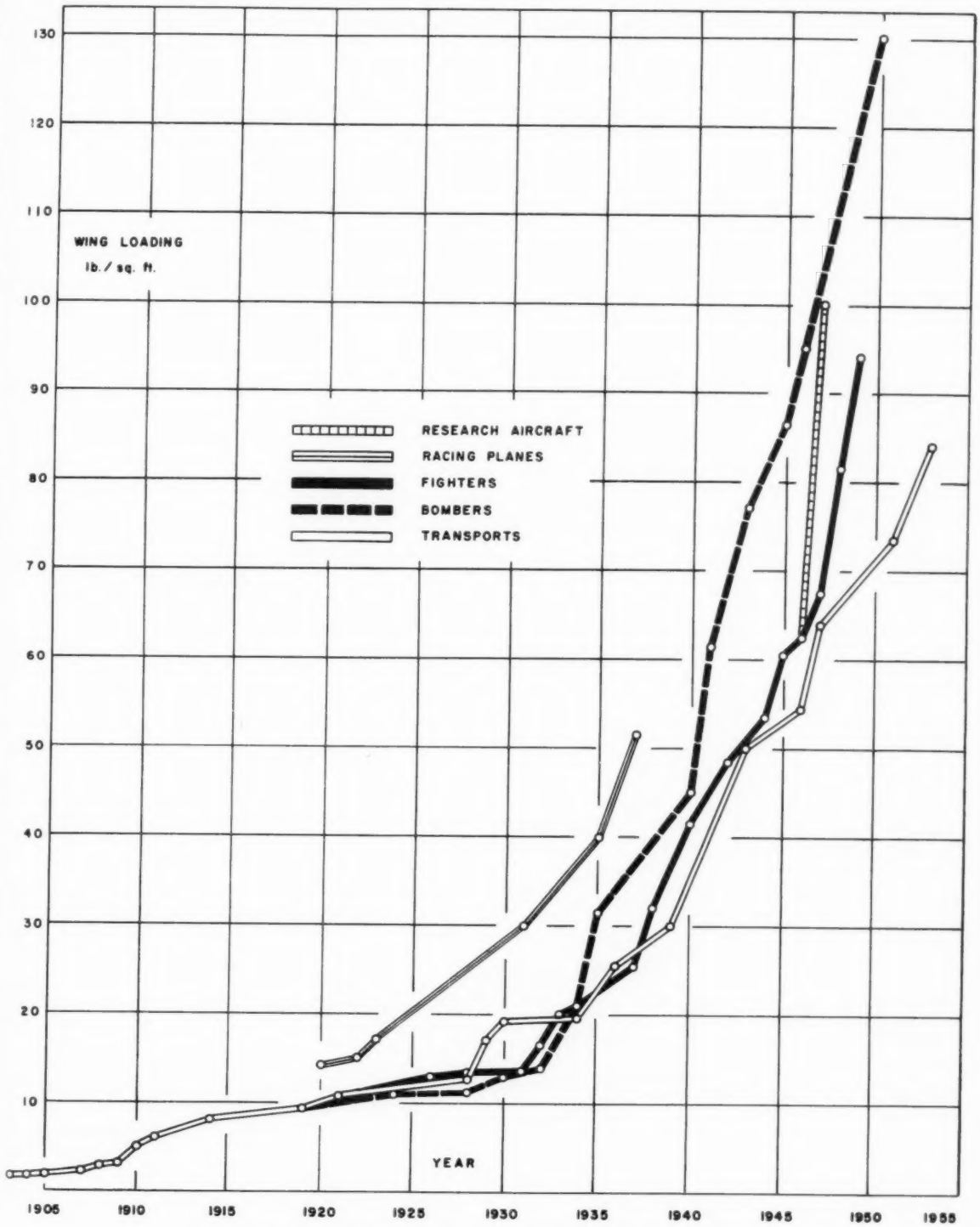

FIG. 4. Variation of wing loading with time for five basic types of U.S. aircraft.

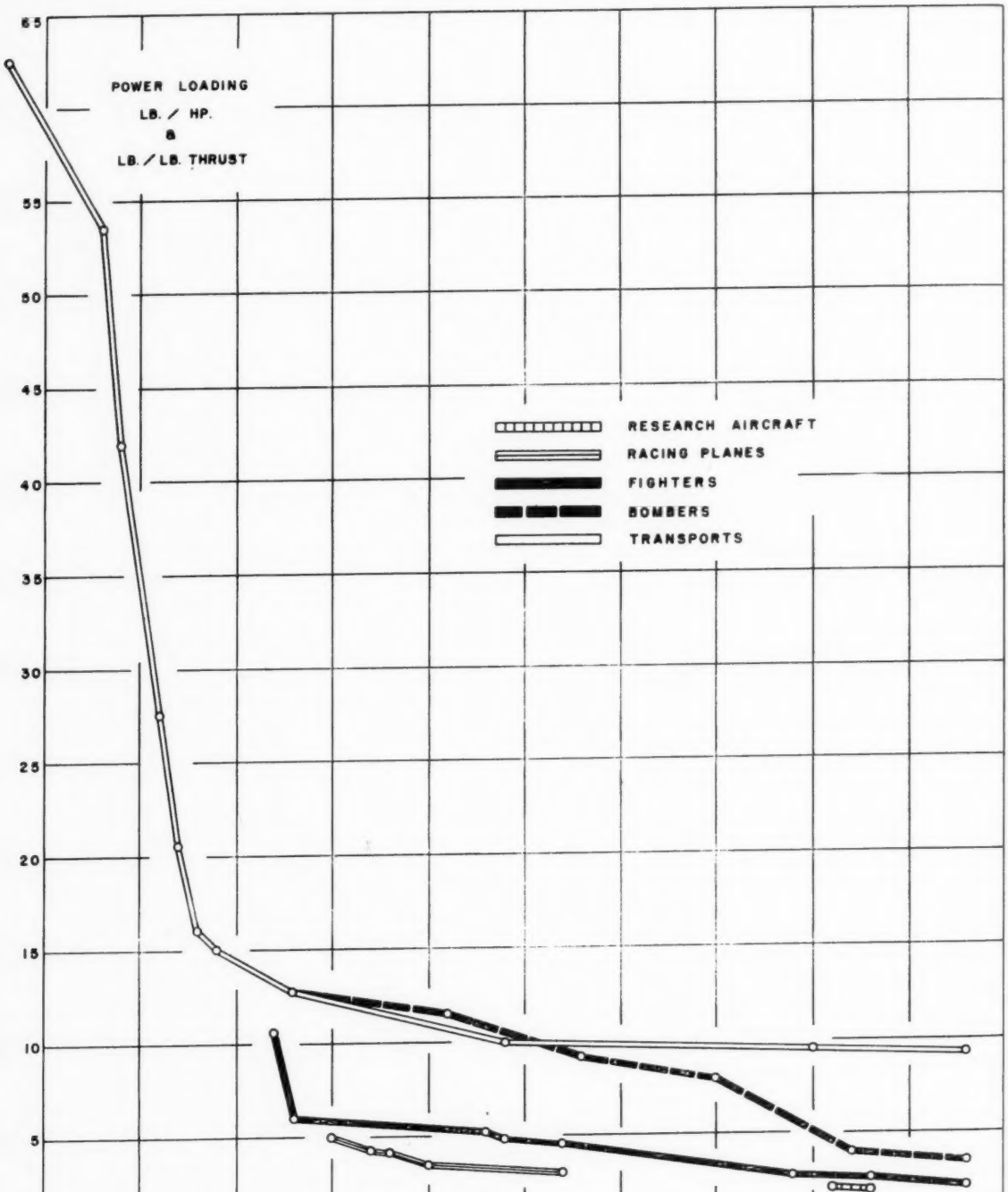

FIG. 5. Variation of power loading with time during the first 50 years of powered flight in America.

ing directly with the size of the anticipated order. Here is the crux of the aircraft manufacturing economic problem and the source of the greatest demands on management acumen. It seems reasonable to assume that about 80 per cent of the structure of a new airplane model will not change throughout its life and that tooling can safely be ordered for such parts. Despite the growth potential and rapid development of a new model in its early years, these things actually effect only about 20 per cent of the major assemblies, and these units may properly be lightly tooled.

Aircraft Engines

The airplane, from its inception, has grown in capacity and performance only at the pace permitted by the aircraft engine, and we have historically selected the engine first and designed our airplane around it. The search for high power has never relaxed for an instant. After their flights in December, 1903, at Kitty Hawk, the Wrights returned to Dayton and immediately began the design of a more powerful engine. After Curtiss made his first flights in 1908 with a 40-hp. Curtiss engine, he immediately began construction of a 50-hp. engine for his next machine. In 1909 I made my first flight with a modified Ford engine of 12 hp. and wasted little time securing an Eldridge marine engine of 30 hp. Thus, from the very first, we have energetically pursued more engine power and our magnificent aircraft engine, propeller, and accessory industries are keeping pace with our demands just as well as science and time permit.

The subject of the turbojet and turboprop forms of aircraft propulsion are well known to you all, and I will touch on them only to express my conviction that we can now have all the power we demand, since the aircraft gas-turbine form has no inherent limitations to its size or output. The rapid maturity of the turbojet in its few brief years of development has been one of the truly amazing stories of this half century of flight. We now have turbojet engines with reliability and durability comparable to our piston-engined types and, when flown at sufficiently high speeds, economy closely approaching that of the piston engine. The rocket and ram-jet forms of propulsion know utterly no limit to their output, and the aircraft designer has had the barrier of power removed from his list of major problems.

Today, on this 50th Anniversary of Powered Flight in America, we have flown at 1,655 m.p.h. and to an altitude of 89,000 ft. in man-carrying aircraft. We have lifted a total disposable load of 200,000 lbs., and we have carried a load of 10,000 lbs. for a distance of more than 10,000 miles. We have flown around the world nonstop, we have carried 308 people in an airplane, and we have flown a distance of 11,236 miles nonstop without refueling. Only a few days ago we witnessed the inauguration of scheduled nonstop transcontinental air service in less than 8 hours. Today we have a combat airplane in quantity production that flies regularly and smoothly at supersonic speed in level flight. The list of such miracles is endless.

Charts Showing Technical Progress

Fig. 1 shows the production history of our industry during its first 50 years. I specifically had this plotted on simple graph paper, rather than the more popular semilogarithmic paper usually used, in order to illustrate the really furious upheavals in our annual rates of production. We see here not only the familiar peaks and valleys in our military output, which is geared to wars, but the identical slopes and proportional magnitudes in commercial production. I think that here, in this simple graph, is portrayed the fundamental problem of the aircraft manufacturing industry and the root of nearly all of it difficulties.

Fig. 2 is the most popular index to our technical progress: the top speed of our aircraft. Although it is customary to pinpoint all of the speeds and then lay down a "trend" curve through a sea of such dots, I have used here the precise maximum speed of each of the years for each of the various aircraft types, since, in my opinion, "trends" are often misleading and the state of the art must always be judged by the best that we have—not the average.

Fig. 3 illustrates our engine progress over 50 years. It shows how the various engine types have progressed and tends to indicate that a radically different powerplant type has been born just as the previous type was beginning to show its age. It might follow that nuclear energy power plants will be available when the turbojet curve starts to flatten. I think it significant, too, that our rate of development of a new engine type has always been much more rapid than the last. At the upper right corner, for example, we see that the flick of an afterburner switch in our currently most powerful turbojet engine instantaneously produces the same amount of power it took us 40 years to obtain with the piston engine.

So far we have seen measurements of our absolute progress, but now let us see some qualitative data on that progress. Fig. 4 shows what has happened to wing loading in 50 years. This chart shows its inevitable and rapid increase through the years, regardless of airplane type. Only the horizontal or time displacement is different for the different types, each following the other within a period of 5 years or less. One point of interest revealed here is that it is the bomber—not the fighter—that has led the way in higher wing loading for the past 20 years. Today's jet bomber wing loading, as a matter of fact, is substantially higher than even our supersonic rocket-powered research aircraft. Our postwar transports have far exceeded even our fastest racing planes of prewar years in wing loading.

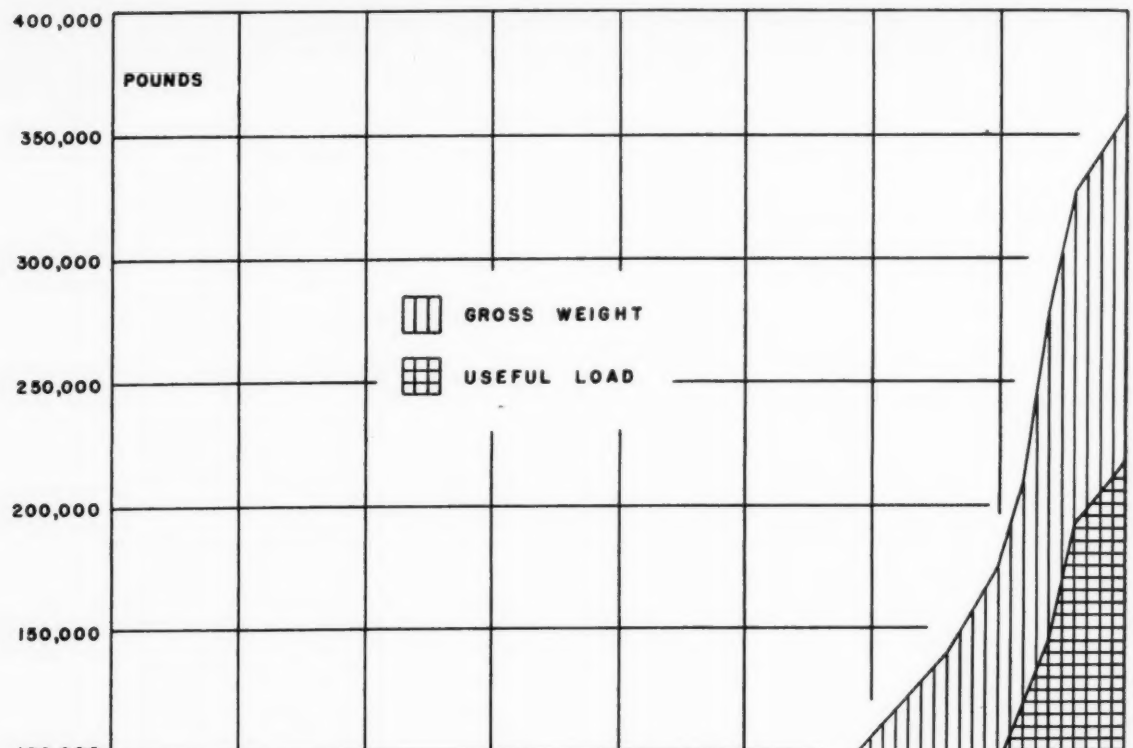

FIG. 6. Increase in aircraft useful load and gross weight during the first half century of flight.

Fig. 5 shows the most consistency in power loading of any of the parameters examined here. It is seen that the transport and the fighter have decreased only slightly in power loading during the past 25 years. This is probably explained by the equal consistency with which we match a power increase in a new aircraft with an almost proportional weight increase. Only the bomber continues to show improvement in power loading, reflecting its multiengined character. With the modern pod arrangement we have reached a point where we can literally "throw in another engine or two" whenever the gross weight shows signs of getting out of hand. For those purists who might quarrel with the apparent interchangeability of horsepower and pounds of thrust in these charts, I might point out that, right or wrong, it certainly simplifies chart-making.

Fig. 6 illustrates a subject that has always been of paramount importance to me. Early in my career I came to the conclusion that only the airplane that could lift a good load was of any long-range importance. This figure shows just how much weight we have been able to lift and is, in my opinion, the most important index of our technical progress. Only quantity production airplanes have been used in this study, and none of the experimental "giant" airplanes of the past has been included. The dark hatched area in the lower right portion of the figure shows that we have managed to lift well over 100 tons in useful load.

This research work was performed by Robert McLarren, the Editor of *Aero Digest* magazine, so we can be assured of its accuracy. Like all engineers, Bob wanted to plot these things on fancy logarithmic paper, but I am old-fashioned enough to prefer simple graph paper. When something is twice as big as something else, I want to see it that way and not only one and one-third as big.

These are the dramatic accomplishments of the first half century of flight in America. More important, I think is our realization that these are only the manifestations of our progress and not progress itself. I have traced briefly the progress of man's *thoughts* on aviation, rather than his deeds, for it is our thinking that builds the lasting foundations for continued future progress.

Discussion

In a free independent society there can be no grand guiding hand controlling the destiny of an industry or a people. We in the aircraft industry have guided our own progress through our faith in, and our loyalty to, each other. The modern airplane constitutes an integration of the thoughts and lifetime work of more individuals than any other industry on earth. This integration was accomplished not by fiat but by understanding cooperation between its many and diverse elements.

This interplay of really diverse avenues of human effort is a monument to man's dependence upon other men, and it has been only the unfettered freedom of America which has created this giant team of cooperating individuals which is our modern aircraft industry. Today there appears to be no limit to the power of this team. We have the aerodynamic knowledge, the structural materials, the power plants, and the manufacturing capacities to perform any conceivable miracle in aviation.

But miracles must be planned, nurtured, and executed with intelligence and hard work. The miracles of the second half century will prove progressively more difficult, more costly, and more time-consuming. They will demand great skills from all of us.

First we must have a clear definition of the miracles to be expected. Our magnificent aircraft manufacturing industry exists only to serve its customers—not itself. It is the customer's requirements that have shaped all that we have done and which have carefully controlled our rate of progress. My files have been bulging for years with proposals for new aircraft, the fruit of engineering imagination and ambition. These are the fundamental ingredients of our capacity for progress, but such beautiful and arresting sketches are not progress until a customer says: "I want that."

Our product must meet someone's need as fully and exactly as we know how to make it. The more widely useful our product, the higher will be our level of activity and the lower the cost to the customer. Today and throughout all our 50 years of aviation history, the Government is the customer for more than 90 per cent of our effort. The grave responsibility of the Air Force and Naval aviation for our national defense is awesome in this atomic age. Their weapons must be the most effective human effort can fashion. The narrow and restrained requirements of the services inevitably create extremely costly aircraft.

The current criticism of the high cost of combat aircraft is nothing new. I heard it in 1918, in 1926, and in 1940. The aircraft is a vehicle, and its cost increases directly with its usefulness. This is true in all forms of transportation, being lowest for the barge and highest for the airplane, but their usefulness varies in direct ratio with their cost. It seems fundamental to me that an airplane capable of operation at 600 m.p.h. at 50,000 ft. is going to cost considerably more than one limited to only 400 m.p.h. at 25,000 ft. An aircraft capable of seeking out and firing upon an unseen target at night in the stratosphere is certainly a more useful and, therefore, more costly weapon than one operable only in daytime at moderate altitude and using the pilot's limited vision and perception for its effectiveness.

I have thought carefully for many years about the pronounced apathy of the American people for the flying machine they invented. While living in Santa Ana, our family Doctor, then living in Los Angeles, mailed the following postcard to my mother:

"September 30, 1910

"*For Heaven's Sake,* if you have any influence with that *wild-eyed hallucinated* young man, *call him off* before he is killed.

"Have him devote his energies to *substantial, feasible,* and profitable pursuits, leaving *Dreaming* to the Professional Dreamers.

H. H. Sutherland"

And this was only one of many. Throughout my participation in aviation, which spans its life history, I have witnessed a public criticism of the high cost of aircraft. There seems to be a pervading public mistrust of its aircraft industry and unrelenting pressure on the Government to keep vigil on aviation profits which resulted, eventually, in severe profit limitations by law. Perhaps this concern is a mistaken heritage from World War I when the term "war profiteer" became almost synonymous with weapons production. I do not know why our citizens heartily approve substantial profits in the manufacture of automobiles and household appliances but become incensed when the word "profit" is even associated with the design and production of vital weapons of national defense.

Without profits there can be no applied research, no advanced machinery and equipment, no progress of any sort. Without profits available for expansion of potential, that expansion becomes the responsibility of the Government. And that responsibility, unchecked, leads inevitably to the political and economic system we are attempting to defeat thoughout the world.

There is a proper role for the Government in aviation progress. As a customer, it must establish clearly and precisely the goals that we will be required to meet. It must assume the financial cost of the research and

development work required in the perfection of that goal. It must make certain that this nation has, at all times, a strong aircraft manufacturing industry, a healthy and progressive accessory and equipment industry, an experienced and capable air-line industry, and a reservoir of educated and skillful young men coming forward to man these industries. The burden of this role, costly as it may seem, will be borne cheerfully by an enlightened American citizen once he understands its full significance to him and his progeny.

When I experienced the indescribable thrill of my first flight, I was convinced that here was a new art that men of vision everywhere must rush to embrace. I was unbounded in my gratitude for having been born into a new race of man privileged to witness the birth of the air age and to share its triumphs during their lifetimes. For me, this age has fulfilled all of its promises, but I am only one of a few hundred thousand of us for whom the dream has come true. For more than a hundred million Americans it seems the dream has proved to be an elusive and a frightening thing.

The salvation of this great nation lies solely in the revival of that dream and its fruits for the American people. That nation will be strongest on earth whose peoples embrace this new age to their hearts. Its destiny must become their destiny, else they perish. The achievements and the problems, the victories and the costs, the dangers and the promises of aviation—all of these things must become a part of the soul of a nation if it is to find security with its prosperity. We must seek out the roots of public apathy and mistrust and, in destroying them, create the omnipotent Air Power we have the brains and the tools to do.

It is not enough to have a core of aviation experts with the sympathy and understanding of Air Power required for its progress. We must have a whole people rising in a great tide of belief in this new art, convinced of its demonstrated ability to usher them into an entirely new age of mankind.

The Future

With such support assuredly no miracle is impossible for aeronautical science and industry. With such support I have no hesitancy in predicting, for the second half century of flight in America:

(1) Interstellar space ships with speeds of 25,000 m.p.h.

(2) Giant 200-passenger jet air liners crossing the continents and the oceans in literally zero time in the westerly direction.

(3) Nuclear-energy-powered aircraft, first as bombers capable of multiple nonstop circumnavigation of the globe and second as passenger air liners.

(4) Helicopters carrying all air-line traffic over distances of 150 miles or less.

(5) Flying boats with speeds matching that of the equivalent landplane but with greater capacity for cargo, passengers, or weapons.

(6) Fully automatic air-line flight operations through electronic guidance and control equipment.

(7) Reductions in the cost of air travel well below that of any other form of transportation.

These predictions are testimony to my faith in the conviction of all of us in aviation today that "the difficult we can do immediately—the impossible takes a little longer." The only real problem we face in the second half century of flight in America is the same one faced by the Wright brothers 50 years ago: to determine the scientific truths and to follow them with bold honesty through all difficulties to inevitable success. This is our great heritage from the two men we honor here, and may God grant us the courage to honor it as well.

An Authorized Binding for Journal of the Aeronautical Sciences

Arrangements have been made by the Institute of the Aeronautical Sciences for members and subscribers to have their Journals bound into distinctively designed books.

Twelve issues, January through December, bound in best grade blue washable buckram, imprinted with your name on cover, cost but $3.45 per volume.

Ship Journals parcel post insured. Within 30 days after receipt, bound volumes will be shipped prepaid in the U.S.A. Full remittance must accompany order.

Publishers' Authorized Bindery Service
(Binders of all Journals)

308 West Randolph St. Chicago 6, Ill.

Skin Friction in Slip Flow*

S. A. SCHAAF† AND F. S. SHERMAN‡
University of California at Berkeley

ABSTRACT

Skin-friction data in the slip flow régime are presented, covering the range: $0.008 < M/\sqrt{Re} < 0.38$; $34 < Re < 2{,}020$ for $2.5 < M < 3.8$; $3 < Re < 500$ for $M \sim 0.2$ and 0.6. The results are discussed in terms of the various relevant theories, and it is inferred that, in the neighborhood of $Re = 1{,}000$, the dominant effect is the interaction between boundary layer and external flow which increases the skin friction, but that, in the neighborhood of $Re = 50$, the dominant effect is that of slip that decreases the skin friction.

NOMENCLATURE

b	=	plate breadth
C_D	=	drag coefficient = total drag force (both sides of plate)/dynamic pressure × area (one side of plate)
D	=	drag force
$\operatorname{erfc}(z)$	=	$\frac{2}{\sqrt{\pi}} \int_z^\infty e^{-x^2}\, dx$
f	=	fraction of diffusely reflected molecules
L	=	plate length
M	=	Mach Number (free stream)
p	=	static pressure
p_i	=	impact pressure
p_0	=	stagnation pressure
p_2	=	cone surface pressure
Pr	=	Prandtl Number
Re	=	Reynolds Number = $u_\infty L/\nu$
T	=	temperature (absolute)
T_∞	=	free-stream temperature
t	=	plate thickness
u	=	tangential velocity
u_∞	=	free-stream velocity
x	=	tangential coordinate
y	=	normal coordinate
z	=	$\sqrt{Re}/1.5M$
α	=	thermal accommodation coefficient
γ	=	specific heat ratio
γ'	=	Euler Number, 0.577
δ	=	boundary-layer thickness
δ_*	=	boundary-layer displacement thickness
λ	=	molecular mean free path
μ_∞	=	viscosity coefficient (free stream)
ν	=	μ_∞/ρ_∞
ρ_∞	=	density (free stream)
σ	=	kinetic theory constant, 0.996
ψ	=	stream function
ω	=	viscosity-temperature exponent, $\mu \sim T^\omega$

Received September 17, 1953.

* This work was sponsored by the Office of Naval Research and the Office of Scientific Research of the Air Force.

† Associate Professor of Engineering Sciences.

‡ Research Engineer, Low Pressures Project.

(1) INTRODUCTION

THE GENERAL FIELD OF RAREFIED GAS DYNAMICS—i.e., the mechanics of a gas so rarefied that mean free path effects become important—has been discussed by Tsien.[1] Theoretical and experimental results for several cases of free molecule flow—i.e., a flow in which the mean free path is large compared to a typical body dimension—have been presented subsequently by Stalder, et al.,[2–4] Heineman,[5] Ashley,[6] Kane and Estermann,[7] and Sauer,[8] among others. Experimental results are, in general, in excellent agreement with theory.

In the slip-flow range, where the mean free path is small but not negligible compared with a typical body dimension or the boundary-layer thickness, experimental results for sphere drag have been obtained by Kane,[9] while heat transfer to spheres and cylinders has been determined by Drake and Backer[10] and Stalder, et al.[11] There has also appeared a considerable body of literature[12–17] dealing with theoretical slip-flow solutions, mostly based on simplifications of the Navier-Stokes equations, and first-order slip and temperature-jump boundary conditions. Comparisons between theory and experiment have been difficult because the complex flow fields for which the experimental results are available are not amenable to easy theoretical analysis. (An exception is the case of the Couette flow between rotating cylinders,[12, 13] which has been investigated experimentally by Kuhlthau.[18])

It is the purpose of this paper to report the results of a series of experiments to determine the drag for a flat plate at zero angle of attack in slip flow. It was felt that skin friction phenomena, which could thus be isolated, were of considerable intrinsic importance and also that there was some possibility of eventual comparison between theory and experiment. The experiments cover the range of Mach Number M and Reynolds Number Re (based on plate length and free-stream conditions): $3 < Re < 500$ for $M \sim 0.2$ and 0.6; and $34 < Re < 2{,}020$ for $2.5 < M < 3.8$. These cover a range of the rarefaction parameter $M/\sqrt{Re}$ (roughly the ratio of mean free path to boundary-layer thickness) of $0.008 < M/\sqrt{Re} < 0.38$.

(2) EXPERIMENTAL RESULTS

The experiments were conducted in the low-density wind tunnel at Berkeley.[19] The technique of Kane[9] was closely followed and will only be summarized here.

TABLE 1
Summary of Flat Plate Drag Data

Drag Plate Dimensions			Pressures				Mach No.,	Static Pressure,	Net Drag,	Drag Coefficient,	Reynolds No.,
			Measured		Corrected						
L (in.)	b (in.)	t (in.)	p_1	p_2	p_1	p_2	M	p (microns)	D (mg.)	C_D	Re
			(micron of mercury)								
1.005	0.5005	0.009	1,127	118	1,133	108	3.05	91	350	0.134	904
			933	104	933	96	2.92	82	318	0.149	708
			653	81	650	74	2.73	64	267	0.182	462
			455	64	446	59	2.51	52	234	0.230	294
			272	37	259	33	2.55	29	162	0.276	173
0.812	0.4995	0.009	1,127	118	1,133	108	3.05	91	297	0.141	734
			933	104	933	96	2.92	82	269	0.155	575
			653	81	650	74	2.73	64	226	0.190	375
			455	64	446	59	2.51	52	187	0.228	239
			272	37	259	33	2.55	29	140	0.294	140
0.597	0.5005	0.009	1,127	118	1,133	108	3.05	91	266	0.171	540
			933	104	933	96	2.92	82	238	0.187	423
			653	81	650	74	2.73	64	197	0.226	276
			455	64	446	59	2.51	52	158	0.263	176
			272	37	259	33	2.55	29	112	0.321	103
0.398	0.5010	0.009	1,127	118	1,133	108	3.05	91	198	0.191	360
			933	104	933	96	2.92	82	176	0.207	282
			653	81	650	74	2.73	64	144	0.248	184
			455	64	446	59	2.51	52	119	0.297	117
			272	37	259	33	2.55	29	87	0.373	69
*0.197	0.4999	0.009	1,127	118	1,133	108	3.05	91	148	0.289	178
			933	104	933	96	2.92	82	132	0.314	139
			653	81	650	74	2.73	64	106	0.369	91
			455	64	446	59	2.51	52	81	0.409	58
			272	37	259	33	2.55	29	55	0.478	34
*0.4008	0.5010	0.018	1,127	118	1,133	108	3.05	91	229	0.219	362
			933	104	933	96	2.92	82	203	0.237	284
			653	81	650	74	2.73	64	163	0.278	185
			455	64	446	59	2.51	52	131	0.324	118
			272	37	259	33	2.55	29	94	0.401	70
0.3995	0.5001	0.0045	1,127	118	1,133	108	3.05	91	193	0.186	361
			933	104	933	96	2.92	82	177	0.207	283
			653	81	650	74	2.73	64	145	0.249	185
			455	64	446	59	2.51	52	119	0.296	117
			272	37	259	33	2.55	29	88	0.377	69
0.3994	1.1976	0.009	1,127	118	1,133	108	3.05	91	496	0.199	361
			933	104	933	96	2.92	82	448	0.219	283
			653	81	650	74	2.73	64	369	0.264	185
			455	64	446	59	2.51	52	300	0.311	117
*0.4000	0.1998	0.009	1,127	118	1,133	108	3.05	91	89	0.214	362
			933	104	933	96	2.92	82	79	0.231	284
			653	81	650	74	2.73	64	65	0.279	185
			455	64	446	59	2.51	52	52	0.323	118
			272	37	259	33	2.55	29	41	0.439	70
1.005	0.5005	0.009	1,936	143	1,936	130	3.77	103	417	0.092	2,020
			1,339	114	1,346	103	3.47	84	357	0.114	1,246
			994	87	999	78	3.43	64	305	0.131	911
			541	57	531	51	3.03	43	224	0.182	422
0.398	0.5010	0.009	1,936	143	1,936	130	3.77	103	266	0.148	800
			1,339	114	1,346	103	3.47	84	220	0.177	494
			994	87	999	78	3.43	64	184	0.199	361
			541	57	531	51	3.03	43	128	0.263	167
			396	44	388	38	3.00	32	105	0.295	120

(*Table 1 continued on page 87*)

Gross and tare drag forces were determined at each of several tunnel flow rate settings for a series of sting-mounted flat plates of various length, breadth, and thickness as indicated in Table 1. The setup for a typical determination is shown in Fig. 3. The forces were detected by means of the balance and quartz-spring arrangement used previously by Kane[9] and indicated in Fig. 3.

The Mach Number and free-stream static pressure were calculated for the supersonic case from measured impact and 5° half-angle cone-static pressures. These readings were corrected for viscous effects[20, 21] to give the ideal values indicated in Table 1 and then were reduced to Mach Numbers and free-stream static pressures by means of the Kopal tables.[22] In the subsonic tests the Mach Number and free-stream static pressure were determined from the measured stagnation chamber pressure, the measured nozzle wall tap static pressure, and the assumption of isentropic flow. Free-stream temperatures were determined from the measured stagnation chamber temperature (standard thermocouple) and the assumption of adiabatic flow. For supersonic flow all pressures were measured with the precision U-tube manometer designed by Maslach[23] or with the earlier oil manometer used by Kane.[9] For subsonic flow the pressures were measured with a precision McLeod gage.

TABLE 1—*Continued*

Drag Plate Dimensions L (in.)	b (in.)	t (in.)	Pressures: Measured p_1 (micron of mercury)	Measured p_2	Corrected p_1	Corrected p_2	Mach No., M	Static Pressure, p (microns)	Net Drag, D (mg.)	Drag Coefficient, C_D	Reynolds No., Re
*0.197	0.4999	0.009	1,936	143	1,936	130	3.77	103	205	0.231	396
			1,339	114	1,346	103	3.47	84	163	0.265	244
			994	87	999	78	3.43	64	136	0.298	178
			541	57	531	51	3.03	43	89	0.370	83
			396	44	388	38	3.00	32	70	0.398	59
0.3995	0.5001	0.0045	1,936	143	1,936	130	3.77	103	250	0.139	803
			1,339	114	1,346	103	3.47	84	208	0.167	495
			994	87	999	78	3.43	64	175	0.189	362
			541	57	531	51	3.03	43	123	0.252	168
			396	44	388	38	3.00	32	99	0.278	121
0.3994	1.1976	0.009	1,936	143	1,936	130	3.77	103	648	0.150	803
			1,339	114	1,346	103	3.47	84	531	0.178	495
			994	87	999	78	3.43	64	435	0.196	362
			541	57	531	51	3.03	43	303	0.259	168
			396	44	388	38	3.00	32	244	0.286	121
*0.400	0.1998	0.009	1,936	143	1,936	130	3.77	103	111	0.155	804
			1,339	114	1,346	103	3.47	84	89	0.179	496
			994	87	999	78	3.43	64	75	0.201	362
			541	57	531	51	3.03	43	46	0.236	168
			396	44	388	38	3.00	32	38	0.267	121

Drag Plate Dimensions L (in.)	b (in.)	t (in.)	Mach No., M	Static Pressure, p (microns of mercury)	Stagnation Pressure, p_0	Net Drag, D (mg.)	Drag Coefficient, C_D	Reynolds No., Re
2.009	1.0011	0.003	0.566	559.3	695.1	308.5	0.141	524
			0.194	1,708	1,753	111.8	0.142	502
			0.683	213.7	292.0	268.7	0.220	250
			0.205	799.1	822.9	82.7	0.201	251
			0.577	67.15	84.15	131.9	0.482	64.2
			0.186	230.7	236.3	46.6	0.477	65.6
			0.460	41.46	47.93	82.2	0.765	30.6
			0.163	121.8	124.1	34.5	0.871	30.4
1.0022	1.0022	0.003	0.546	1,121	1,373	287.0	0.140	496
			0.199	3,188	3,277	108.5	0.140	483
			0.590	541.3	685.1	220.0	0.190	263
			0.194	1,706	1,751	79.8	0.203	252
			0.721	202.0	285.6	187.1	0.290	125
			0.205	806.2	830.2	59.6	0.286	126
			0.597	65.33	83.14	89.6	0.626	32.2
			0.186	232.5	238.2	33.5	0.678	32.9
			0.466	41.49	48.14	53.9	0.974	15.3
			0.164	122.8	125.1	25.3	1.245	15.2
0.5029	1.0010	0.003	0.196	3,282	3,371	82.0	0.211	242
			0.586	548.5	692.1	163.9	0.283	132
			0.196	1,708	1,754	61.1	0.303	126
			0.707	209.5	292.4	139.7	0.433	62.9
			0.207	804.2	828.6	45.8	0.432	63.0
			0.626	62.39	81.25	66.0	0.878	16.1
			0.188	231.4	237.2	25.4	1.009	16.5
			0.516	37.32	44.75	39.7	1.296	7.69
			0.166	121.6	124.0	18.4	1.782	7.64
0.2070	1.0005	0.003	0.586	543.8	686.2	117.4	0.497	54.2
			0.195	1,714	1,760	44.4	0.537	52.0
			0.710	205.5	287.6	97.9	0.745	25.8
			0.207	805.1	829.6	34.3	0.785	25.9
			0.622	62.03	80.52	42.2	1.387	6.64
			0.188	232.8	238.6	18.5	1.776	6.79
			0.521	36.43	43.83	25.9	2.064	3.17
			0.167	122.5	124.9	14.1	3.257	3.15

The No. 2 and No. 3 supersonic nozzles[19] used in the experiments produced test-section flows for which the Mach Number and static pressures varied by the order of ±10 per cent in general. For a few of the worst cases, the values given in Table 1 are the result of averaging over the space occupied by the model. The departure from uniformity in these test-section flows probably represents one of the major sources of random experimental error in these tests. The subsonic nozzle produced a flow that was uniform to within ±0.2 per cent.

In the supersonic tests, a systematic attempt was made to eliminate aspect ratio and thickness effects. Analysis of the data obtained with plates of varying thickness and span indicated that such effects become less than the general overall order of uncertainty for all the unstarred data of Table 1 for supersonic conditions. Only this material has been used in the figures. No systematic attempt to eliminate thickness and aspect ratio effects was made in the subsonic tests. It is probable that there are no serious thickness effects. The effect of the varying aspect ratio probably con-

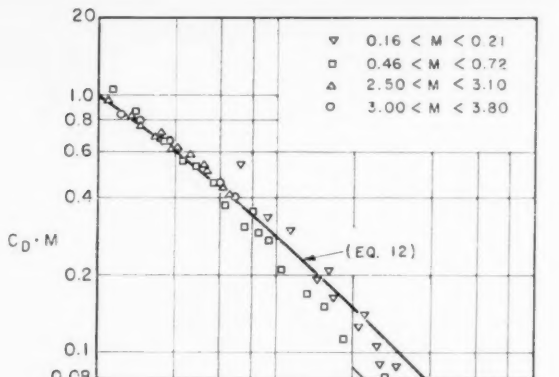

FIG 1. $C_D M$ vs. $\sqrt{Re}/1.5M$.

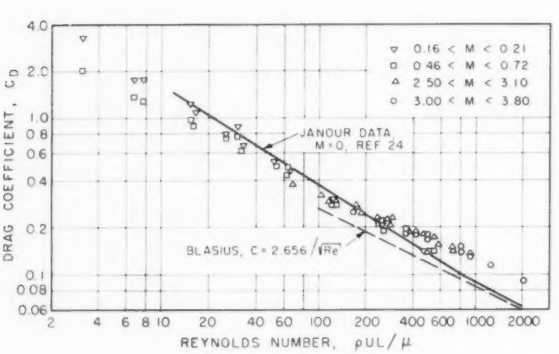

FIG 2. C_D vs. Re.

tributes considerably to the relatively large scatter of the subsonic data, but no systematic trends could be determined. For the worst case, the approximate theory of Howarth[24] indicates an aspect ratio effect of 32 per cent. This theory predicts a decrease in the effect with increasing Reynolds Number, a conclusion that apparently agrees roughly with the reduction in the scatter of the present data for higher Reynolds Numbers.

Summarizing the sources of error, it is estimated that the indicated experimental skin-friction coefficients are, in general, good to within ±5 per cent. It will be observed that the skin-friction coefficient itself varies by approximately 25 to 1 over the range of these experiments.

The results are tabulated in Table 1 and are also presented graphically in Figs. 1 and 2, along with various theoretical curves and a curve summarizing the experimental work of Janour[25] for incompressible flow.

(3) Theoretical Considerations

There is as yet no satisfactory theory for predicting skin friction in the range of Mach and Reynolds Numbers covered by these experiments. The range of Reynolds Numbers is too low for the Prandtl boundary-layer theory to be completely valid and is at the same time too high to warrant use of the Stokes or Oseen approximations based on partial or complete neglect of inertia forces. On the other hand, the rarefaction parameter M/Re is not high enough to warrant use of free-molecule flow theory. These three theories constitute known end points for any applicable theory, however, and in a sense bracket the possibilities. The corresponding total drag coefficients are:

Boundary-layer theory:[26] $[(Re \gg 1),\ M/Re \sim 0]$.

$$C_D = (2.656/\sqrt{Re})\,\{1 + 0.365M^2 \times (\gamma - 1)Pr^{1/2}\}^{(\omega-1)/2} \quad (1)$$

Oseen theory:[27] $[(Re \sim 0),\ M/Re \sim 0]$.

$$C_D = 8/Re[1 - \gamma' - \ln (Re/16)] \quad (2)$$

Free-molecule flow theory:[4] $[(Re \sim 0),\ M/Re \gg 1]$.

$$C_D = 1.35/M \qquad \text{(diffuse reflection)} \quad (3)$$

None of these theories considers the effects of slip, which is known to be an important phenomenon in the range covered by these experiments. From kinetic theory considerations, one has the boundary condition at a wall, $y = 0$,

$$u_{slip} = \sigma[(2 - f)/f]\lambda(\partial u/\partial y) + \ldots \quad (4)$$

where f is the reflection coefficient (approximately unity for most engineering surfaces) and σ is a numerical constant very close to 1. There is also a corresponding temperature jump boundary condition,

$$\Delta T \equiv T_{gas} - T_{wall} = \sigma \frac{2 - \alpha}{\alpha} \frac{\gamma}{\gamma + 1} \frac{\lambda}{Pr} \frac{\partial T}{\partial y} + \ldots \quad (5)$$

where α is the thermal accommodation coefficient and Pr is the Prandtl Number. Higher order terms have been calculated by Schamberg[12] and Grad.[28]

The effects of slip by itself on incompressible flat-plate boundary-layer flow were determined to first order by Lin and Schaaf.[15] The first two terms in a perturbation series for the stream function were obtained in the form

$$\psi = \psi_0 + \lambda\psi_1 + \ldots \quad (6)$$

There is a decrease in the boundary-layer displacement thickness,

$$\delta_*/x = (1.73/\sqrt{Re})\,[1 - 0.866\,(M/\sqrt{Re}) \ldots] \quad (7)$$

but no corresponding change to relative order $\lambda\ \delta$ (or $M/\sqrt{Re}$) in the skin-friction coefficient. This is apparently associated with the fact that the tangential velocity distribution function for the flat plate boundary

layer with no free-stream pressure gradient has an inflection point at the surface. In the general case, a correction term of relative order λ/δ to the skin friction could be expected. Maslen[17] has extended these results to the compressible boundary-layer flow case.

It should be emphasized at this point that rarefaction effects are not confined to the phenomena of slip and temperature jump, even in the so-called slip-flow range. These latter phenomena are associated with the boundary conditions only, and in general it is to be expected that modifications in the differential equations used to describe the flow will also have to be made. These modifications in the differential equations consist in the addition of neglected terms of two general kinds: (1) terms contained in the complete Navier-Stokes equations but neglected in the first approximation—e.g., the stress term $\mu(\partial^2 u/\partial x^2)$ for boundary-layer theory or the inertia term $\rho(Du/Dt)$ for Stokes theory—and (2) correction terms to the Navier-Stokes stress and heat flux formulas themselves—e.g., the Burnett terms[1] obtained from the kinetic theory of monatomic gases. (It might be noted at this point that it is quite possible that corrections of this second kind should be made by considering more equations in more dependent variables, rather than adding more terms to the Navier-Stokes stress and heat flux formulas, following the treatment of Grad.[28])

Writing Eqs. (4) and (5) in dimensionless form,

$$\frac{u_{slip}}{u_\infty} \sim \frac{M}{\sqrt{Re}} \frac{\partial(u/u_\infty)}{\partial(y/\delta)} \sim \frac{M}{Re} \frac{\partial(u/u_\infty)}{\partial(y/L)} \tag{8}$$

$$\frac{\Delta T}{T_\infty} \sim \frac{M}{\sqrt{Re}} \frac{\partial(T/T_\infty)}{\partial(y/\delta)} \sim \frac{M}{Re} \partial(T/T_\infty) \tag{9}$$

one observes that terms of relative order $M/\sqrt{Re}$ neglected in the boundary-layer flow equations must be considered if slip at high Re is to be considered, while terms of relative order M/Re neglected by the Oseen equations must be considered for slip flows at low Re. The problem is further complicated by the fact that the flow equations depend upon M and Re independently and not merely on a rarefaction parameter. Corrections to boundary-layer theory in the form of asymptotic series expansions of the flow equations for the no-slip case and based on the Navier-Stokes expressions have been investigated for $M = 0$ by Alden[29] and for $M \gg 1$ by Lees and Probstein.[30, 31] Alden finds correction terms to the Blasius expression for the *local* skin-friction coefficient in the form of an additive term proportional to $1/Re^{5/2}$. Lees and Probstein find additive terms for the *local* skin-friction coefficient proportional to M^3/Re for $M^3/\sqrt{Re} < 1$ and proportional to $M^{7/2}/Re^{3/4}$ for $M^3/\sqrt{Re} \gg 1$. (In this latter range the "corrective" term dominates the "first-order" term.) The physical basis for the increased skin friction is the interaction between the boundary layer and the free-stream pressure disturbance induced by the boundary layer. The corresponding local drag coefficients, it will be noted, are, except for the last case, nonintegrable. The analytic solution for the flow field must thus apparently be obtained by "matching" a solution valid near the leading edge to the asymptotic solution valid downstream. Some preliminary results of this kind for the case $M = 0$ have been obtained by Lewis and Carrier.[33]

In addition to these terms, which must be retained in the flow equations, it is to be expected, as indicated above, that higher order approximations to the stress tensor and heat flux vector than given by the Navier-Stokes expressions must also be considered. Kinetic theory permits calculation of such correction terms for the case of a monatomic gas; these are the so-called Burnett terms. However, the equivalent expressions for air are not available, and the work of Truesdell[32] indicates that they may be of considerably greater complexity than the monatomic gas relations of Burnett.

To summarize, it appears that an asymptotic series type of solution valid for the range covered by these experiments may be possible, correcting boundary-layer theory with respect to neglected terms in the flow equations, including the still-undetermined stress and heat flux expressions for air, as well as slip and temperature jump in the boundary conditions. It is further to be expected, from the partial results of Alden and Lees and Probstein, indicated above, that only local nonintegrable skin-friction values will result. The complete analytic determination for the total drag coefficient would probably involve a matching of the asymptotic solution to one that is valid near the leading edge. A direct numerical analysis is probably not warranted for air until the higher order stress and heat flux terms have been determined.

(4) Approximate Overall Solutions

In view of the great complexity attached to the solution of the problem of skin friction in the range covered

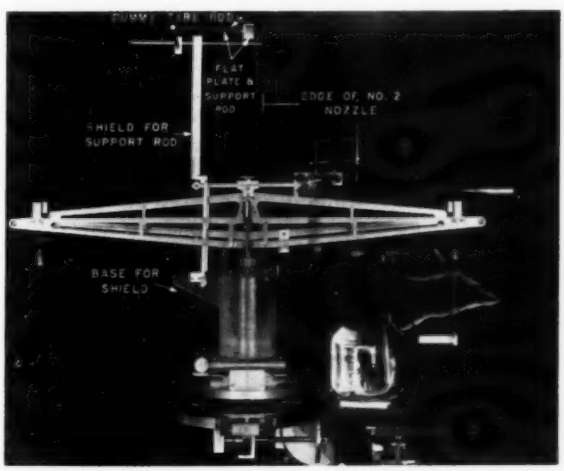

Fig 3. Photograph of experimental setup.

by these experiments, it has seemed desirable to develop a rough approximate theory that spans in closed form the entire range from continuum to free-molecule flow. Such a theory gives an idea of the overall trend and assists in the analysis of the data.

The Rayleigh equation[3,4]

$$\rho_\infty u_\infty(\partial u/\partial x) = \mu_\infty(\partial^2 u/\partial y^2) \tag{10}$$

is used in conjunction with the first-order slip boundary condition, Eq. (4) with $f = 1$, to obtain the solution

$$\frac{u}{u_\infty} = 1 + \exp\left(\frac{\nu x}{\lambda^2 u_\infty} + \frac{y}{x}\right)\operatorname{erfc}\left(\sqrt{\frac{ux}{\lambda^2 u_\infty}} + \sqrt{\frac{u_\infty y^2}{4\nu x}}\right) - \operatorname{erfc}\left(\sqrt{\frac{u_\infty y^2}{4\nu x}}\right) \tag{11}$$

The corresponding total drag coefficient is

$$C_D M = \frac{2.67}{z^2}\left\{e^{z^2}\operatorname{erfc}(z) - 1 + \frac{2z}{\sqrt{\pi}}\right\} \qquad z^2 = Re/2.25M^2 \tag{12}$$

This has the limiting forms of

$$\left.\begin{aligned} C_D &\to 8/\sqrt{\pi Re}, & M^2/Re &\to 0 \\ C_D &\to 2.67/M, & M^2/Re &\to \infty \end{aligned}\right\} \tag{13}$$

which are correct in form although not in numerical value. Mirels[16] has extended this calculation to include the effect of compressibility and has introduced an empirical relation so as to ensure a correct matching for $Re \to \infty$. In view of the discussion above such extensions seem of somewhat limited value. Both the foregoing analysis and that of Mirels imply no first-order effect of slip on skin friction, in agreement with the more detailed analyses of Lin and Schaaf and Maslen.

A casual inspection of Fig. 1 would seem to indicate that, within reasonable scatter, the data seem to lie on the curve defined by Eq. (12) for high rarefaction, the boundary-layer curve of Blasius for low rarefaction, and an interpolating curve in between. However, closer inspection reveals additional interrelations and strongly indicates that no such single correlation of $C_D M$ vs. $M/\sqrt{Re}$ in fact exists. The departure of the skin-friction coefficient from its continuum boundary-layer theory value seems to be associated with at least two phenomena—namely, slip effects and interaction effects. (The word interaction is used to include all effects stemming from modifications in the flow differential equations.) It can be guessed from the work of Alden and Lees, et al., that these interaction effects will increase the skin friction, and do so increasingly with higher Mach Numbers. It appears in Fig. 2 that in the vicinity of $Re \sim 1{,}000$ this phenomenon dominates the slip effect, in agreement with the theories of Lin and Schaaf and of Maslen which indicate that slip effects are initially negligible. However, at lower Reynolds Number, $Re \sim 50$ say, slip apparently begins to be the dominant effect, and the skin friction decreases with increasing Mach Number. Slip can certainly be expected to be a dominant effect for $M/\sqrt{Re} \sim 1$. The fact that the Rayleigh limiting value of Eq. (13) happens to be approximately as much higher than the Blasius value as the actual increase at the higher Reynolds Numbers in these experiments, due presumably to the interaction effects, is probably only a fortuitous coincidence.

References

[1] Tsien, H. S., *Superaerodynamics, Mechanics of Rarefied Gases*, Journal of the Aeronautical Sciences, Vol. 13, No. 12, pp. 653–664, December, 1946.

[2] Stalder, J. R., and Jukoff, D., *Heat Transfer to Bodies Traveling at High Speed in the Upper Atmosphere*, Journal of the Aeronautical Sciences, Vol. 15, No. 7, pp. 381–391, July, 1948. (Also NACA TN No. 1682, August, 1948, NACA Report No. 944, 1949.)

[3] Stalder, J. R., Goodwin, G., and Creager, M., *A Comparison of Theory and Experiment for High Speed Flow*, NACA TN No. 2244, December, 1950.

[4] Stalder, J. R., and Zurich, V. J., *Theoretical Aerodynamic Characteristics of Bodies in a Free Molecule Flow Field*, NACA TN No. 2423, 1951.

[5] Heineman, M., *Theory of Drag in Highly Rarefied Gases*, Communications on Applied Mathematics, Vol. 1, pp. 259–273, September, 1948.

[6] Ashley, H., *Applications of the Theory of Free Molecule Flow to Aeronautics*, Journal of the Aeronautical Sciences, Vol. 16, No. 2, pp. 95–104, February, 1949.

[7] Estermann, I. B., and Kane, E. D., *A Torsion Balance for Measuring Forces in Low Density Gas Flows*, Jour. Appl. Phys., Vol. 20, June, 1949.

[8] Sauer, F. M., *Convective Heat Transfer from Spheres in a Free-Molecule Flow*, Journal of the Aeronautical Sciences, Vol. 18, No. 5, pp. 353–354, May, 1951.

[9] Kane, E. D., *Sphere Drag Data at Supersonic Speeds and Low Reynolds Numbers*, Journal of the Aeronautical Sciences, Vol. 18, No. 4, pp. 259–270, April, 1951.

[10] Drake, R. M., and Backer, G. H., *Heat Transfer from Spheres in Supersonic Flow to a Rarefied Gas*, Trans. ASME, Vol. 74, October, 1952.

[11] Stalder, J. R., Goodwin, G. C., and Creager, M. O., *Heat Transfer to Bodies in a High-Speed Rarefied Gas Stream*, NACA TN No. 2438, August, 1951.

[12] Schamberg, R., *The Fundamental Differential Equations and the Boundary Conditions for High Speed Slip-Flow and Their Application to Several Specific Problems*, C.I.T. Thesis, 1947.

[13] Lin, T. C., *The Effect of Variable Viscosity and Thermal Conductivity on the High-Speed Couette Flow of a Semi-Rarefied Gas*, Univ. of Wash. Eng. Experiment Station Bulletin, No. 118, pp. 26–49, 1951.

[14] Drake, R. M., and Sauer, F. M., *Forced Convection Heat Transfer from Horizontal Cylinders in a Rarefied Gas*, Journal of the Aeronautical Sciences, Vol. 20, No. 3, p. 175, March, 1953.

[15] Lin, T. C., and Schaaf, S. A., *The Effect of Slip on Flow Near a Stagnation Point and in a Boundary Layer*, NACA TN No. 2568, December, 1951.

[16] Mirels, H., *Estimate of Slip Effect on Compressible Laminar Boundary Layer Skin Friction*, NACA TN No. 2609, January, 1952.

[17] Maslen, S. A., *Second Approximation to Laminar Boundary Layer Flow on Flat Plate in Slip Flow*, NACA TN No. 2818, November, 1952.

(*Concluded on page 144*)

Turbulent Boundary Layers in Adverse Pressure Gradients*

FRANCIS H. CLAUSER†
The Johns Hopkins University

SUMMARY

An experimental study has been made of turbulent boundary layers in adverse pressure gradients which were established in such a way that for each layer the profiles, when plotted in a set of universal coordinates, are of similar shape. A comparison is made with the corresponding set of laminar profiles. Results are presented for the effects of Reynolds Number, pressure gradient, and roughness on skin friction. It is shown that boundary layers in moderately high adverse gradients will not exhibit what is termed downstream stability. A comparison is made of the present experimental results with conventional methods of predicting the effect of pressure gradients on turbulent boundary layers, and it is shown that the agreement is poor.

INTRODUCTION

ONE OF THE MOST CHALLENGING PROBLEMS in fluid mechanics today is that of understanding the behavior of turbulent boundary layers, particularly with regard to their separation or detachment. A great deal of our technology is concerned with devices that are fluid mechanical in nature such as fans, compressors, turbines, pumps, torque converters, reciprocating engines, jet engines, aircraft, missiles, ships, and the like. In almost all cases, the limiting performance of these devices is determined by flow separation. The ultimate lift of a wing or thrust of a propeller is determined by stalling—i.e., separation. Similarly, the maximum compression of an axial-flow fan and the maximum torque of a converter are limited by separation. Even the simplest water faucet depends on separation for its throttling action.

Near every solid surface immersed in a moving fluid there is a layer of fluid retarded by friction. For the fluids that are commonly used, together with the velocities and sizes that most frequently occur, the Reynolds Numbers are sufficiently large that the layers are not only thin but also turbulent. Thus we find that the greater number of our fluid mechanical machines are directly limited in their capabilities by separation of turbulent boundary layers. This separation is caused by the action of adverse or rising pressure gradients, retarding the fluid in the boundary layer, bringing it to rest, and forcing the outer stream to leave the surface and ride out over this stagnant fluid.

In spite of the great technical importance of turbulent separation, our knowledge of the action of pressure gradients on turbulent layers is poor. First, no theory worthy of the name exists for any turbulent shear flow. Second, several empirical methods exist for predicting the effect of pressure gradients on turbulent boundary layers, but experience indicates that none of them is reliable. They do little more than correlate the set of data on which they were based originally.

Early, it was found that the state of affairs in the turbulent boundary layer depends not only upon the local environment such as the local values of the pressure gradient, the wall shear, the surface roughness, the boundary layer thickness, etc., but also upon a long portion of the history of the layer. The forces acting on a boundary layer are surprisingly small. Skin-friction coefficients show that shearing stresses are only a few thousandths of the kinetic energy per unit volume. Furthermore, because the layers are thin, the pressure forces that act upon an effective area across the face of the layer are also very small in size. With such diminutive forces present, the boundary layer reacts slowly to a changing environment. It is for these reasons that the previous history of the layer is so important.

When we began our turbulent boundary-layer research at Johns Hopkins, we wanted to study in detail a few cases that would have simple and well-defined pressure histories and which could be measured with a fair degree of precision. In specifying the history, nondimensional parameters must, of course, be used. The pressure gradient acts across some effective face area δ' of the layer with a force per unit length and width of $\delta'(dp/dx)$. The only other gross force on the layer is the wall shear, τ_0. Consequently, the boundary layer will have a constant history, nondimensionally speaking, if $(\delta'/\tau_0)\ (dp/dx)$ is held constant throughout its length. Since a constant history is a particularly simple and well-defined case, we decided to attempt to obtain such cases, even though we were not sure that it would be easy in practice to set up such "simple" histories. Throughout the rest of this paper we shall, for convenience, call this class of profiles "equilibrium" profiles. This paper describes the results of the work accomplished so far on layers having such profiles.

Received August 11, 1953.

* The research work described in this report was sponsored by the Office of Scientific Research of the U.S. Air Research and Development Command through Contract AF 33(038)9862. The experimental work was carried out by Dr. Giles Corcos, Miss Ingeborg Busemann, and Mr. Donald Johnson. Dr. Stanley Corrsin assisted in the supervision of the project.

† Chairman, Department of Aeronautics.

NOTATION

C	= a constant
c_f	= local skin-friction coefficient
F	= power spectrum
F_1, F_2	= Reynolds Number factors for effect of roughness and pressure gradient on skin friction
f, g	= functions used in describing velocity profiles
G	= family parameter of equilibrium profiles
H	= δ^*/θ
k	= height of roughness elements
m	= constant in Falkner-Skan solution
n	= spectral wave number
p	= local static pressure
dp/dx	= static pressure gradient
q	= local free-stream dynamic pressure
R	= Reynolds Number
u, v, w	= components of velocity
U	= free-stream velocity
u_*	= friction velocity = $\sqrt{\tau_0/\rho}$
x, y, z	= position coordinates
$\frac{\Delta u_1}{u_*}$, $\frac{\Delta u_2}{u_*}$	= shifts of semilogarithmic profiles caused by roughness and pressure gradient
β	= constant in Hartree solution
δ	= distance to outer edge of boundary layer
δ^*	= displacement thickness
δ'	= effective boundary-layer thickness used in $(\delta'/\tau_0)(dp/dx)$
Δ	= universal turbulent boundary-layer thickness
θ	= displacement thickness
ρ	= fluid density
ν	= kinematic viscosity
τ_0	= shearing stress at wall

EXPERIMENTAL PROGRAM

Description of Boundary-Layer Tunnel

Our program of turbulent boundary-layer research is a long-range one which has as its goal both the determination of the behavior of turbulent layers and an exploration of their internal structure. A relatively inexpensive wind tunnel was built especially for this research. In establishing conditions for the tunnel design, it was considered necessary that the layers themselves and their associated sublayers should be sufficiently thick that microinstrumentation would not be required. This led to a test section 37 ft. long, 4 ft. high, and 3 ft. wide with velocities ranging from 6 to 40 ft. per sec. Measurements are made on the boundary layer that develops on the floor. The layers range from 2 to 20 in. thick. Because separating boundary layers were to be one of the subjects of investigation, there was great likelihood that adverse gradients would induce separation on the walls and ceiling before it occurred on the floor. This indicated the need for boundary-layer control on the upper three surfaces. To accomplish this without suction ducting and at the same time to simplify the pressure distribution control, the tunnel was arranged as shown in Fig. 1. A large blower is used to force air into the tunnel under pressure. A screened diffusor and a large settling chamber with four single-piece precision screens makes the air stream uniform and of low turbulence. The tunnel is open-return, and a heavily screened diffusor at the exit maintains a controllable overpressure in the working section.

On the sides, simple variable-width slots with rounded edges are provided every 8 in. for boundary-layer removal, the air simply being blown into the atmosphere by the overpressure in the tunnel. Flaps are provided on the top for exhausting relatively large amounts of air to slow down the central stream and establish a variable adverse pressure gradient. A portion of the floor is a flexible masonite sheet, controlled by automobile jacks for more detailed pressure control. A traversing gear for both pitot tubes and hot-wire probes can be used at any location in the test section.

Preliminary Analysis

At first sight it would appear simple to establish a pressure distribution giving a sequence of equilibrium turbulent boundary-layer profiles. Falkner and Skan[1] obtained the theoretical solution for the corresponding set of laminar profiles. The Falkner and Skan solutions show that, if $(\delta/\tau_0)\ (dp/dx)$ is held constant throughout the length of the layer, then the profiles of u/U versus y/δ are all identical, even though the Reynolds Number (and, hence, c_f) is changing with x. Further, if x is measured from the origin of the boundary layer, then $(x/q)\ (dp/dx)$ is likewise constant throughout the length of the layer. This shows that U is proportional to x^m, where $m = -(1/2)\ (x/q)\ (dp/dx)$. It is of interest that neither $(\delta/q)\ (dp/dx)$ nor $(x/\tau_0)\ (dp/dx)$ is constant. Since for these laminar layers the profiles are all identical throughout the length of the layer, the choice of thickness in the expression $(\delta/\tau_0)\ (dp/dx)$ is arbitrary since all thicknesses will be in constant ratio for a given layer. A simple special case of the above analysis is the Blasius solution, obtained when the pressure is constant.

When we turn to the case of turbulent layers, the situation is not so simple. In contrast to the Blasius case, turbulent profiles are not similar, even when the pressure is constant. At lower Reynolds Numbers, the profiles are roughly one-seventh power profiles, and as the Reynolds Numbers increase, the profiles are more nearly one-eighth or one-ninth power profiles. The typical difference can be seen in Fig. 2 for the profiles of Hama and Klebanoff and Diehl. Further, it is seen that a profile on a rough wall shows even greater lack of similarity.

Normally, one might overlook the deviation for the the smooth plate profiles. However, with our long test section, such discrepancies were likely to show up, and, since we had a chance to make careful measurements under well-defined conditions, we did not want to have effects due to pressure gradients confused with such Reynolds Number effects.

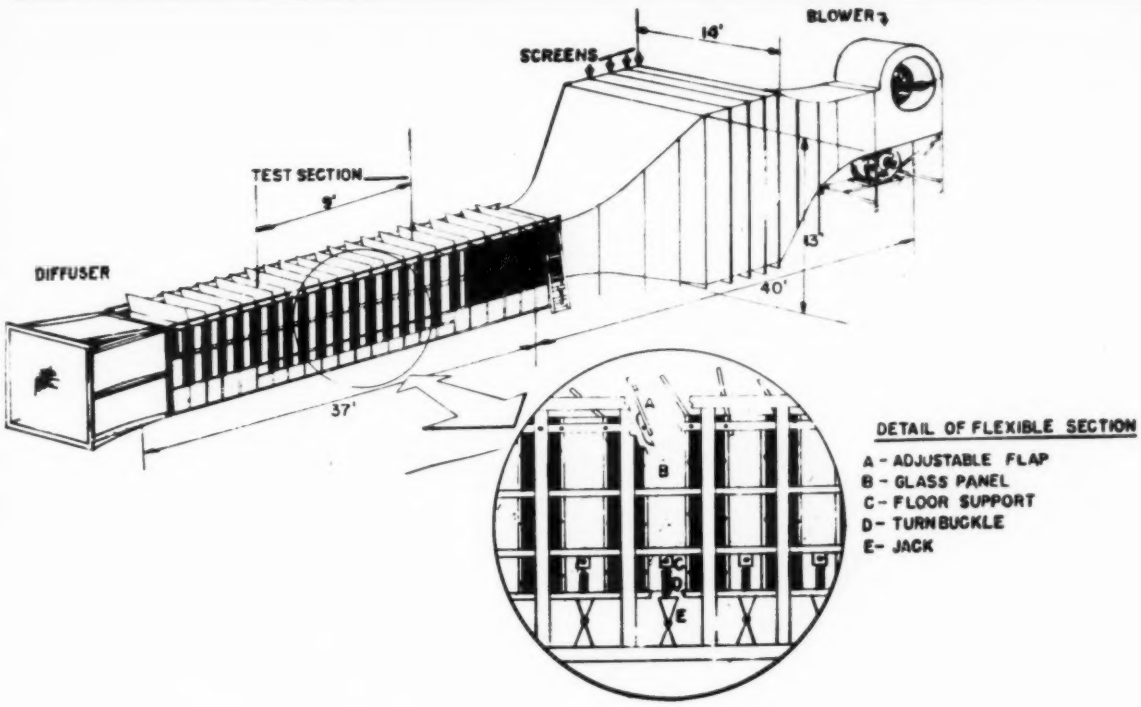

FIG.1 SKETCH OF WIND TUNNEL FOR BOUNDARY LAYER TESTS

Now it has been known for many years that, if we measure velocities relative to the free stream and abandon U as a nondimensionalizing velocity, using in its place $u_* = \sqrt{\tau_0/\rho}$, the friction velocity, then all constant pressure turbulent profiles are similar. In Fig. 3, a collection of profiles has been plotted, and it will be seen they all fall together, including the dissimilar profiles of Fig. 2. This way of plotting retains the typical shape of turbulent profiles. The customary zero velocity point is located at the now variable height, $-\sqrt{2/c_f}$.

It should be emphasized that this plot correlates the profiles independently of both Reynolds Number and roughness. When the roughness size becomes comparable to the thickness of the layer, then the origin of y is undefined. Moore[2] has shown that, even for very large roughness elements, an origin exists which will give agreement with this universal law, as can be seen from his data plotted on Fig. 3. It is believed that all turbulent profiles for which reliable wall shears are known are in agreement with the method of plotting used in Fig. 3. In fact, it is seldom, either in turbulence research or boundary layer research, that a collection of data from varied sources shows such consistency.

The method of correlating turbulent profiles given in the preceding paragraphs offers a possible foundation on which to build an analysis of equilibrium profiles. It appears reasonable that a family of equilibrium profiles should be characterizable by a dimensionless parameter containing the pressure gradient as one of the factors in the parameter. If this is true, then all of the constant pressure profiles must correspond to a single member of the equilibrium family, since for all these profiles the parameter will be zero. This in turn necessitates that a correlation scheme be adopted for which all the constant pressure profiles will be a single member of the family—i.e., they are all identical when plotted nondimensionally. This has been achieved by the method just described.

When we consider equilibrium turbulent layers for which the pressure is not constant, it is necessary to attempt to define more precisely what we mean by equilibrium layers. What we should like, of course, is to have

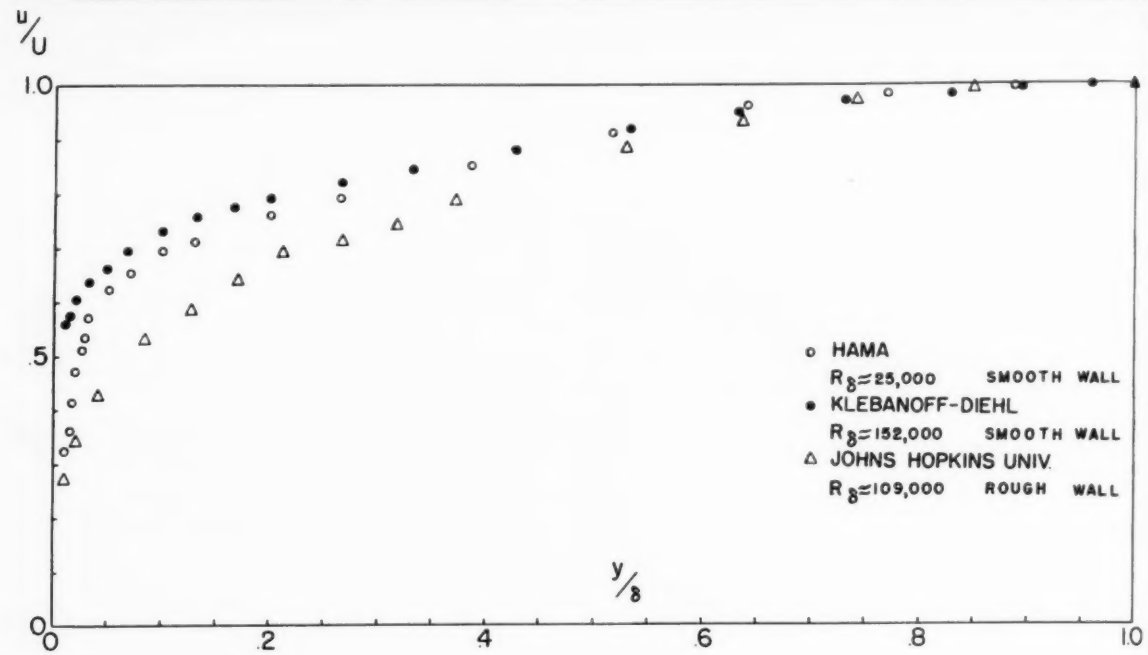

FIG. 2 CONVENTIONAL PLOT OF SEVERAL TURBULENT BOUNDARY LAYER PROFILES FOR CONSTANT PRESSURE

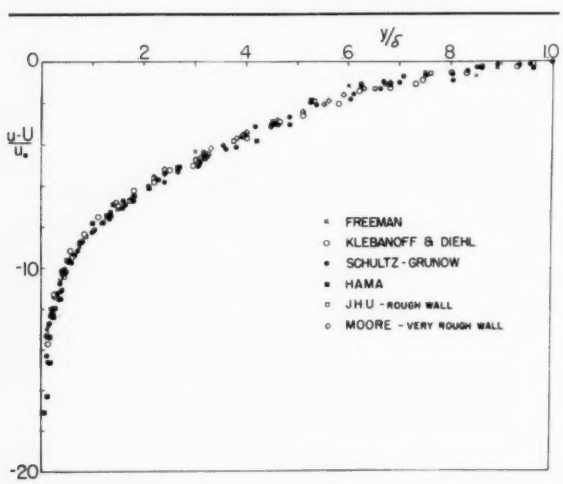

FIG. 3 UNIVERSAL PLOT OF CONSTANT PRESSURE TURBULENT BOUNDARY LAYER PROFILES

a layer for which at every cross section the flow is completely dynamically similar. By this is meant that at each section both the mean velocity patterns and the statistical patterns of the fluctuations will be similar. It is almost certain this cannot be achieved, because as the layer moves down the plate its Reynolds Number increases and this changes the high wave number end of the spectrum compared to the low wave number end. This is clearly seen in the recent measurements of Laufer,[15] which show this change in statistical structure of turbulent shear flow in a pipe when the Reynolds Number is altered.

On the other hand, this same state of affairs must exist in constant pressure layers, and in spite of this an important property such as mean velocity distribution can be correlated on a single plot even when the Reynolds Number is varying. Since large eddies determine the shear distribution, which in turn determines the mean velocities, this probably indicates that for constant pressure layers the small wave number (large eddy size) end of the spectrum is always similar in pattern (i.e., similar as a function of the two variables, wave number, and distance from the wall). The appropriate nondimensional variables would be $F/U_*^2\delta$, $n\delta$, and y/δ.

The foregoing leads to the hope that a like state of affairs may exist for equilibrium layers with varying pressures. If this is true, then it is plausible that equilibrium layers should be those layers for which the profiles at each cross section are identical when $(u - U)/u_*$ is plotted against y/δ. In this report, we shall accept this as a tentative criterion that layers

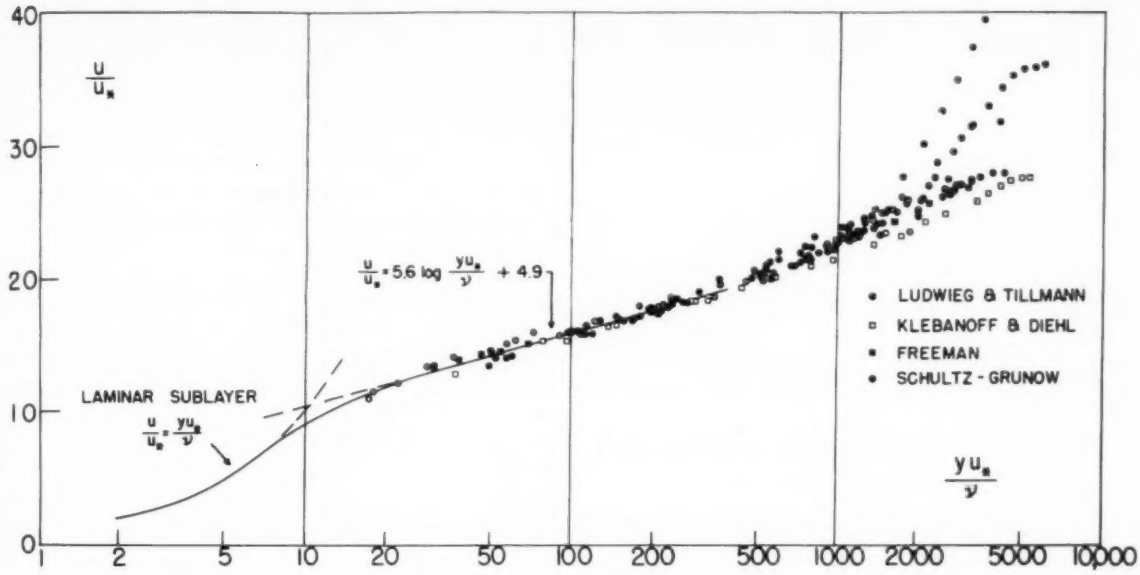

FIG. 4 UNIVERSAL VELOCITY DISTRIBUTION FOR TURBULENT VELOCITY PROFILES NEAR SMOOTH WALLS

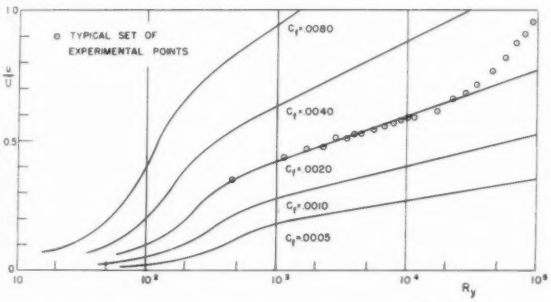

FIG. 5 CHART FOR EXPERIMENTAL DETERMINATION OF TURBULENT SKIN FRICTION

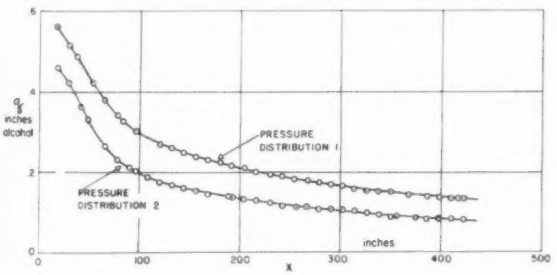

FIG. 6 EXPERIMENTAL PRESSURE DISTRIBUTIONS

are indeed equilibrium layers. Eventually, it will be necessary to show that similarity also exists for some significant set of properties of the fluctuating quantities.

There also remains the question of obtaining a proper parameter of the form $(\delta'/\tau_0)(dp/dx)$. We shall show presently that the choice of δ' is not arbitrary as in the case for laminar layers. This point is discussed in some detail later.

Experimental Procedures and Results

It was apparent at the outset of the experimental work that it would be necessary to measure wall skin friction. Not only is τ_0 a useful piece of information in itself but, as has been shown above, it is also a primary datum in the correlation of turbulent profiles. An instrument for measuring τ_0 is being built; however, this instrument was not ready for use when the present results were being obtained so an alternate method was used. Ludwieg and Tillmann[3] found that near a smooth wall, the mean velocity points fall on the well-known universal curve of u/u_* vs. yu_*/ν, even when a pressure gradient is present. A collection of data has been plotted on Fig. 4 to show this agreement. It is sufficiently convincing that the following method of measuring shear has been used. Since $u/u_* = (u/U)\sqrt{2/c_f}$ and $yu_*/\nu = y(U/\nu)\sqrt{c_f/2}$, the universal curve of Fig. 4 can be replotted as a universal family with c_f as a parameter as shown in Fig. 5.† Experimental points taken near the wall are plotted on the figure as shown, and c_f is determined by selecting the appropriate member of the family which fits the points. This method should prove to be of value in turbulent boundary-layer research, since it provides a method of obtaining the skin-friction coefficient simply

† In a private communication, D. Ross has independently proposed to use this same method.

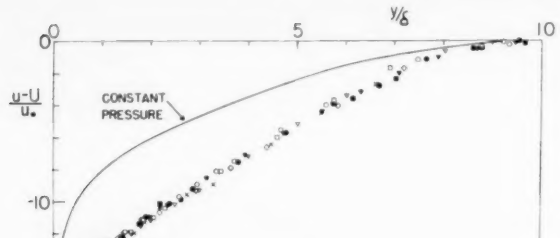

FIG. 7 UNIVERSAL PLOT OF TURBULENT VELOCITY PROFILES FOR PRESSURE DISTRIBUTION I

from the mean velocity profile. This method should make available for analysis a great deal of data taken in the past for which no skin-friction coefficients were obtained but for which accurate velocity profiles were taken.

For the first attempt at establishing an equilibrium set of profiles, it was decided to use a relatively mild dimensionless gradient. This was done because it was known that, with gradients that produce near separating conditions, the velocities close to the wall are small and the turbulence levels large, making accurate measurements difficult because of the lack of existence of instruments having strictly linear response. This initial choice was fortunate for other reasons, as will be seen presently. The procedure adopted was to set up a trial pressure distribution and to measure the velocity profiles at a number of stations, determining the skin-friction coefficients and making a plot of $(u - U)/u_*$ vs. y/δ. For the first trial pressure distribution, the profiles were not similar, and it was necessary to alter the pressure distribution a great number of times before similar profiles were obtained. The final pressure distribution for this first set of measurements is shown in Fig. 6. The corresponding set of similar profiles is shown in Fig. 7. Although the profiles were similar from $x = 83$ to 387 in., the adverse pressure started very near the beginning of the test section. A tripping wire was used at the entrance of the test section to induce a uniform transition. The initial run of the turbulent layer from $x = 0$ to 83 in. was used to give the boundary layer a chance to settle down and attain a reasonably uniform internal dynamical state. The conditions existing during the settling down process have not yet been explored. It is expected this will be done later in the program.

It will be noticed that the profiles of Fig. 7 show an expected difference from those with constant pressure. Compared with this difference the profiles show little scatter from a single curve, indicating that they are nearly identical members of what must be an equilibrium set. The same profiles have been plotted in the conventional manner of u/U vs. y/θ in Fig. 8. It will be seen that there is a consistent variation with increasing x caused by the decrease of c_f as the Reynolds

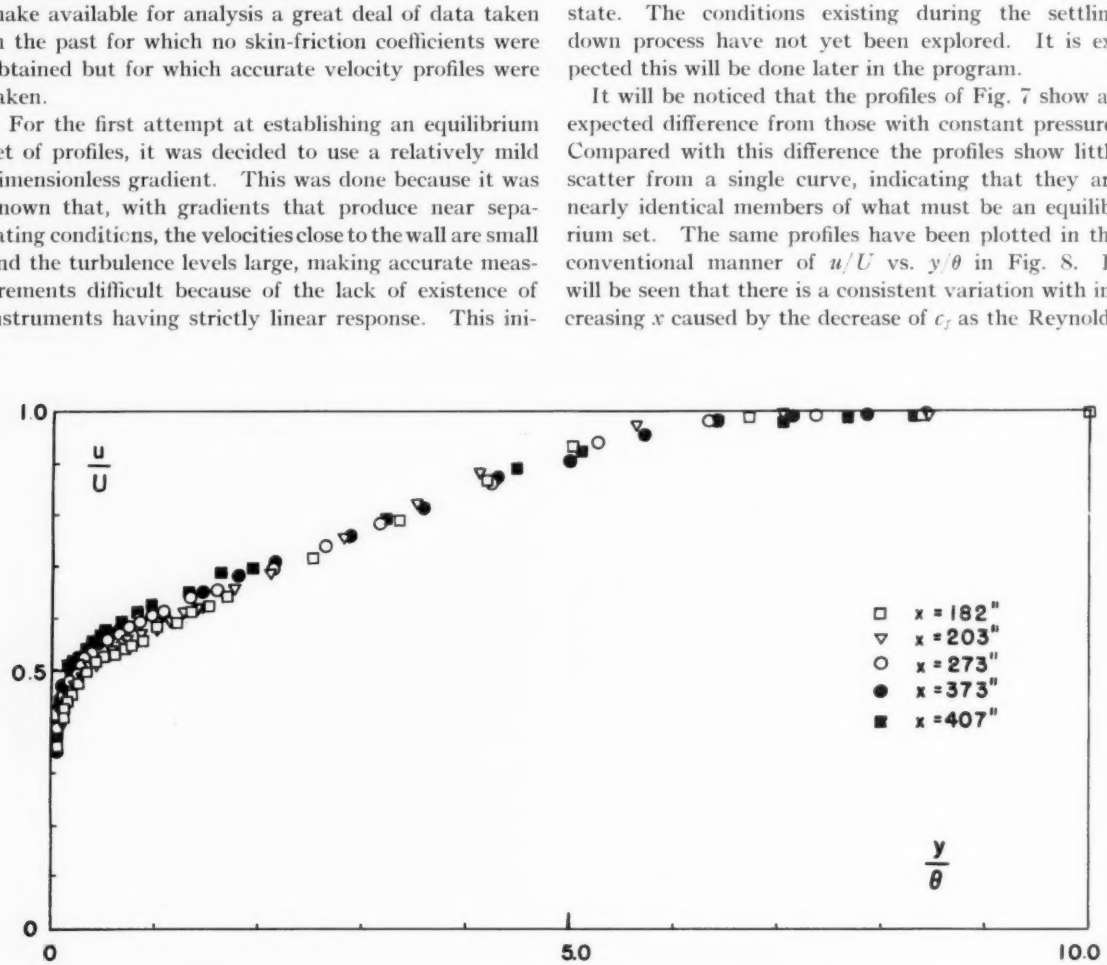

FIG. 8 CONVENTIONAL VELOCITY PROFILES FOR PRESSURE DISTRIBUTION I

Number increases. This variation of c_f with x is shown in Fig. 9. The change in shape of the profiles on Fig. 8 causes a change in H from about 1.4 to 1.5. Since H for constant pressure profiles is about 1.3 and for separating profiles is about 2.5, it is clear that this set of profiles is far from separation. In spite of this, the skin-friction coefficients are much smaller than corresponding values for constant pressure profiles.

Next it was decided to attempt using a steeper dimensionless gradient. Immediately, serious difficulties were encountered. The first of these was the appearance of strong disagreements with the simple two-dimensional momentum equation,

$$\frac{d\theta}{dx} = \frac{C_f}{2} + \frac{(H+2)}{2}\frac{\theta}{q}\frac{dp}{dx}$$

The c_f term was insignificant, and the dp/dx term was larger than the $d\theta/dx$ term by as much as a factor of two, indicating a lateral divergence of the flow. The second difficulty was an inability to obtain a set of constant dimensionless characteristics for the profiles. Corrections in dp/dx which had previously led to convergence in obtaining equilibrium profiles now produced wild variations at downstream stations. After considerable work these difficulties were understood and corrected. A detailed discussion of the reasons will be given later. The final profiles obtained for the steeper pressure distribution are plotted in Fig. 10. The pressure distribution itself is shown on Fig. 6, along with the first pressure distribution. The skin-friction distribution is also shown on Fig. 9. It is felt that these two sets of constant history profiles, along with the data on constant pressure profiles, give a useful cross section of such nonseparating turbulent profiles in adverse gradients.

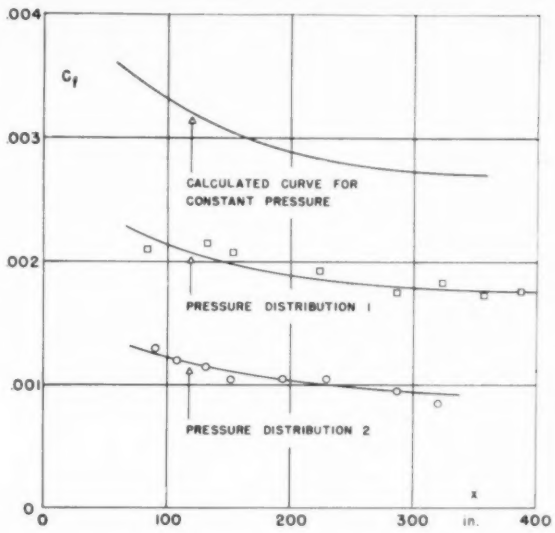

FIG. 9 DISTRIBUTION OF SKIN FRICTION DURING EXPERIMENTS ON TURBULENT VELOCITY PROFILES

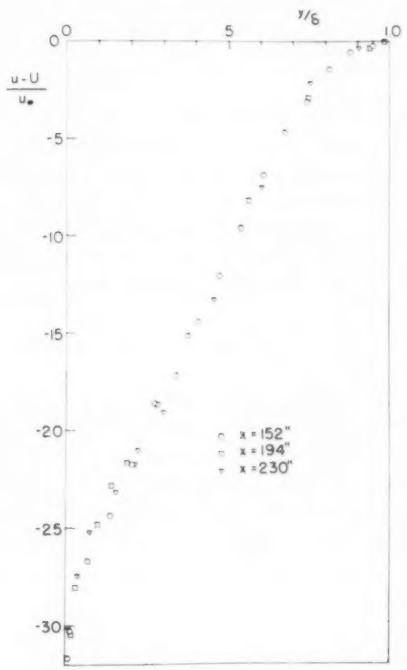

FIG. 10 UNIVERSAL PLOT OF TURBULENT VELOCITY PROFILES FOR PRESSURE DISTRIBUTION 2

Analysis and Discussion

Parameters for Analysis

A question arises as to what parameters can be used to analyze the data that have been obtained. First consider the boundary-layer thickness. The distance δ to the outer edge of the profile has the difficulty that the outer edge of the layer is ill-defined. The displacement thickness

$$\delta^* = \int_0^\infty [1 - (u/U)]\, dy$$

and the momentum thickness

$$\theta = \int_0^\infty [1 - (u/U)]u/U\, dy$$

are not satisfactory for analyzing turbulent profiles because they cannot be obtained directly from the universal plot that forms the basis for our correlation of turbulent profiles. To see this we note that, for each member of the family, $(u - U)/u_*$ is a universal function of y/δ. Thus if we put $(u - U)/u_* = \zeta$ and $y/\delta = \eta$, then $\zeta = f(\eta)$ and we have

$$\delta^* = -\delta\sqrt{\frac{2}{c_f}}\int_0^\infty f(\eta)\, d\eta$$

Since the integral is simply a number, the ratio of δ^* to δ is not fixed, but is a function of c_f—that is, of Rey-

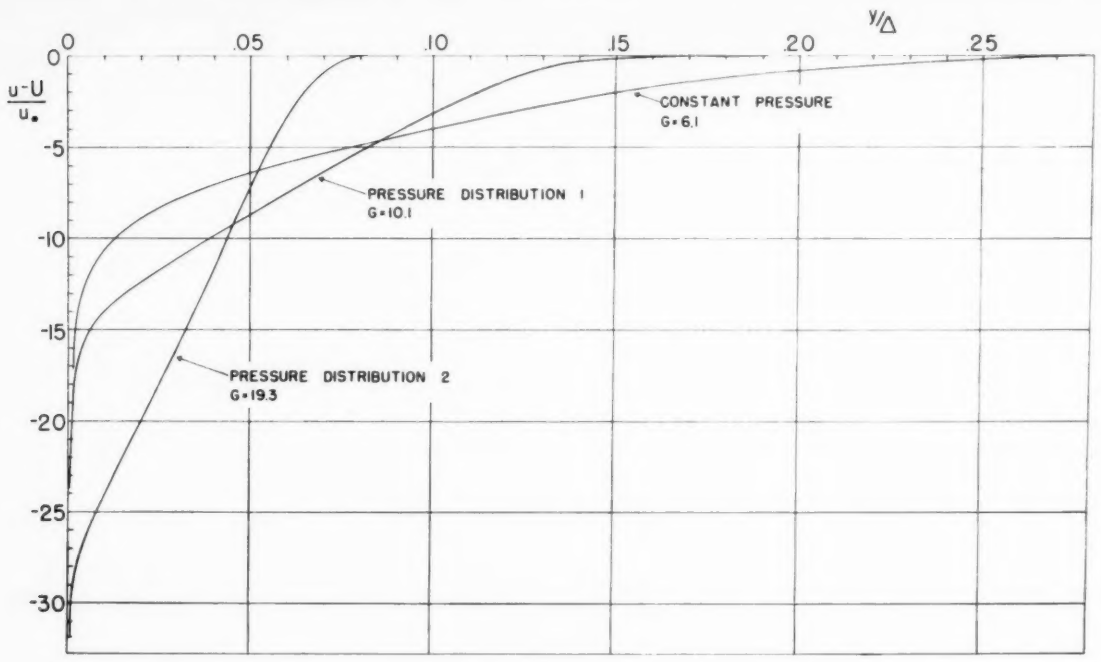

FIG. 11 UNIVERSAL PLOT OF EQUILIBRIUM TURBULENT VELOCITY PROFILES

nolds Number and roughness. A similar statement holds for θ. This dependence of δ^* and θ on Reynolds Number and roughness makes them unsuitable for analyzing a universal family. It is, of course, desirable to have a thickness that does not need these additional data for its specification. It is clear that the simplest universal thickness that is so defined is

$$\Delta = \int_0^\infty \frac{U - u}{u_*}\, dy = -\delta \int_0^\infty f(\eta)\, d\eta$$

For constant pressure profiles the integral has the value 3.6. Each set of equilibrium profiles will have a different value for the integral, but for each set Δ is in constant ratio to δ. This means that we may substitute Δ for δ in our universal plots and eliminate the uncertainty in determining δ. It will be found that Δ is well suited to analyses of turbulent profiles.

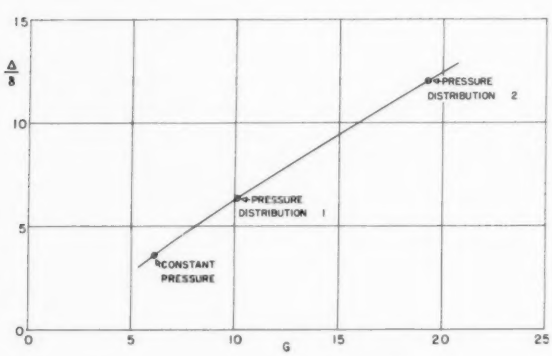

FIG. 12 RELATIONSHIP BETWEEN $\frac{\Delta}{\delta}$ AND G FOR EQUILIBRIUM TURBULENT VELOCITY PROFILES

In addition to Δ, we need a suitable parameter to characterize the various members of our universal family. Customarily, $H = \delta^*/\theta$ is used; however, this suffers from the same shortcoming as δ^* and θ. When profiles are plotted using u/U, δ^* is a first moment of the profile around the axis $u/U = 1$. Similarly, θ is a mixed second moment around the axes $u/U = 0$ and $u/U = 1$, and H is the ratio of these two moments. As a substitute for H, we can ask for a ratio of moments on our universal plot. Since the only axis with significance is $(u - U)/u_* = 0$, the proper choice of parameter is the ratio of the second to the first moment around this axis—i.e.,

$$G = \int_0^\infty \left(\frac{U - u}{u_*}\right)^2 dy \Big/ \int_0^\infty \frac{U - u}{u_*}\, dy = \int_0^\infty \left(\frac{U - u}{u_*}\right)^2 d(y/\Delta)$$

We can relate our new thickness, Δ, and integral family parameter, G, to θ, δ^*, and H as follows:

$$\delta^* = \sqrt{c_f/2}\ \Delta$$

$$\theta = \sqrt{c_f/2}\,(1 - G\sqrt{c_f/2})\,\Delta$$

$$H = 1/(1 - G\sqrt{c_f/2})$$

In addition to the integral parameter G, we also have the dynamic parameter $(\delta'/\tau_0)\ (dp/dx)$, which, if δ' is properly chosen, will be constant throughout the length of an equilibrium layer. This should, of course, be

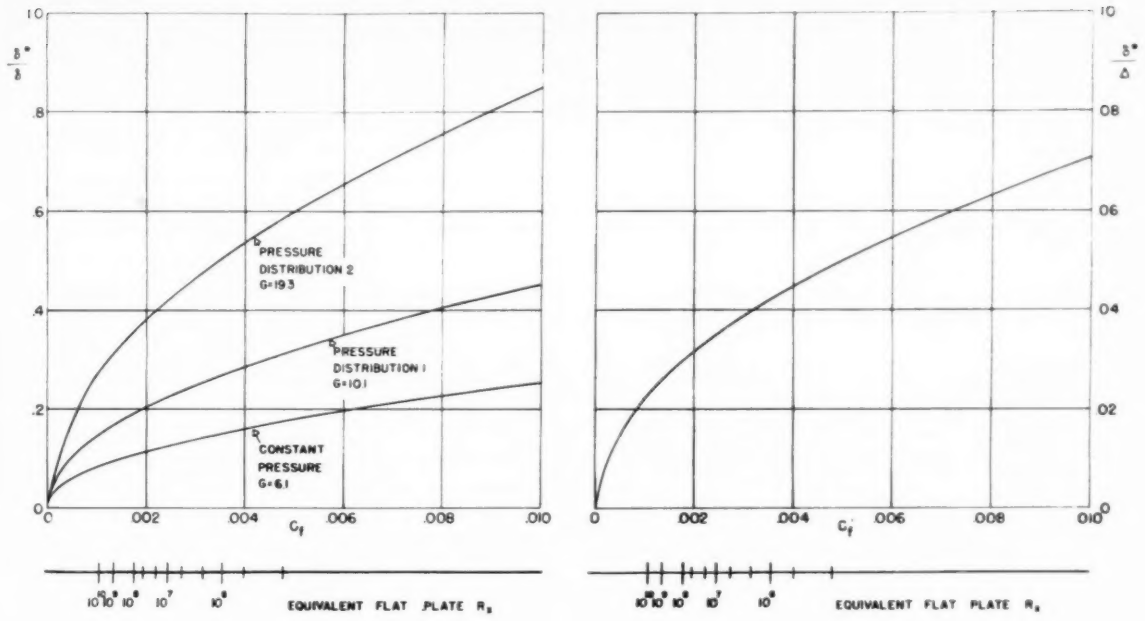

FIG. 13 EFFECT OF C_f ON δ^* FOR EQUILIBRIUM TURBULENT VELOCITY PROFILES

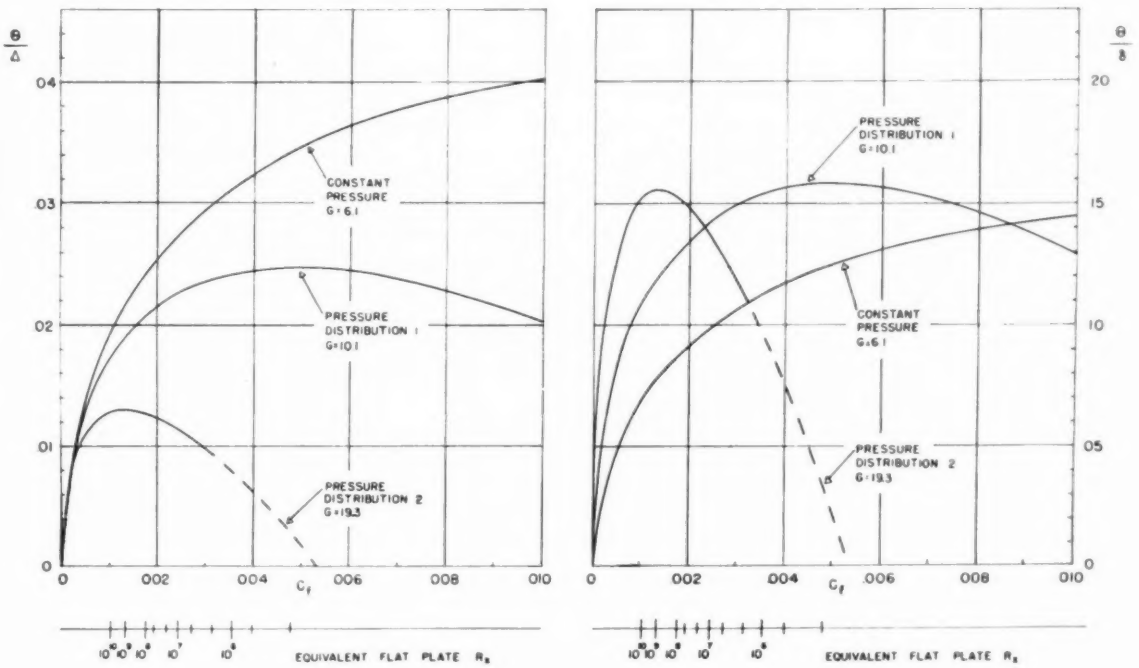

FIG. 14 EFFECT OF C_f ON θ FOR EQUILIBRIUM TURBULENT VELOCITY PROFILES

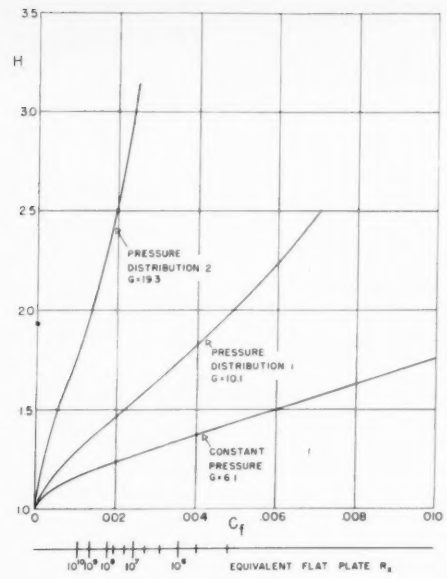

FIG. 15 EFFECT OF C_f ON H FOR EQUILIBRIUM TURBULENT VELOCITY PROFILES

true independently of the value of c_f. However, we have seen that the various thicknesses δ, Δ, θ, and δ^* are not all in constant ratio independent of c_f. Consequently, the choice of thickness to use for δ' is not arbitrary, and we do not know ahead of time which of these thicknesses, if any, is the one that will be appropriate for equilibrium layers. As yet there appears to be no sound theoretical basis for determining which thickness is the proper one. Experimentally this can be obtained fairly simply by establishing equilibrium profiles on both smooth and rough plates, taking care that both have the same values of G, and then finding what choice of δ' will make $(\delta'/\tau_0)\ (dp/dx)$ constant. This has not been done as yet.

Analysis of Properties of the Family of Equilibrium Profiles

The data from the two sets of equilibrium profiles, plus the accumulated data for constant pressure profiles, give us three points in plotting the characteristics of the family of equilibrium profiles. A summary of the values found is given in the following table.

Designation	G	Δ/δ
Constant Pressure	6.1	3.6
First Pressure Distribution	10.1	6.4
Second Pressure Distribution	19.3	12.0

In Fig. 11 the profiles have been replotted in terms of the universal parameters given above. The ratio of Δ to δ has been plotted against G in Fig. 12. We also have sufficient information to show the variation of δ^*, θ, and H with c_f. This has been done in Figs. 13, 14, and 15. For convenience, a scale is also given showing the variations of Reynolds Numbers on a smooth flat plate corresponding to the values of c_f. It is apparent that variations of δ^*, θ, and H with c_f are not negligible, showing that an analysis using them as universal parameters would be unsound.

At this point a word of caution is in order. Thus far we have assumed that the entire profile is represented by the universal function of $(u - U)/u_*$ vs. y/δ. This is not true near the wall. On a smooth wall, the profile departs from this universal law in the vicinity of the laminar sublayer. On a rough wall, the departure occurs at a distance from the wall comparable to the height of the roughness. The integrals for Δ and G for a given distribution of $(u - U)/u_*$ vs. y/δ in the outer portion of the layer will have the values quoted above only as long as the laminar sublayer or the roughness elements are small compared with the thickness of the layer. Fortunately this is usually true. This same effect appears in another way. On the profiles of Fig. 11, zero velocity occurs at an ordinate of $-\sqrt{2/c_f}$. As c_f increases, this point occurs at greater values of y/δ on the profile. If this value of y/δ is not small, then substantial portions of the universal profiles will correspond to negative values of u, whereas actual values of u will be positive corresponding to the conditions in the laminar sublayer or in the roughness elements. This will give false values for θ and H. On Figs. 14 and 15, the solid curves have been terminated where this error is no longer negligible. The dotted portions show this incorrect prediction.

Family of Laminar Boundary-Layer Profiles

Since it is of interest to compare our results for the universal family of turbulent boundary layers in adverse pressure gradients with the corresponding results for laminar profiles, we pause at this point to review the properties of the laminar family. We start by asking if a pressure distribution exists such that all the profiles are similar—i.e., that $u/U = f'(y/\delta)$, where δ is some characteristic thickness of the profile and U and δ are functions of x. For convenience of integration, we start with f' as the derivative of a function (stream function) which can be taken so that $f(0) = 0$. We put $\eta = y/\delta$ and insert the expression for u in the continuity equation,

$$(\partial u/\partial x) + (\partial v/\partial y) = 0$$

Remembering that U and δ are functions of x only, we find

$$\frac{v}{U} = \delta' \int_0^\eta \left[\xi f''(\xi) - \frac{\delta U'}{\delta' U} f'(\xi) \right] d\xi$$

where prime denotes differentiation.

Similarity demands that $\delta U'/\delta' U$ be a constant. We can integrate thus

$$\frac{v}{U} = \delta' \left[\eta f'(\eta) - \left(1 + \frac{\delta U'}{\delta' U} \right) f(\eta) \right]$$

and substitute the result into the boundary-layer equation of motion, giving

$$f'^2 - \left(1 + \frac{\delta' U}{\delta U'}\right) ff'' = 1 + \frac{\nu}{U'\delta^2} f'''$$

This equation was studied by Hartree,[4] who chose the as yet undefined thickness, δ, in such a way that

$$(\nu/U'\delta^2 = 1 + (\delta' U/\delta U')$$

Since $\delta' U/\delta U'$ is constant, $U'\delta^2/\nu$ must be a constant, which Hartree calls β. Falkner and Skan use the constant $m = \beta/(2 - \beta)$. The equation for f becomes

$$\beta(f'^2 - 1) = f''' + ff''$$

The two differential equations for U and δ as functions of x can be integrated explicitly, and, when fitted to the appropriate initial conditions, the solutions are

$$u = Cx^m$$

$$\delta = \sqrt{\frac{2\nu x}{(m+1)U}} = \sqrt{\frac{2\nu}{(m+1)Cx^{m-1}}}$$

Hartree has obtained a family of solutions of the equation for f. Using them, we can compute

$$\delta^* = \int_0^\infty = [1 - (u/U)]\, dy = \delta \int_0^\infty (1 - f')\, d\eta$$

$$\theta = \int_0^\infty u/U[1 - (u/U)]\, dy = \delta \int_0^\infty f'(1 - f')\, d\eta$$

$$c_f = \frac{\tau_0}{\rho(U^2/2)} = \frac{\mu(\partial u/\partial y)_0}{\rho(U^2/2)} = \frac{2\nu}{U\delta} f''(0) = \frac{2f''(0)}{R_{\delta^*}} \int_0^\infty (1 - f')\, d\eta$$

We also see that

$$\frac{\theta}{\tau_0}\frac{dp}{dx} = \frac{\beta}{f'(0)} \int_0^\infty f'(1 - f')d\eta$$

$$\frac{x}{U}\frac{dU}{dx} = -\frac{x}{\rho U^2}\frac{dp}{dx} = m$$

both of which are constant independently of x. We have obtained numerical values for θ/δ, δ^*/δ, H, and $(\theta/\tau_0)\ (dp/dx)$ for the Hartree profiles. These profiles are plotted in Fig. 16 with an accompanying legend of useful information.

Effect of Pressure Gradient on Skin Friction for Laminar and Turbulent Profiles

Most methods of treating turbulent boundary layers in adverse pressure gradients assume that the pressure gradients have no effect on the skin friction. Ludwieg and Tillmann[3] and Schubauer and Klebanoff[5] showed that adverse gradients reduced c_f, but neither group was able to make a quantitative statement about the relationship of c_f and dp/dx.

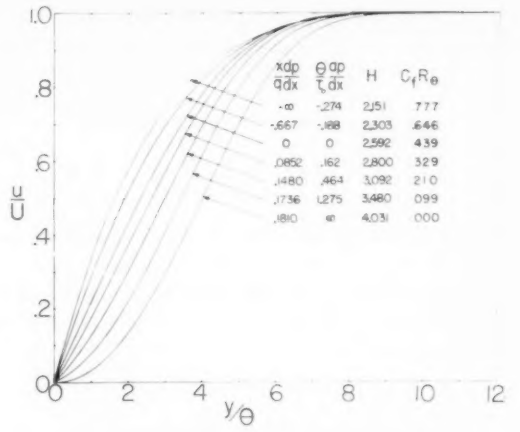

FIG. 16 EQUILIBRIUM LAMINAR VELOCITY PROFILES

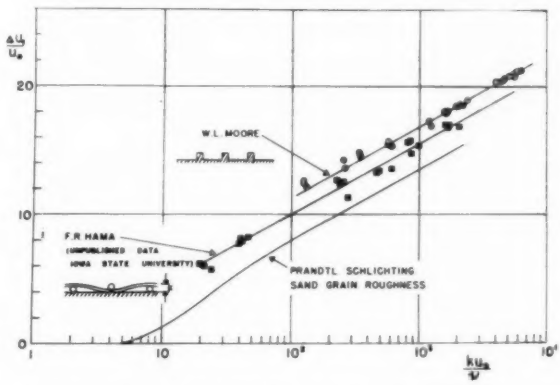

FIG. 17 EFFECT OF ROUGHNESS ON UNIVERSAL TURBULENT VELOCITY PROFILES

Early in the course of the present work it was apparent that pressure gradients had an unexpectedly large effect on skin friction. Even though our first pressure distribution had relatively gentle gradients, the skin-friction coefficients were nearly half of those for constant pressure profiles at the same Reynolds Number.

By combining the results of our present investigation with those of others in the field, we are able to present a relatively complete picture of turbulent skin friction. As mentioned previously, Fig. 4 shows that for smooth plates there is a region outside the laminar sublayer in which the velocity distribution can be represented by the law

$$u/u_* = 5.6 \log_{10} (u_* y/\nu) + 4.9$$

even when pressure gradients are present. Prandtl[6] has shown that, when the wall is rough, the semilogarithmic part of the curve is displaced downward parallel to itself by an amount $\Delta u_1/u_*$, which depends on the roughness Reynolds Number ku_*/ν. In Fig. 17 are

shown experimental data on the relations between these two parameters for the case of sand grain roughness and also for transverse square bars and wire screening laid on a flat surface. It will be noticed that, when u_*k/ν is greater than approximately 100, the asymptotic form is

$$\Delta u/u_* = 5.6 \log (u_*k/\nu) + \text{constant}$$

Since yu_*/ν at the outer edge of the laminar sublayer is approximately 50, we see that, when the roughness is greater than about twice the thickness of the laminar sublayer, the universal law for the turbulent region near the wall becomes

$$u/u_* = 5.6 \log (y/k) + \text{constant}$$

The above results are known to hold for smooth, moderately rough, and extremely rough walls without pressure gradient and for smooth walls with pressure gradients. Dimensional reasoning, which shows that the effects of pressure gradients on conditions near the wall must be small, indicates that the results are also true for rough walls with pressure gradients.

For all these cases, there exists a turbulent region next to the wall for which u/u_* is linearly related to log y. Turning now to our universal plot of $(u - U)/u_*$ vs. y/Δ, we readily see that, for the inner portion of this plot, $(u - U)/u_*$ should be linearly proportional to log y/Δ. Further, the slope of this semilogarithmic curve should be 5.6—i.e., the same as that on the plot of u/u_* vs. log yu_*/ν or log y/k. This is seen to be true in Fig. 18, where the members of the equilibrium family have been plotted on semilogarithmic scales. The existence of this region of overlapping between the two different plots on which data for the inner and outer portions of the layer may be correlated is of great importance. The overlapping can be used to prove *ab initio* that this portion of the layer must be semilogarithmic,[7] and it serves to establish skin-friction laws for turbulent layers.

On one plot, u/u_* is a universal function of yu_*/ν independent of the free-stream velocity or boundary-layer thickness. The function depends on the surface roughness Reynolds Number u_*k/ν.

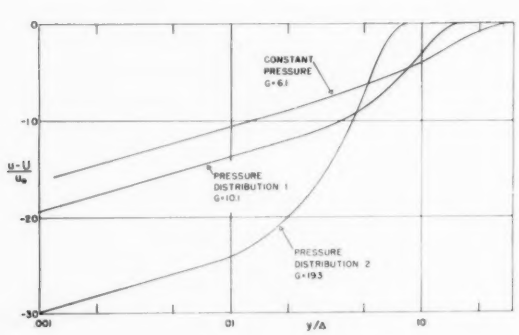

FIG 18 LOGARITHMIC PLOT OF EQUILIBRIUM TURBULENT VELOCITY PROFILES

On the other plot, $(u - U)/u_*$ is a universal function of y/Δ with the function depending on the pressure gradient but being independent of the viscosity (Reynolds Number) or of the roughness. We put

$$u/u_* = g(yu_*/\nu)$$
$$(u - U)/u_* = f(y/\Delta)$$

These two can be rewritten

$$u/u_* = g[(y/\Delta)\cdot(u_*\Delta/\nu)]$$
$$u/u_* = f(y/\Delta) + (U/u_*)$$

Now the experimental data show that there is a common region near the wall where these two quite different relations will simultaneously correlate the velocity profiles. In the overlapping region, both represent the same functional relation between u and y. However, one contains the factor $u_*\Delta/\nu$ as a multiplier of y/Δ inside the function, while the other contains U/u_* as an additive term outside the function. The equivalence of the two equations is maintained even though $u_*\Delta/\nu$ and U/u_* vary through a wide range of values. This implies both that a relation exists between $u_*\Delta/\nu$ and U/u_* and that the functions f and g must be logarithms, since this is the only function for which a multiplicative factor inside the function has the same effect as an additive factor outside the function. This, of course, is in agreement with the experimental data that show that the functions are indeed logarithmic.

The function g can be written

$$u/u_* = 5.6 \log_{10} yu_*/\nu - (\Delta u_1/u_*) + 4.9$$

and the function f can be written

$$(u - U)/u_* = 5.6 \log (y/\Delta) - (\Delta u_2/u_*) + 0.6$$

for those portions of the curves on Fig. 18 that are semilogarithmic. The function $\Delta u_1/u_*$ is the shift in vertical ordinate of the straight line on Fig. 4 when roughness is present. It is a function of the variable ku_*/ν as shown on Fig. 17. The function $\Delta u_2/u_*$ is the corresponding shift of the straight-line portion of the curves on Fig. 18. The shift is measured from the line of the constant pressure profile. It is a function of the pressure gradient, G, or equivalently of the parameter $(\delta'/\tau_0)\ (dp/dx)$.

The relationship between U/u_* and $u_*\Delta/\nu$, mentioned above, can be obtained by subtracting the above equations, which eliminates both u and y; thus,

$$U/u_* = 5.6 \log (u_*\Delta/\nu) - (\Delta u_1/u_*) + (\Delta u_2/u_*) + 4.3$$

or since $u_*/U = \sqrt{c_f/2}$ and $\sqrt{c_f/2}\,\Delta = \delta^*$,

$$\sqrt{\frac{2}{c_f}} = 5.6 \log R_{\delta^*} - \frac{\Delta u_1}{u_*}\left(R_k\sqrt{\frac{c_f}{2}}\right) + \frac{\Delta u_2}{u_*}(G) + 4.3$$

This equation is of remarkable significance. It is the universal skin-friction law for all turbulent boundary layers having equilibrium pressure gradients. It includes the effects of Reynolds Number, pressure gradient, and surface roughness. It is probably the most general "universal" law that exists, because other pressure distributions will have an arbitrariness of definition that will make the appelation "universal" inappropriate.

This law contains the four parameters c_f, R_{δ_*}, G, and R_k. R_{δ_*} may be replaced by R_θ and H by G from the following formulas:

$$R_\theta = (1 - G\sqrt{c_f/2})R_{\delta_*}$$

$$H = 1/(1 - G\sqrt{c_f/2})$$

The existence of four parameters makes the skin-friction law difficult to plot for practical use. In Fig. 19, a useful set of curves is given for the case of smooth plates where $k = 0$. Lines are shown for both G constant and H constant. Although H is frequently more convenient to use, a given equilibrium boundary layer will move along a G curve in its development. Although it is cumbersome to plot the four-parameter skin-friction law, it can fortunately be put in a form for ready engineering applications. If we introduce two factors F_1 and F_2, the skin-friction law can be written

$$\sqrt{2/C_f} = 5.6 \log [R_{\delta_*} F_2/F_1] + 4.3$$

When F_1 and F_2 are unity, this is the well-known skin-friction law for smooth plates with constant pressure, which has been plotted in Fig. 20. The factors

$$F_1 = 10^{\Delta u_1/5.6u_*}, \qquad F_2 = 10^{\Delta u_2/5.6u_*}$$

have been plotted in Figs. 21 and 22, using the data of the present report for pressure gradients and the Prandtl-Schlichting data for sand grain roughness. In use, after F_1 and F_2 have been obtained from Figs. 21 and 22, a fictitious Reynolds Number $R_{\delta_*} F_2/F_1$ is computed. This is used in place of the actual Reynolds Number, R_{δ_*}, to find c_f in Fig. 20.

Referring back to the analysis for laminar profiles, the formula

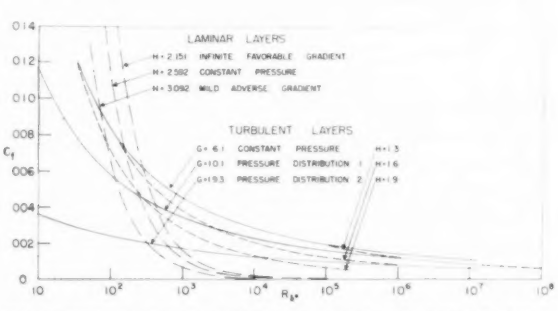
LAMINAR LAYERS
H = 2.151 INFINITE FAVORABLE GRADIENT
H = 2.592 CONSTANT PRESSURE
H = 3.092 MILD ADVERSE GRADIENT
TURBULENT LAYERS
G = 6.1 CONSTANT PRESSURE H = 1.3
G = 10.1 PRESSURE DISTRIBUTION 1 H = 1.6
G = 19.3 PRESSURE DISTRIBUTION 2 H = 1.9
c_f
R_{δ_*}

FIG. 19 EFFECT OF PRESSURE GRADIENTS ON LAMINAR AND TURBULENT SKIN FRICTION FOR SMOOTH PLATES

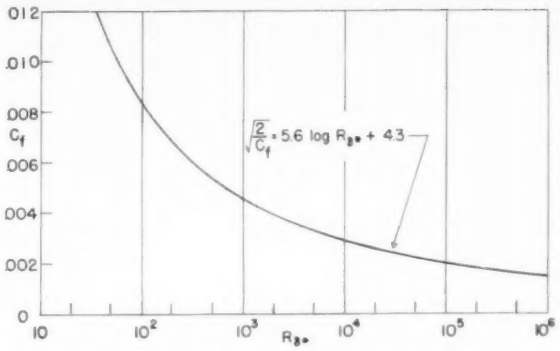

FIG. 20 CONVENTIONAL TURBULENT SKIN FRICTION LAW FOR SMOOTH PLATES WITH CONSTANT PRESSURE

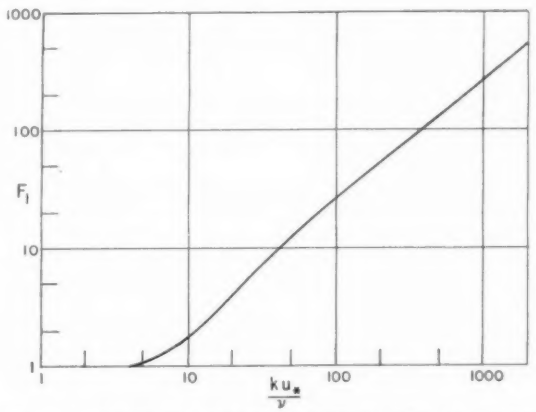

FIG. 21 REYNOLDS' NUMBER FACTOR FOR THE EFFECT OF SAND PAPER ROUGHNESS ON SKIN FRICTION

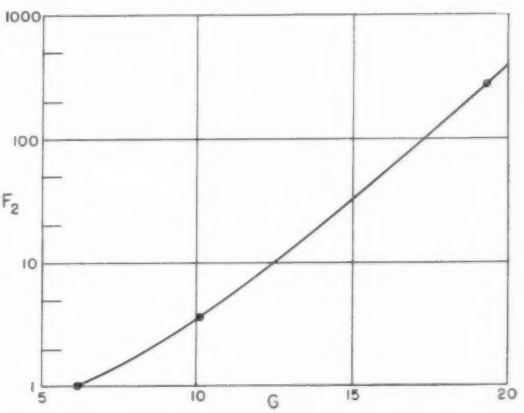

FIG. 22 REYNOLDS' NUMBER FACTOR FOR THE EFFECT OF PRESSURE GRADIENT ON SKIN FRICTION

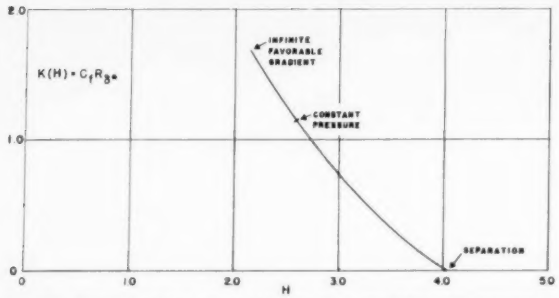

FIG. 23 EFFECT OF H ON LAMINAR SKIN FRICTION COEFFICIENTS

$$c_f = \frac{2f''(0)}{R_{\delta^*}} \int_0^\infty (1 - f')\, d\eta = \frac{K(H)}{R_{\delta^*}}$$

was obtained. The factor $K(H)$ has been evaluated and is plotted in Fig. 23. Laminar skin-friction coefficients have been plotted in Fig. 19, along with the data for turbulent layers. It will be noticed that the effects of pressure gradient on skin friction are large, both for laminar and turbulent layers. Gradients considerably smaller than those required to produce separation are effective in reducing the surface friction. It is felt that this reduction is of great technical importance.

Comparison of Present and Past Results

It is of interest to give a comparison of the results of the present paper with those of previous authors. Since an understanding of turbulent processes under the combined influences of shear and pressure gradients does not exist, analyses have necessarily used the momentum integral equation,

$$\frac{d\theta}{dx} = (c_f/2) + \frac{(H + 2)}{2} \frac{\theta}{q} \frac{dp}{dx}$$

as a starting point. Since the momentum equation is not complete in itself, it is necessary to make assumptions about how the terms in the equation are to be obtained. These assumptions may generally be cataloged as follows:

(1) It is assumed that only a single family of possible turbulent profiles exists. This permits the necessary relationship between δ^* and θ to be determined. Different authors have used different parameters to characterize the various members of the family of profiles.

(2) It is necessary to introduce an auxiliary equation to determine the successive values of the family parameter. This auxiliary equation is invariably based on empirical correlations of collections of experimental data.

(3) A law for the variation of skin friction must be assumed. Most authors have assumed a power-law variation with Reynolds Number, neglecting any influence of pressure gradient on skin friction.

In making the comparison we shall follow the above three points. We shall deal principally with the method of analysis proposed by von Doenhoff and Tetervin,[8] since this method is one of the better known in this country and is generally typical of the rest.

Von Doenhoff uses a universal family of profiles in which u/U is plotted against y/θ. The family parameter is H. Since all the quantities entering into this formulation may be obtained directly from a velocity profile, it is an easy matter to check to see if any given profile fits the family. This has been done for typical profiles from our first and second pressure distributions, and the results have been plotted on Fig. 24. The great and consistent difference between the two sets of profiles, which should agree, was quite unexpected. It had been felt that this single-parameter family assumption was one of the relatively reliable points of prior analyses. The difference shown is sufficient to cast serious doubt upon this assumption for general boundary-layer behavior. The difference is probably caused by the fact that in our profiles H was nearly constant whereas, in von Doenhoff's profiles, H was increasing fairly rapidly. Apparently this has an effect on the shape of the profile.

Von Doenhoff uses, as an auxiliary equation,

$$\theta \frac{dH}{dx} = e^{4.68(H-2.975)} \left[2 \frac{\theta}{\tau_0} \frac{dp}{dx} - 2.035\,(H - 1.286) \right]$$

In analyzing his data, he assumes that the base profile for zero pressure gradient is a one-seventh power profile for which $H = 1.286$. As explained earlier, this is not in agreement with our knowledge of constant pressure profiles as shown in Figs. 2 and 3. Actually, H varies with c_f even for constant pressure, as shown in Fig. 15. If the range of Reynolds Number is small and only smooth plates are considered, the variation of H with c_f is not large, and it can be argued that neglecting the variation is not serious. Consistently with this, one may follow von Doenhoff in viewing any H = constant set of profiles as analogous to what we have been calling equilibrium profiles. The reasoning here is analogous to that given later in connection with Fig. 26. For H = constant, von Doenhoff's equation becomes

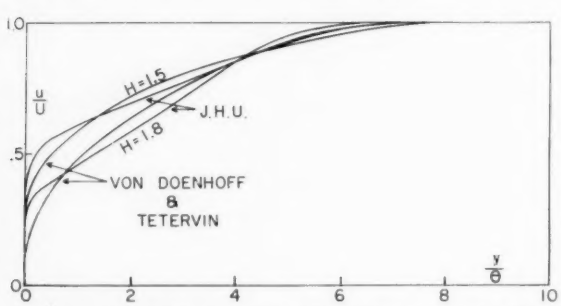

FIG. 24 COMPARISON OF EQUILIBRIUM PROFILES AND THE VON DOENHOFF - TETERVIN ONE PARAMETER FAMILY OF PROFILES

$$(\theta/\tau_0)\ (dp/dx) - 1.018\ (H - 1.286)$$

This can be compared directly with our data, which have been plotted as a band on Fig. 25 along with von Doenhoff's line. The results are quite discrepant. The only agreement is for $(\theta/\tau_0)\ (dp/dx) = 0$—i.e., for constant pressure profiles where they must agree reasonably well. After that, the trends are quite different. Von Doenhoff's equation predicts a small value of $(\theta/\tau_0)\ (dp/dx)$ at separation, whereas in actuality it must be infinite because τ_0 goes to zero. His linear relation misses completely the bending over of the experimental data. As will be explained in more detail in connection with Fig. 26, the reason the present data are plotted as a band is because the parameters H and $(\theta/\tau_0)\ (dp/dx)$ are not consistent with the universal parameters we find appropriate for turbulent layers. The scatter is caused by the variation of H and θ with c_f.

For skin friction, von Doenhoff uses a power-law variation with Reynolds Number and assumes that there is no effect of pressure gradient. As has been seen, the present results show that the pressure gradient effect is large.

In summary, it is seen that the experimental results we have obtained show little or no agreement with the predictions of the von Doenhoff method. The same is true of other methods with which the author is familiar. Since these methods do not agree with the relatively simple and well-defined experimental results we have obtained, one can conclude that the field is still wide open for the advent of a reliable method of predicting the behavior of turbulent layers under the influence of pressure gradients.

Downstream Stability

It will be recalled that difficulty was experienced in obtaining constant values of G for the steeper set of pressure gradients. Throughout most of turbulent boundary-layer work there exists a fundamental proposition that is seldom enunciated explicitly but which is generally believed to be true. It states that a turbulent boundary layer has a downstream stability such that in a given environment the effect of any small perturbation, such as local changes in roughness or pressure distribution, will die out downstream, leaving no trace other than a possible slight thickening of the layer. Thus, the effect of a crack or a wave in the wall will have no significant effects on the structure of the boundary layer far downstream. Klebanoff and Diehl[9] found, indeed, that constant pressure layers can be violently disturbed and yet return to a universal state downstream, several times thicker but otherwise none the worse for their rough treatment. Similarly, for our experiments with the flatter pressure distribution, the layer possessed this downstream stability, permitting corrections to be made at one point without unduly disturbing downstream points.

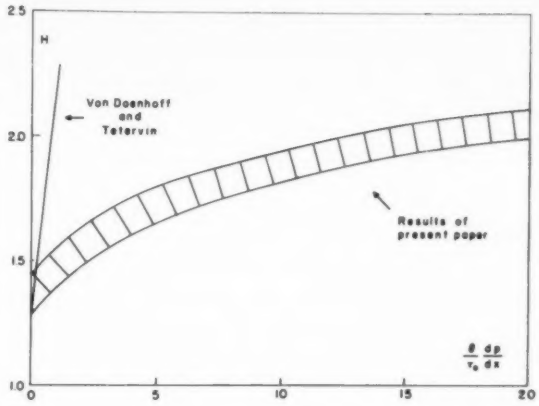

FIG. 25 COMPARISON OF PRESENT AND PREVIOUS RESULTS FOR H versus $\frac{\theta}{\tau_0}\frac{dp}{dx}$ FOR EQUILIBRIUM TURBULENT LAYERS

When work was first started on the steeper gradients, it was not realized that the situation might be different. Corrections were made simultaneously at several points, and it quickly became apparent that something was wrong. It will be seen that downstream stability is necessary to ensure that such simultaneous changes will lead to a converging result. Since we were sufficiently far from separation that upstream influences were not present, the chaotic response that occurred when this procedure was followed indicated that some kind of downstream instability might be present. The following analysis shows why this was so.

Intuitively, one believes that $(\theta/\tau_0)\ (dp/dx)$ should be a reasonably well-behaved dynamic parameter. For constant pressure profiles it is zero. For separating profiles it is ∞, because τ_0 vanishes at separation. In between, it should provide a reasonably reliable indication of the state of the layer. Particularly for equilibrium profiles, it should monotonically increase as one proceeds from constant pressure profiles to separating profiles. As explained previously, its value for turbulent profiles will be somewhat dependent on c_f, but this will not affect the present analysis. The

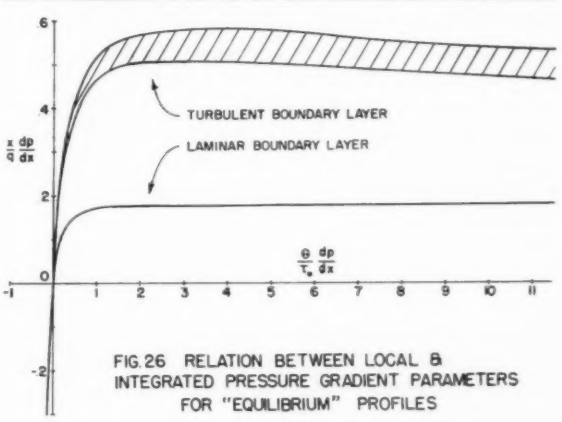

FIG. 26 RELATION BETWEEN LOCAL & INTEGRATED PRESSURE GRADIENT PARAMETERS FOR "EQUILIBRIUM" PROFILES

difficulty in its use is that when one is setting up a pressure distribution, either for a boundary-layer test or for the more general problem of the design of fluid mechanical machinery, one deals not with θ and τ_0 but with x and p or q. Correspondingly, one would like to use, instead of $(\theta/\tau_0)\ (dp/dx)$, dimensionless parameters such as $(x/q)\ (dp/dx)$ or $(x/U)\ (dU/dx)$. For specific families such as the equilibrium profiles, we can ask for the relationship between the two types of parameters.

To illustrate, consider the equilibrium laminar profiles. We have seen previously that for these profiles $(x/q)\ (dp/dx)$ and $(\theta/\tau_0)\ (dp/dx)$ are both constant throughout the length of the layer. Consequently, for equilibrium layers there will be an exact relation between these parameters. This is shown in Fig. 26. Near zero, $(x/q)\ (dp/dx)$ increases proportionately to $(\theta/\tau_0)\ (dp/dx)$; however, when $(\theta/\tau_0)\ (dp/dx)$ is greater than 1, $(x/q)\ (dp/dx)$ is nearly constant at its asymptotic value of 0.181. This means that, if one were to attempt to obtain profiles having a value of $(\theta/\tau_0)\ (dp/dx)$ greater than approximately unity, the pressure gradient would have to be set with an almost impossible precision to avoid getting a different $(\theta/\tau_0)\ (dp/dx)$. Stated differently, all of the members of the equilibrium family of laminar layers with rising gradients are obtained with practically the same pressure distribution, p vs. x, except those for which the gradients are relatively mild. Let us see what the effect of this condition is on downstream stability. Suppose that an equilibrium laminar layer is disturbed so that in one region θ, say, is increased, $(\theta/\tau_0)\ (dp/dx)$ will be increased, but $(x/q)\ (dp/dx)$ will be unchanged (we suppose the boundary layer has no effect on the outer flow). Now if the boundary layer originally corresponded to a point near the origin of the curve of Fig. 26, the disturbance will shift the point to the right of the curve. Any local irregularities in the profile will be ironed out by viscosity. In addition, there will be a progressive change in the gross characteristics of the profiles because they no longer lie on the equilibrium curve of Fig. 26. Intuition and experience say that the profiles will asymptotically return to a point on this curve.

Now suppose the original layer corresponded to a point on the flat part of the curve of Fig. 27. Again the disturbed point moves to the right, but there will be no tendency to return because it is still on the equilibrium curve. Such a layer would not possess downstream stability.

Let us see what happens in the case of turbulent profiles. As shown earlier, our family of turbulent profiles is not expressible in terms of θ, which is related to the universal length parameter Δ through the skin-friction coefficient c_f. However, since the Reynolds Number effect is not great for turbulent profiles, we may establish upper and lower limits for the relation between $(x/q)\ (dp/dx)$ and $(\theta/\tau_0)\ (dp/dx)$ if we are willing to restrict the range of Reynolds Numbers. We have

$$\frac{x}{q}\frac{dp}{dx} \equiv \frac{(\theta/\tau_0)\ (dp/dx)}{\theta/xc_f}$$

The momentum equation,

$$\frac{d\theta}{dx} = \frac{c_f}{2} + \frac{(H+2)}{2}\frac{\theta}{q}\frac{dp}{dx} = c_f\left[1 + (H+2)\frac{\theta}{\tau_0}\frac{dp}{dx}\right]$$

with appropriately averaged c_f (denoted $\bar{c}_f$) can be integrated to give

$$\frac{\theta}{x\bar{c}_f} = \frac{1}{2}\left[1 + (H+2)\frac{\theta}{\tau_0}\frac{dp}{dx}\right]$$

Substituting this in the equation above, we have

$$\frac{x}{q}\frac{dp}{dx} = \frac{2(\theta/\tau_0)\ (dp/dx)}{1 + (H+2)\ (\theta/\tau_0)\ (dp/dx)}$$

This equation with upper and lower limits on the variation of c_f (and on H, which also varies with C_f) has been plotted on Fig. 26, using values obtained from our experimental profiles. This band has a number of interesting features. It shows that turbulent boundary layers can withstand about three times the nondimensional pressure gradient $(x/q)\ (dp/dx)$ that laminar profiles can. The greatest value for this parameter for equilibrium profiles is about 0.58. This means that a flow with

$$\frac{x}{q}\frac{dp}{dx} = -\frac{2x}{U}\frac{dU}{dx} = 0.58$$

or $U = \text{const.}\ x^{-0.29}$ can be decelerated to zero velocity without separation, but this is the maximum rate of deceleration which can be accomplished without eventual separation.

In Fig. 26, it is also seen that the turbulent boundary layer behaves similarly to the laminar boundary layer in that $(x/q)\ (dp/dx)$ is proportional to $(\theta/\tau_0)\ (dp/dx)$ for small pressure gradients, but the curve quickly levels off for values of $(\theta/\tau_0)\ (dp/dx)$ between 1 and 5. Above this point, a surprising thing happens. The dimensionless pressure gradient $(x/q)\ (dp/dx)$ actually decreases for profiles closer to separation. The peak values of $(x/q)\ (dp/dx)$ lie between 0.5 and 0.58. As $(\theta/\tau_0)\ (dp/dx)$ approaches ∞, corresponding to separation, $(x/q)\ (dp/dx)$ approaches $2/(H+2)$. At separation, however, H lies between 2.2 and 2.6.[8] The corresponding values of $(x/q)\ (dp/dx)$ at separation are 0.43 and 0.48, showing a definite decrease from the peak values. At first sight this behavior seems to be entirely incorrect, for it implies that the pressure distributions producing near-separating profiles are definitely flatter than those producing profiles well removed from separation. Further, since the curve has a maximum, this says that there are cases where two quite different boundary layers will be produced by exactly the same pressure distribution. Both will be shape-preserving, but one will have a shape only slightly different from the familiar constant

pressure profile while the other will be very near separation. A typical example is $(x/q)\ (dp/dx) = 0.48$, which can be integrated to give $U = \text{const}\ x^{-0.24}$. In such a velocity distribution, Fig. 26 shows that an equilibrium boundary layer can exist for which $(\theta/\tau_0)\ (dp/dx) = 1.2$ with $H = 1.3$, a value very near that for constant pressure profiles. In exactly this same velocity distribution, a second layer can exist for which $(\theta/\tau_0)\ (dp/dx) = 15.0$ and $H = 2.1$, which is near the separation limit of $2.2 < H < 2.6$. This shows that two layers in the same pressure distribution can be at opposite extremes of the family for adverse pressure gradients.

This unexpected behavior can perhaps best be explained by examining the identity

$$\frac{x}{q}\frac{dp}{dx} \equiv \frac{(\theta/\tau_0)\ (dp/dx)}{\theta/xc_f}$$

When the pressure gradient is small, the rate of growth of θ with x is governed primarily by c_f, and if x is measured from the apparent origin of the boundary layer, θ/xc_f will be nearly constant. For this condition, the formula shows that $(x/q)\ (dp/dx)$ will be nearly proportional to $(\theta/\tau_0)\ (dp/dx)$, as one would intuitively think it should. However, as the pressure gradient increases, the pressure gradient quickly begins to dominate the small skin-friction term in the momentum equation. Under this condition, θ/xc_f is more nearly proportional to $[(H + 2)/2]\ (\theta/\tau_0)\ (dp/dx)$, and $(x/q)\ (dp/dx)$ becomes nearly equal to $2/(H + 2)$. If H were constant, $(x/q)\ (dp/dx)$ would be constant. However, H increases with $(\theta/\tau_0)\ (dp/dx)$, causing $(x/q)\ (dp/dx)$ to *decrease* for large $(\theta/\tau_0)\ (dp/dx)$, explaining the observed shape of the curve. The above discussion shows that, for values of $(\theta/\tau_0)\ (dp/dx)$ greater than 1 to 1.5, both laminar and turbulent layers will have little downstream stability and turbulent layers can show instability.

Our experience in obtaining our second set of equilibrium profiles confirms the above analysis. It will be remembered that these profiles were closer to separation. The $(\theta/\tau_0)\ (dp/dx)$ was approximately 5. Whenever a change in conditions was made, the effect of the change was felt with increasing amplitude downstream. However, the rate of divergence was not unmanagably large. Once the phenomenon was understood, the method of obtaining equilibrium profiles was changed from a process of simply correcting the pressure distribution to a process of "steering" the boundary layer along a G = constant course. Experimentally, the experience greatly resembled the process of driving a mildly unstable automobile that always wants to wander off the road and must be brought back. Once a satisfactory equilibrium layer had been obtained, it showed little tendency to wander off with time. The downstream instability is an instability in x and not in t.

Difficulties Obtaining Two-Dimensional Flow

During the course of our investigation, considerable difficulty was experienced obtaining two-dimensional flow. It is felt that these results have considerable influence on the question raised recently by several authors about the proper form for the momentum equation.

Wieghardt[10] and Mangler[11] conducted experiments on turbulent boundary layers in rising pressure gradients. They used the two-dimensional momentum equation to deduce the values of c_f. Their results indicate that c_f, instead of decreasing as separation was approached, actually increases. Schubauer[3] and Ludwieg,[2] using direct measurements of shear, found that c_f decreases in rising pressures. However, when the two-dimensional momentum equation is used to obtain c_f from Schubauer's data, rising values of c_f are obtained. Ludwieg has suggested that lack of two-dimensionality is the cause for the discrepancy. On the other hand, Newman,[12] Goldschmied,[13] and Bidwell[14] suggest that the discrepancy is caused by the momentum equation being in error through the omission of terms containing the turbulent fluctuations.

During the course of the present experiments, it was found that agreement with the two-dimensional momentum equation was obtained when the pressure was constant, but when the pressure was rising, definite disagreement was obtained. For our second rising pressure distribution, with near-separating profiles, the disagreement was very great. The skin-friction term was negligible compared with the $d\theta/dx$ and $[(H + 2)/2]\ (\theta/q)\ (dp/dx)$ terms. Further, the $[(H + 2)/2]\ (\theta/q)\ (dp/dx)$ term was 50 to 100 per cent greater than the $d\theta/dx$ term. If c_f had been computed from the momentum equation, a large negative value would have been obtained.

An attempt was made to obtain agreement with the momentum equation by taking into account the fluctuation terms as suggested by Newman, Goldschmied, and Bidwell. However, this procedure led to corrections far too small to explain the observed discrepancies. In the case of equilibrium profiles, with similar conditions existing at each station, the fluctuation terms in the momentum equation are either zero or very small. The reason for this is that these terms usually occur as an x derivative of an integral of the fluctuations. With similarity in conditions, these integrals are substantially constant.

An investigation was made to see if the discrepancy was caused by nonlinearity in the instrumentation, which would give incorrect mean velocity measurements in the presence of turbulent fluctuations. Mean velocities were measured by flattened hypodermic probes and by hot-wires. Turbulence measurements were also made by hot-wires. The hypodermic probes were calibrated against angles of attack and yaw. Knowing the levels of the u fluctuations and estimating

the levels of the v and w fluctuations, estimates were made of the effect of the turbulence on the mean velocity readings of both the hypodermic probes and the hot-wires. Reasonable agreement was obtained except near the wall where the turbulence levels were relatively large. It was found that the corrections had insufficient effect on the integrated values of θ and δ^* to explain the momentum discrepancy.

From the above it was concluded that neither the additional terms proposed by Newman, Goldschmied, and Bidwell nor instrumentation errors could account for observed disagreement with the momentum equation. The evidence pointed to the possibility that the flow was not two-dimensional. Apparently, the flow was spreading laterally in such a way as to tend to thin out the boundary layer. If w is the local component of lateral velocity parallel to the plate (w is assumed constant with y), then a term $(\delta^*/U)\ (\partial w/\partial z)$ must be included in the momentum equation. Calculations showed that the lateral flow required to explain the discrepancy appearing in the momentum equation was small. At the sides of the tunnel, a divergence angle of about $1^1/_2{}^\circ$ would have been sufficient. Attempts were made with yawmeters to measure the lateral flow, but these were unsuccessful because the lateral turbulent fluctuations were so large (greater than $\pm$ 10° in flow inclination) that they masked any small shift in mean flow direction.

It will be remembered that the tunnel is constructed so that the boundary layers on the side walls are removed. It was conjectured that this removal might be causing the flow to diverge laterally. The slots were taped up, and the discrepancy was reduced but not eliminated. This was surprising because now the wall boundary layers should have caused the flow on the test floor to converge and reverse the discrepancy. Next, it was noticed that a crack, about 1/32 to 1/16 in. wide, existed where the walls joined the floor. This was taped up, and the discrepancy was again improved but not eliminated or reversed. At one section of the tunnel, this last change caused a previously well-behaved boundary layer on the floor to separate. This indicates that these fine cracks had been removing sufficient low-velocity air to prevent separation. An analysis of this situation showed that, when a leak such as these cracks exists, there is a strong tendency for the swiftly moving central stream to travel straight down the tunnel but for the slowly moving air next to the floor and walls to move laterally toward the leak.

Next we considered the possibility that the boundary layer air on the floor was moving laterally to the walls and then up through the wall boundary layers to the outlet flaps on the top of the tunnel, which were used to control the pressure distribution. Measurements of the wall boundary layers indicated they were not growing, even though the wall slots were closed. This strengthened our belief that low-velocity air was moving through the boundary layers to the outlet flaps. To prevent this movement, the ends of the outlet flap openings next to the walls were closed. This was finally sufficient to reverse the discrepancy. Once the discrepancy was under control, it was an easy matter to adjust conditions so that the two-dimensional momentum equation was satisfied.

After working to cure this discrepancy as long as we did, we came to have a great respect for the ease with which air can move laterally in boundary layers subjected to adverse pressures gradients. None of this trouble appeared when the pressure was constant. After having had this experience, it is easy to believe that the results of Mangler, Wieghardt, and Schubauer should be interpreted as indicating that their flows were not two-dimensional.

References

[1] Falkner, V. M., and Skan, S. W., *Some Approximate Solutions of the Boundary Layer Equations*, A.R.C. Reports & Memoranda No. 1314, 1930.

[2] Moore, W. L., *An Experimental Investigation of the Boundary-Layer Development Along a Rough Surface*, Ph.D. Dissertation, State University of Iowa, 1951.

[3] Ludwieg, H., and Tillmann, W., *Investigations of the Wall-Shearing Stress in Turbulent Boundary Layers*, NACA TM No. 1285, 1950.

[4] Hartree, D. R., *On an Equation Occurring in Falkner and Skan's Approximate, Treatment of the Equation of the Boundary Layer*, Proc. Camb. Phil. Soc., Vol. 33 pp. 223–239, 1937.

[5] Schubauer, G. B., and Klebanoff, P. S., *Investigation of Separation of the Turbulent Boundary Layer*, NACA TN No. 2133, 1950.

[6] Durand, W. F., *Aerodynamic Theory*, Vol. III, Division G (L. Prandtl, "The Mechanics of Viscous Fluids").

[7] Millikan, C. B., *A Critical Discussion of Turbulent Flows in Channels and Circular Tubes*, Proceedings of the Fifth International Congress for Applied Mechanics, 1938.

[8] von Doenhoff, A. E., and Tetervin, N., *Determination of General Relations for the Behavior of Turbulent Boundary Layers*, NACA TR No. 772, 1943.

[9] Klebanoff, P. S., and Diehl, F. W., *Some Features of Artificially Thickened Fully Developed Turbulent Boundary Layers with Zero Pressure Gradient*, NACA TN No. 2475, 1951.

[10] Wieghardt, K., *Uber die Wandschubspannung in Turbulenten Reibungsschichten bei Veranderlichem Aussendruck*, ZWB UM 6603, 1943.

[11] Mangler, W., *Das Verhalten der Wandschubspannung in Turbutenten Reibungsschichten mit Druckanstieg*, ZWB UM 3052, 1943.

[12] Newman, B. G., *Skin Friction in a Retarded Turbulent Boundary-Layer Near Separation*, Report A. 73, Department of Supply Aeronautical Research Laboratories, Australia, 1950.

[13] Goldschmied, F. R., *Skin Friction of Incompressible Turbulent Boundary Layers Under Adverse Pressure Gradients*, NACA TN No. 2431, 1951.

[14] Bidwell, J. M., *Application of the von Kármán Momentum Theorem to Turbulent Boundary Layers*, NACA TN No. 2571, 1951.

[15] Laufer, J., *Investigation of Turbulent Flow in a Two-Dimensional Channel*, NACA TN No. 2123, 1950.

General Instability of Simply Supported Rectangular Plates

J. R. M. RADOK*

Aeronautical Research Laboratories, Melbourne, Australia

SUMMARY

The problem of lateral bending of thin plates, stiffened by line reinforcements, is reduced to the limiting case of uniform plates under triangular loading, distributed over a strip, when the width of the strip tends to zero. Using the basic solutions, arising from this limiting process, the characteristic equations for the compressive buckling loads of rectangular plates, reinforced by stringers, by ribs, by distributed stringers, and by discrete ribs, are deduced. In all these cases closed expressions in terms of elementary functions are obtained for arbitrary spacing of the reinforcing members, and it is shown that the case of discrete stringers and ribs cannot be solved in a similarly simple manner.

NOTATION

a, b	= dimensions of plate
h	= thickness of plate
k	= $1 + (12I_x/h^3)(1 - \nu^2)$
q	= lateral loading of plate
s_m, r_n	= arbitrary coefficients for stringer and rib loading functions
w	= lateral deflection of plate
x, y	= coordinates
x_i, y_j	= positions of ribs or stringers
A	= area of stringer
B	= flexural stiffness of reinforcing member
D	= flexural rigidity of plate
I_x	= second moment of area of distributed stringer
M_x, M_{xy}, M_y	= moment resultants
N_x	= normal compressive force per unit length of plate edge
β	= a/b
γ	= B/bD
δ_{ij}	= Kronecker's delta—i.e., $\delta_{ij} = \begin{cases} 1, i = j \\ 0, i \neq j \end{cases}$
δ	= A/bh
ν	= Poisson's ratio
$\Delta[\ ]$	= discontinuity of expression in brackets

(1) INTRODUCTION

THE PROBLEM OF GENERAL INSTABILITY of rectangular plates with reinforcing members parallel to their edges was first investigated by Timoshenko in 1913. This work is reproduced in the same author's book on *Elastic Stability*.[1] Since then several other authors have dealt with this problem, among whom mention should be made of Cox and his coauthors[2–4] in England, Seide and his coauthors[9, 10] in America, and of Lokshin[8] in Russia, whose papers were not accessible to the author of this report.

Received August 14, 1953.

* Senior Scientific Officer, Structures & Materials Division.

In the references quoted above, results have been deduced by means of the energy method. This method is known to lead always to infinite systems of equations, and in the case of reference 1 conclusions with regard to the buckling stresses are deduced by considering progressive approximations, obtained by neglecting all but the first few unknowns of these equations. On the other hand, it is shown in references 3 and 4 that the variables in these equations may be rearranged into infinite series that are easily summed and that in this way the infinite system may be reduced to a finite one involving new variables. A similar approach has also been adopted in references 9 and 10.

The method of the present report is equivalent to that applied in reference 5 to the problem of general instability of circular cylinders. It avoids the indirect approach of the energy method and leads immediately to a determinant of order equal to the number of reinforcing members parallel to one of the sides of the plate. It also shows that the case of a plate with stringers, as well as ribs, cannot be reduced to a closed expression. This last fact was first suggested in reference 4 and also in reference 7, which partly deals with the buckling problem of plates clamped along all four edges; it is easily shown that this latter problem is equivalent to the former.

The present approach deduces the characteristic equations directly from the equilibrium equation for a plate in compression. It will be seen below that in the cases of ribs or stringers it leads directly to the buckling equations of references 3 and 4. Apart from these cases, a detailed discussion is given of the case of stringers and ribs and of the case of distributed stringers and discrete ribs which is of importance for aircraft construction when the stringer spacing is often so close that each buckling wave comprises several stringers.

(1.1) Discussion and Interpretation of the Method of Solution

Before stating the basic assumptions, a short physical interpretation of the mathematical procedure will greatly assist the understanding of this report and of the significance of the assumptions made (cf. also reference 5).

In order to ensure the compatibility of displacements and stresses in a plate reinforced, for example, by stringers, certain relations must be satisfied between the shear stresses at adjacent edges of neighboring

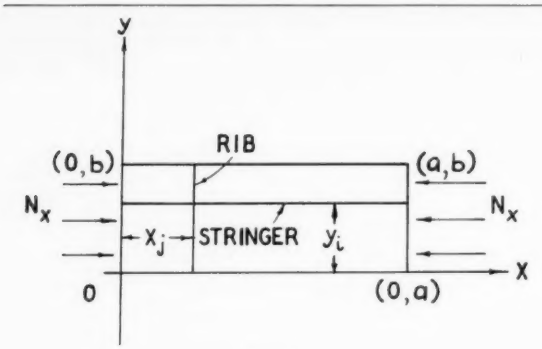

FIG. 1

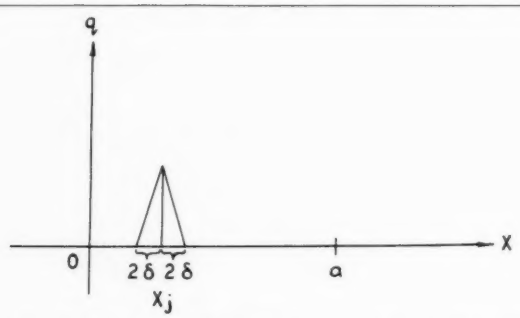

FIG. 2. Triangular load distribution over a strip, parallel to the 0y axis.

panels, or, in other words, these stress resultants undergo discontinuous changes at the stringers. As the equilibrium equation to be used here represents the condition of lateral equilibrium of a plate element, the stringers, if idealized into lines, must be loci of infinite pressures. This was the basic idea of the method of solution of reference 5. Accordingly, the homogeneous differential equation

$$\nabla^4 w + (N_x/D)\,(\partial^2 w/\partial x^2) = 0 \qquad (1.1.1)$$

which is relevant for the case of a simple plate without lateral loads, would have to be replaced by the nonhomogeneous equation

$$\nabla^4 w + (N_x/D)\,(\partial^2 w/\partial x^2) = q/D \qquad (1.1.2)$$

where q is infinite along the lines of attachment of the stringers while it is zero elsewhere.

However, the approach of reference 5 suffers still from the disadvantage that it is not analytically rigorous. In fact, the differential equations of that report, as well as Eq. (1.1.1), are based on the assumption that the displacements have continuous derivatives up to and including the fourth order. For this reason, the use of a conditionally convergent series for q which is divergent at the reinforcement is not strictly justified. In the present report this formal objection has been overcome by means of a limiting process that is applied to the solutions corresponding to local lateral loading of finite magnitude.

The above loading q is thus introduced by means of a suitably chosen Fourier series, which is zero everywhere except along a strip surrounding the stringer where it represents a finite triangular distribution of pressure. (Fig. 2.) Eq. (1.1.2) may then be solved by substituting for w a Fourier series with unknown coefficients, the values of which can be determined in terms of the coefficients of the earlier series. In this way one obtains the solutions of Section (2.2).

In Section (2.3) the above-mentioned limiting process is applied to the solutions of Section (2.2), which leads to the basic solutions to be used in Section (3) for the solution of the buckling problems. These basic solutions may be interpreted as sources of shear stress. So far, solutions of this type have only been used in plate theory when dealing with point loads.[6]

Finally, a few remarks will be made with regard to the analytical properties of the solutions of Sections (2.2) and (2.3). It is easily seen that the solutions of Section (2.2) satisfy all the necessary conditions with regard to continuity of derivatives which are demanded by the differential equation. The basic solutions of Section (2.3), on the other hand, do not belong to the same class of continuous functions, because certain of their third derivatives are discontinuous. However, this property of discontinuity is essential for the purpose of satisfying the "internal" boundary conditions so that the basic solutions are suitable for the solution of the problems in hand.

(1.2) *Assumptions*

Only those assumptions that refer directly to the reinforcing members will be stated explicitly. Some of these are not essential and have only been introduced in order to simplify the presentation of the theory. For example, it is not difficult to relax the conditions that the flexural axis of the reinforcing members should lie in the middle plane of the plate and that their torsional deformation may be neglected. In reference 3, which deals with the case of ribs, this last assumption has not been made.

(A.1) The theory of thin plates is applicable.

(A.2) The plate is simply supported along its edges.

(A.3) The flexural axes of the reinforcing members lie in the middle plane of the plate.

(A.4) The reinforcing members do not possess torsional stiffness.

(A.5) The stringers or ribs may be idealized into lines.

(A.6) In the case of stringers and ribs the former are so closely spaced that each transverse buckling wave includes several stringers that may hence be distributed.

(2) Equilibrium Equations and Basic Solutions

Throughout this report, whenever possible, use will be made of the notation of references 1 and 6. In particular, stringers will be reinforcements in the direction in which the plate is compressed, while ribs will be transverse reinforcements (see Fig. 1). As far as the deduction of the equilibrium equations is concerned, the work of the above references will be fully utilized, and only the final stages will be reproduced in order to illustrate the modifications caused by the presence of distributed stringers.

(2.1) *Equilibrium Equations*

In terms of the moment resultants, the equilibrium equation of a plate subject to lateral loads and compression in the $0x$ direction is given by[6]

$$\frac{\partial^2 M_x}{\partial x^2} - 2\frac{\partial^2 M_{xy}}{\partial x\,\partial y} + \frac{\partial^2 M_y}{\partial y^2} = -\left(q + N_x\frac{\partial^2 w}{\partial x^2}\right) \tag{2.1.1}$$

For an isotropic plate the following relations hold between these resultants and the lateral displacement w, provided the last is small:

$$\left.\begin{aligned} M_x &= -D[(\partial^2 w/\partial x^2) + \nu(\partial^2 w/\partial y^2)] \\ M_y &= -D[(\partial^2 w/\partial y^2) + \nu(\partial^2 w/\partial x^2)] \\ M_{xy} &= D(1-\nu)\,(\partial^2 w/\partial x\,\partial y) \end{aligned}\right\} \tag{2.1.2}$$

Hence, Eq. (2.1.1) becomes

$$\nabla^4 w + \frac{N_x}{D}\frac{\partial^2 w}{\partial x^2} \equiv \frac{\partial^4 w}{\partial x^4} + 2\frac{\partial^4 w}{\partial x^2\,\partial y^2} + \frac{\partial^4 w}{\partial y^4} + \frac{N_x}{D}\frac{\partial^2 w}{\partial x^2} = \frac{q}{D} \tag{2.1.3}$$

In the case of distributed stringers, one is effectively dealing with an orthotropic plate and Eqs. (2.1.2) must be replaced by

$$\left.\begin{aligned} M_x &= -D[k(\partial^2 w/\partial x^2) + \nu(\partial^2 w/\partial y^2)] \\ M_y &= -D[(\partial^2 w/\partial y^2) + \nu(\partial^2 w/\partial x^2)] \\ M_{xy} &= D(1-\nu)\,(\partial^2 w/\partial x\,\partial y) \end{aligned}\right\} \tag{2.1.4}$$

where

$$k = 1 + (12I_x/h^3)\,(1-\nu^2) \tag{2.1.5}$$

Instead of Eq. (2.1.3), one then obtains, from Eq. (2.1.1),

$$\nabla^4 w + (k-1)\frac{\partial^4 w}{\partial x^4} + \frac{N_x}{D}\frac{\partial^2 w}{\partial x^2} \equiv k\frac{\partial^4 w}{\partial x^4} + 2\frac{\partial^4 w}{\partial x^2\,\partial y^2} + \frac{\partial^4 w}{\partial y^4} + \frac{N_x}{D}\frac{\partial^2 w}{\partial x^2} = \frac{q}{D} \tag{2.1.6}$$

(2.2) *Solutions for Lateral Loading over a Finite Width Strip*

Following reference 5 the desired loading would have to be introduced by means of the following loading functions:

$$q = D\sum_{m=1}^{\infty}\sum_{n=1}^{\infty} s_{mi}\sin\frac{m\pi x}{a}\sin\frac{n\pi y_i}{b}\sin\frac{n\pi y}{b} \tag{2.2.1a}$$

for a stringer at the station y_i,

$$q = D\sum_{m=1}^{\infty}\sum_{n=1}^{\infty} r_{nj}\sin\frac{n\pi y}{b}\sin\frac{m\pi x_j}{a}\sin\frac{m\pi x}{a} \tag{2.2.2a}$$

for a rib at the station x_j. As indicated in the introduction, these loading functions, while corresponding to the basic solutions of the next section, lead to solutions of Eqs. (2.1.4), which have certain discontinuous third derivatives. For this reason the ensuing analysis would not be justifiable, since the solutions of this equation must have continuous derivatives up to and including the fourth order.

The loading functions, Eqs. (2.2.1a) and (2.2.1b), will now be replaced by the functions

$$q = D\sum_{m=1}^{\infty}\sum_{n=1}^{\infty} s_{mi}\sin\frac{m\pi x}{a}\sin\frac{n\pi y_i}{b}\sin\frac{n\pi y}{b}\,\frac{\sin^2 n\delta}{n^2\delta^2} \tag{2.2.1}$$

$$q = D\sum_{m=1}^{\infty}\sum_{n=1}^{\infty} r_{nj}\sin\frac{n\pi y}{b}\sin\frac{m\pi x_j}{a}\sin\frac{m\pi x}{a}\,\frac{\sin^2 m\delta}{m^2\delta^2} \tag{2.2.2}$$

which are easily seen to correspond to triangular loadings over strips of width 4δ surrounding the respective reinforcements. The widths of these strips must, of course, be restricted in such a way that the loading stays within the region of the plate (see Fig. 2).

It is easily seen that the series (2.2.1) and the series (2.2.2) are absolutely and uniformly convergent in the region of the plate, provided δ has a finite value. It is also readily verified that, in the limit when $\delta \to 0$, these series tend formally to those given by Eqs. (2.2.1a) and (2.2.1b).

First consider the case of the isotropic plate, subject to the loadings in Eqs. (2.2.1) and (2.2.2). Substituting for w in Eq. (2.1.3) the series

$$W = \sum_{m=1}^{\infty}\sum_{n=1}^{\infty} C_{mn}\sin\frac{m\pi x}{a}\sin\frac{n\pi y}{b} \tag{2.2.3}$$

and comparing coefficients of $\sin(m\pi x/a)\sin(n\pi y/b)$, one finds

$$C_{mn}{}^{i} = \frac{s_{mi}\sin(n\pi y_i/b)}{\pi^4\left\{\left(\frac{m}{a}\right)^2 + \left(\frac{n}{b}\right)^2\right\}^2 - \left(\frac{m}{a}\right)^2\pi^2\frac{N_x}{D}}\cdot\frac{\sin^2 n\delta}{n^2\delta^2} \tag{2.2.4}$$

for the case of triangular loading on a x-wise strip at y_i, and

$$C_{mn}{}^{j} = \frac{r_{nj}\sin(m\pi x_j/a)}{\pi^4\left\{\left(\frac{m}{a}\right)^2 + \left(\frac{n}{b}\right)^2\right\}^2 - \left(\frac{m}{a}\right)^2\pi^2\frac{N_x}{D}}\cdot\frac{\sin^2 m\delta}{m^2\delta^2} \tag{2.2.5}$$

for the case of triangular loading on a y-wise strip at x_j, where in both cases the width of the strip is 4δ.

In the case of the orthotropic plate with ribs, one finds from Eq. (2.1.6)

$$\bar{C}_{mn}{}^{j} = \frac{\bar{r}_{nj} \sin (m\pi x_j/a)}{\pi^4\left[\left\{\left(\frac{m}{a}\right)^2 + \left(\frac{n}{b}\right)^2\right\}^2 + (k-1)\left(\frac{m}{a}\right)^4\right] - \left(\frac{m}{a}\right)^2 \pi^2 \frac{N_x}{D}} \times \frac{\sin^2 m\delta}{m^2\delta^2} \tag{2.2.6}$$

where obviously

$$k - 1 > 0 \tag{2.2.7}$$

Substituting for C_{mn} in Eq. (2.2.3) the above values, one obtains the relevant solutions for the plate with strip loading of the indicated type.

(2.3) *The Basic Solutions*

The required solutions for the problem of general instability of plates with line reinforcements can be obtained from the solutions of Section (2.2) by means of the same limiting process that transforms the loadings in Eqs. (2.2.1) and (2.2.2) into the basic loadings in Eqs. (2.2.1a) and (2.2.2a). In fact, letting $\delta \to 0$, one obtains, finally, for the isotropic plate,

$$C_{mn}{}^{i} = \frac{s_{mi} \sin (n\pi y_i/b)}{\pi^4\left\{\left(\frac{m}{a}\right)^2 + \left(\frac{n}{b}\right)^2\right\}^2 - \left(\frac{m}{a}\right)^2 \pi^2 \frac{N_x}{D}} \tag{2.3.1}$$

for a stringer at y_i,

$$C_{mn}{}^{j} = \frac{r_{nj} \sin (m\pi x_j/a)}{\pi^4\left\{\left(\frac{m}{a}\right)^2 + \left(\frac{n}{b}\right)^2\right\}^2 - \left(\frac{m}{a}\right)^2 \pi^2 \frac{N_x}{D}} \tag{2.3.2}$$

for a rib at x_j, while for the orthotropic plate with a rib at x_j,

$$\bar{C}_{mn}{}^{j} = \frac{\bar{r}_{nj} \sin m\pi x_j/a}{\pi^4\left[\left\{\left(\frac{m}{a}\right)^2 + \left(\frac{n}{b}\right)^2\right\}^2 + (k-1)\left(\frac{m}{a}\right)^4\right] - \left(\frac{m}{a}\right)^2 \pi^2 \frac{N_x}{D}} \tag{2.3.3}$$

where

$$W = \sum_{m=1}^{\infty} \sum_{n=1}^{\infty} C_{mn}{}^{j} \sin \frac{m\pi x}{a} \sin \frac{n\pi y}{b} \tag{2.3.4}$$

These expressions for w are easily seen to have the properties required by the present problem. For example, substituting for C_{mn} the values in Eq. (2.3.1), it is seen that the derivative $\partial^3 w/\partial y^3$ has a discontinuity at $y = y_i$, since the corresponding solution contains series of the form

$$\sum_{n=1}^{\infty} \frac{1}{n} \cos \frac{n\pi y}{b} \sin \frac{n\pi y_i}{b} \tag{2.3.5}$$

The discontinuity of this series at the station $y = y_i$ is obviously

$$\pi/2 \tag{2.3.6}$$

Similar reasoning may be applied to the remaining series.

In the next section the characteristic equations for the general instability of stiffened plates will be obtained by satisfying the "internal" boundary conditions that are known to relate the deformations of the reinforcements to the above discontinuities.

(3) The Buckling Equations

(3.1) *Case of Discrete Stringers or Ribs*

The basic solutions of Section (2.3) contain the arbitrary constants s_{mi} and r_{nj}, which are required to satisfy the internal boundary conditions at the reinforcing members. On the basis of the remarks at the end of the last section, these conditions are

$$\left[B_k \frac{\partial^4 w}{\partial x^4} + \frac{A_k N_x}{h} \frac{\partial^2 w}{\partial x^2}\right]_{y=y_k} = -D\Delta\left[\frac{\partial^3 w}{\partial y^3}\right]_{y=y_k} \tag{3.1.1}$$

for a stringer at y_k, and

$$\left[B_l \frac{\partial^4 w}{\partial y^4}\right]_{x=x_l} = -D\Delta\left[\frac{\partial^3 w}{\partial x^3}\right]_{x=x_l} \tag{3.1.2}$$

for a rib at x_l. In these formulas, Δ indicates the discontinuity in the respective derivatives that are the only discontinuous parts of the relevant shear resultants.

First consider the case of f stringers. The relevant basic solution is obtained from Eqs. (2.3.1) and (2.3.4) by summing with respect to i over all stringers. Substituting this solution in the f conditions, Eqs. (3.3.1), corresponding to the stations $y_k (k = 1, 2, \ldots, f)$, one finds

$$\left|\delta_{ik} + 2\left(\gamma_k m^4 - \delta_k \frac{N_x \beta^2 m^2 b^2}{D\pi^2}\right) \sum_{n=1}^{\infty} \frac{\sin(n\pi y_i/b)\sin(n\pi y_k/b)}{\{m^2 + \beta^2 n^2\}^2 - (N_x \beta^2 m^2 b^2/D\pi^2)}\right| = 0$$

$$\left(i, k = 1, 2, \ldots, \quad \delta_{ik} = \begin{cases} 0, & i \neq k \\ 1, & i = k \end{cases}\right) \tag{3.1.3}$$

which is the condition for the existence of nonzero values for the constants s_{mi}. Eq. (3.1.3) is a determinant of order f, and it is easily seen to agree with the results on page 374 of reference 1, which were obtained by means of the energy method. In fact, the result given there may be rewritten as

$$a_{mn}\left\{(m^2 + \beta^2 n^2)^2 - \frac{N_x \beta^2 m^2 b^2}{D\pi^2}\right\} + 2\sum_{i=1}^{\infty}\left[\gamma_k m^4 - \delta_k \frac{N_x \beta^2 m^2 b^2}{D\pi^2}\right] \sin\frac{m\pi y_i}{b} \sum_{p=1}^{\infty} a_{mp} \times \sin\frac{p\pi y_i}{b} = 0$$

which is an infinite system of equations for the arbitrary coefficients a_{mn}. Dividing the above equation by the coefficient of a_{mn}, multiplying by $\sin n\pi y_k/b$, and summing with respect to n, one obtains a system of f equations in the new variables

$$\sum_{p=1}^{\infty} a_{mp} \sin\frac{p\pi y_i}{b}, \quad (i = 1, 2, \ldots, f)$$

the determinant of which is Eq. (3.1.3). Thus it is seen that the constants s_{mi} of the basic solutions are proportional to the above variables. The same process of summation has been used frequently in references 2–4.

Next, the case of g ribs will be investigated. The same procedure may be applied as in the case of stringers, using this time Eqs. (2.3.2), (2.3.4), and (3.1.2). The characteristic equation is now

$$\left|\delta_{jl} + 2\gamma_l \beta^3 n^4 \sum_{m=1}^{\infty} \frac{\sin\frac{m\pi x_j}{a}\sin\frac{m\pi x_l}{a}}{\{m^2 + n^2\beta^2\}^2 - \frac{N_x \beta^2 m^2 b^2}{D\pi^2}}\right| = 0, \quad (j, l = 1, 2, \ldots, g) \tag{3.1.4}$$

On page 379 of reference 1, a related result has been obtained using again an energy method and assuming that $n = 1$. By a process analogous to that indicated for the case of stringers, it can be shown that Eq. (3.1.4) is equivalent to the special result obtained there if one puts $n = 1$. It can also be shown that the coefficients r_{nj} of the basic solutions are proportional to

$$\sum_{p=1}^{\infty} a_{pn} \sin\frac{p\pi x_j}{a}$$

Finally, consider the series, figuring in the determinants (3.1.3) and (3.1.4). These series can be summed in the manner used in reference 3, and the corresponding sums are

$$\sum_{n=1}^{\infty} \frac{\sin\frac{n\pi y_i}{b}\sin\frac{n\pi y_k}{b}}{\{m^2 + \beta^2 n^2\}^2 - \frac{N_x \beta^2 m^2 b^2}{D\pi^2}} = \left[\frac{\pi}{8\beta^4 c\theta} \frac{\sinh\left\{\pi B\left(1 - \frac{y_i}{b}\right)\right\}\sinh\left\{\pi B\frac{y_k}{b}\right\}}{B\sinh\pi B} - \frac{\sinh\left\{\pi A\left(1 - \frac{y_i}{b}\right)\right\}\sinh\left\{\pi A\frac{y_k}{b}\right\}}{A\sinh\pi A}\right] \quad (\text{for } y_i < y_k) \tag{3.1.5}$$

where

$$c^2 = \frac{m^2}{\beta^2}, \quad \theta^2 = \frac{N_x b^2}{4D\pi^2}, \quad A^2 = c(c + 2\theta), \quad B^2 = c(c - 2\theta) \tag{3.1.6}$$

$$\sum_{m=1}^{\infty} \frac{\sin \frac{m\pi x_j}{a} \sin \frac{m\pi x_l}{a}}{\left\{m^2 + \beta^2 n^2\right\}^2 - \frac{N_x \beta^2 m^2 b^2}{D\pi^2}} = \frac{\pi}{8FG}\left[\frac{\sin \pi(F+G)\left(1 - \frac{x_j}{a}\right) \sin \pi(F+G)\frac{x_l}{a}}{(F+G)\sin(F+G)\pi} - \right.$$

$$\left. \frac{\sin \pi(F-G)\left(1 - \frac{x_j}{a}\right) \sin \pi(F-G)\frac{x_l}{a}}{(F-G)\sin(F-G)\pi}\right] \tag{3.1.7}$$

where

$$F^2 = \frac{a^2}{4\pi^2}\frac{N_x}{D}, \quad G^2 = F^2 - n^2\beta^2, \quad x_j \leqslant x_l \tag{3.1.8}$$

Thus, the determinants (3.1.3) and (3.1.4) can be written in closed form, using Eqs. (3.1.5) and (3.1.7), respectively. The final characteristic will be independent of n or m—i.e., of the wave lengths at right angles to the reinforcing members. The equations deduced here are somewhat more general than those of references 3 and 4, which assume constant stringer or rib spacing.

(3.2) *Case of Discrete Stringers and Ribs*

This problem is referred to in reference 4 and also in reference 7, since the analytical difficulties that it presents are of equal nature to those encountered in dealing with the buckling problem of a plate clamped along all edges. The purpose of the present discussion is to provide a proof that the characteristic equation cannot be presented in closed form or, quoting from reference 4, that the "difficulties in respect of mathematical summations" are irresolvable. The proof given here is indirect and leads to the conclusion that summation will only be possible if all the reinforcing members are parallel.

Using Eqs. (2.3.1), (2.3.2), and (2.3.4) and assuming f stringers and g ribs, the relevant basic solution is

$$w = \sum_{m=1}^{\infty}\sum_{n=1}^{\infty} \frac{\sin \frac{m\pi x}{a} \sin \frac{n\pi y}{b}}{\pi^4\left\{\left(\frac{m}{a}\right)^2 + \left(\frac{n}{b}\right)^2\right\}^2 - \left(\frac{m}{a}\right)^2 \pi^2 \frac{N_x}{D}} \cdot \left\{\sum_{i=1}^{f} s_{mi} \sin \frac{n\pi y_i}{b} + \sum_{j=1}^{g} r_{nj} \sin \frac{m\pi x_j}{a}\right\} \tag{3.2.1}$$

Substituting this solution in Eqs. (3.1.1) and (3.1.2), one finds the following set of equations:

$$\sum_{i=1}^{f} s_{mi}\left\{D\frac{b}{2} - \left[B_k\left(\frac{m\pi}{a}\right)^4 - \frac{A_k N_x}{h}\left(\frac{m\pi}{a}\right)^2\right] A_m^{ik}\right\} + \left[B_k\left(\frac{m\pi}{a}\right)^4 - \frac{A_k N_x}{h}\left(\frac{m\pi}{a}\right)^2\right] \cdot \sum_{j=1}^{g} R_m^{jk} \sin \frac{m\pi x_j}{a} = 0$$

$$\sum_{i=1}^{f} B_l\left(\frac{n\pi}{b}\right)^4 \sin \frac{n\pi y_i}{b} S_n^{il} + \sum_{j=1}^{g} r_{nj}\left\{D\frac{a}{2} + B_l\left(\frac{n\pi}{b}\right)^4 A_n^{jl}\right\} = 0$$

$$(k = 1, 2, \ldots, f, \quad l = 1, 2, \ldots, g, \quad m = 1, 2, \ldots, \infty, \quad n = 1, 2, \ldots, \infty) \tag{3.2.2}$$

where

$$A_m^{ik} = \sum_{n=1}^{\infty} \frac{\sin \frac{n\pi y_i}{b} \sin \frac{n\pi y_k}{b}}{A_{mn}}, \quad A_n^{jl} = \sum_{m=1}^{\infty} \frac{\sin \frac{m\pi x_j}{a} \sin \frac{m\pi x_l}{a}}{A_{mn}} \tag{3.2.3}$$

$$R_m^{jk} = \sum_{n=1}^{\infty} \frac{r_{nj}}{A_{mn}} \sin \frac{n\pi y_k}{b}, \quad S_n^{il} = \sum_{m=1}^{\infty} \frac{s_{mi}}{A_{mn}} \sin \frac{m\pi x_l}{a} \tag{3.2.4}$$

$$A_{mn} = \pi^4\left\{(m/a)^2 + (n/b)^2\right\}^2 - (m/a)^2 \pi^2 (N_x/D) \tag{3.2.5}$$

In agreement with the deductions at the end of the preceding section, the first f equations and the remaining g equations of Eqs. (3.2.2) (for constant m and n) are independent of n and m, respectively. However, in order to achieve this state, the new variables R_m and S_n had to be introduced so that these equations are no longer in terms of the same variables. Thus there arises the question whether a further summation can be

applied to these equations so that one obtains a finite set of equations in consistent variables.

Rewrite Eqs. (3.2.2) in the following manner:

$$\left.\begin{aligned} s_m \left\{ \frac{Db}{2\left[B_s\left(\frac{m\pi}{a}\right)^4 - \frac{A_s N_x}{h}\left(\frac{m\pi}{a}\right)^2\right]} + A_m \right\} + \\ R_m \sin\frac{m\pi x_r}{a} = 0 \\ S_n \sin\frac{n\pi y_s}{b} + r_n \left\{ \frac{Da}{2B_r(n\pi/b)^4} + A_n \right\} = 0 \end{aligned}\right\} \quad (3.2.2')$$

assuming that there is only one stringer at y_s and one rib at x_r. It is now easily seen to be impossible to reduce these equations to two equations with consistent variables. In fact, having introduced the variable R_m in the second set of equations in conformity with Eqs. (3.2.4), this variable can be eliminated by means of the first set of equations. But this process will not lead to a closed expression, since S_n already involves all s_m ($m = 1, 2, \ldots, \infty$). A similar reasoning applies with respect to S_n. Hence, these equations will only reduce to a closed expression if either all s_m or all r_n are zero—i.e., if only parallel reinforcing members are present.

The physical interpretation of this result is largely contained in the final conclusions of Section (3.1). It has been seen there that in the cases of stringers or ribs the buckling equations involve the number of waves in the directions of the reinforcing members. In the case of stringers and ribs the wave lengths in the x and in the y directions are of equal importance. If this were not so, it would follow that the case of only parallel reinforcements would also be independent of the corresponding wave lengths.

(3.3) *Case of Distributed Stringers and Discrete Ribs*

It has been seen in the previous section that it is not possible to obtain a closed expression for the characteristic equation in the case of a plate with stringers and ribs. However, in many practical cases, the stringer spacing will be sufficiently close as compared with the rib spacing to justify the introduction of the assumption (A.6). In that case one obtains, as before, using Eqs. (2.3.3), (2.3.4), and (3.1.2),

$$\left| \delta_{jl} + 2k\gamma_l\beta^3 n^4 \sum_{m=1}^{\infty} \frac{\sin\frac{m\pi x_j}{a}\sin\frac{m\pi x_l}{a}}{\left\{m^2 + n^2\beta^2\right\}^2 + (k-1)m^4 - \frac{N_x\beta^2 m^2 b^2}{D\pi^2}} \right| = 0 \quad (j, l = 1, 2, \ldots, g) \qquad (3.3.1)$$

The sums of the series in Eqs. (3.3.1) are

$$\sum_{m=1}^{\infty} \frac{\sin\frac{m\pi x_j}{a}\sin\frac{m\pi x_l}{a}}{\left\{m^2 + n^2\beta^2\right\}^2 + (k-1)m^4 - \frac{N_x\beta^2 m^2 b^2}{D\pi^2}} = \frac{\pi}{4kP}\left[\frac{\sinh\pi(Q-P)^{1/2}\left(1-\frac{x_j}{a}\right)\sinh\pi(Q-P)^{1/2}\frac{x_l}{a}}{(Q-P)^{1/2}\sinh\pi(Q-P)^{1/2}} - \frac{\sinh\pi(Q+P)^{1/2}\left(1-\frac{x_j}{a}\right)\sinh\pi(Q+P)^{1/2}\frac{x_l}{a}}{(Q+P)^{1/2}\sinh\pi(Q+P)^{1/2}}\right] \qquad (3.3.2)$$

where

$$P^2 = \frac{1}{4k^2}\left\{2n^2\beta^2 - \frac{N_x a^2}{D\pi^2}\right\}^2 - \frac{n^4\beta^4}{k}, \quad Q = \frac{1}{k}\left(n^2\beta^2 - \frac{N_x a^2}{2D\pi^2}\right) \quad (x_j \ll x_l) \qquad (3.3.3)$$

(4) Conclusions

The characteristic equations for the general instability of rectangular plates with stringers or ribs, with stringers and ribs, and with distributed stringers and discrete ribs have been deduced directly from the equilibrium equations. The method used leads in all but one of these cases to a determinantal equation the order of which equals the number of discrete reinforcing members. For the case of stringers and ribs it has been shown that the present approach leads to an infinite determinant.

Some of these buckling equations have been previously obtained by the use of the energy method.[1–4] However, comparison of the present work with that of references 3 and 4 shows that the energy approach leads to more involved calculations.

Another advantage of the present approach is that the basic solutions of the equilibrium equations, ob-

tained in Section (2.3) have a simple physical interpretation in that they represent the mathematical formulation of discrete reinforcements. For this reason, the analytical process leading to the characteristic equations may be directly related to the physical aspects of the buckling process, and a clearer understanding of the mechanism of general instability thus becomes possible.

References

[1] Timoshenko, S., *Theory of Elastic Stability;* McGraw-Hill Book Company, Inc., New York, London, 1936.

[2] Cox, H. L., and Smith, H. E., *The Buckling of Grids of Stringers and Ribs*, Proc. Lond. Math. Soc., Ser. 2, Vol. 48, pp. 1–26, 1943.

[3] Cox, H. L., and Smith, H. E., *The Buckling of a Thin Sheet Transversely Stiffened*, Proc. Lond. Math. Soc., Ser. 2, Vol. 48, pp. 27–34, 1943.

[4] Cox, H. L., and Riddell, J. R., *Buckling of a Longitudinally Stiffened Flat Panel*, Aeron. Quarterly, Vol. 1, pp. 225–244, November, 1949.

[5] Radok, J. R. M., *The Theory of General Instability of Cylindrical Shells*, College of Aeronautics, Cranfield Rep. 61, June, 1952.

[6] Timoshenko, S., *Theory of Plates and Shells;* McGraw-Hill Book Company, Inc., New York, London, 1940.

[7] Cox, H. L., *The Buckling of a Flat Rectangular Plate Under Axial Compression and Its Behaviour After Buckling*, R. and M. 2041, May, 1945.

[8] Lokshin, A. S., *On the Calculation of Plates with Ribs*, Jour. Appl. Math. and Mech., Vol. 2, p. 225, 1935 (Russian).

[9] Budiansky, B., and Seide, P., *Compressive Buckling of Simply Supported Plates with Transverse Stiffeners*, NACA TN No. 1557, April, 1948.

[10] Seide, P., and Stein, M., *Compressive Buckling of Simply Supported Plates with Longitudinal Stiffeners*, NACA TN No. 1825, March, 1949.

Conference on Supersonic Flow

An unclassified conference on Supersonic Flow will be held in the Mathematics Building, University of Maryland, from 9:30 a.m. to 5:00 p.m. on March 19–20, 1954.

Information concerning the conference may be obtained from Dr. E. L. Resler, Associate Research Professor, Institute of Fluid Dynamics and Applied Mathematics, University of Maryland, College Park, Md.

Changes of Address

Since the Post Office Department does not as a rule forward magazines to forwarding addresses, it is important that the Institute be notified of changes in address 30 days in advance of publishing date to ensure receipt of every issue of the JOURNAL and REVIEW.

Notices should be printed legibly and sent directly to:

Institute of the Aeronautical Sciences, Inc.
2 East 64th Street, New York 21, New York

Survey of Friction Coefficients, Recovery Factors, and Heat-Transfer Coefficients for Supersonic Flow*

JOSEPH KAYE†

Massachusetts Institute of Technology

SUMMARY

A brief survey is presented of the progress made in the last 4 years on theoretical and experimental work on friction coefficients, recovery factors, and heat-transfer coefficients for supersonic flow of air.

NOMENCLATURE

A	=	heat-transfer area
c_f	=	local skin-friction coefficient
c_H	=	Stanton Number of Van Driest
c_p	=	specific heat at constant pressure
D	=	inside diameter of pipe
f	=	local apparent coefficient of friction, $2g\tau/\rho V^2$
G	=	flow per unit area
g	=	acceleration given to unit mass by unit force
h	=	heat-transfer coefficient, $(q/A)/(t_w - t_{aw})$
M	=	Mach Number, $V/\sqrt{gkRT}$
Nu_L	=	length Nusselt number, hL/k
Pr	=	Prandtl Number, $c_p\mu g/\lambda$
p	=	static pressure
q	=	rate of heat transfer
r	=	recovery factor, $(t_{aw} - t_1)/(t_0 - t_1)$
Re_D	=	diameter Reynolds Number, $DG/\mu g$
Re_L	=	length Reynolds Number, $LG/\mu g$
St	=	Stanton Number, h/c_pG
T	=	temperature, °F. abs.
t	=	temperature, °F.
V	=	velocity
ρ	=	density
λ	=	thermal conductivity
μ	=	viscosity
τ	=	shear stress at wall

Subscripts:

0	refers to stagnation conditions
aw	refers to adiabatic wall conditions
1	refers to mean-stream conditions
∞	refers to free stream conditions
i	refers to flow of incompressible fluid
w	refers to wall conditions

Presented at the Aerodynamics Session, Twenty-First Annual Meeting, IAS, New York, January 26–29, 1953.

* The assistance of Prof. T. Y. Toong and George A. Brown in the preparation of Figs. N, O, P, and Q is gratefully acknowledged. This survey report was written mainly under the sponsorship of the Office of Naval Research of the United States Navy under Contract Number N5-ori-07805. Permission has been received to reproduce the figures taken from the JOURNAL OF THE AERONAUTICAL SCIENCES, the reports of the National Advisory Committee for Aeronautics, and the reports of the U.S. Naval Ordnance Laboratory.

† Associate Professor of Mechanical Engineering.

INTRODUCTION

THE IMPORTANCE OF DESIGNING AIRCRAFT for safe operation at higher and higher supersonic speeds is apparent to all. Twenty years ago designers of aircraft were concerned with the effects resulting from an aircraft passing through the speed of sound—"the sonic barrier." But having shown that it is feasible to design an aircraft that can start from rest and exceed sonic speed safely, the designer is at present concerned with safe operation of aircraft at supersonic and hypersonic speeds.

Safe operation of supersonic aircraft implies safety for both the inhabitants of the aircraft and its equipment. It is evident that, as the speed increases to five or ten times the sonic speed, the function of the human beings on board must be reduced considerably, since the human being represents a poorly designed servomechanism at these high rates of action and reaction. Hence, as the speed increases, more and more of the normal human operations will be taken over by electronic gadgets. But here the designer is faced with an obstacle similar to the "sonic barrier."

If the speed of the plane is sufficiently high, its surface temperature may reach a value of the order of 1,000°F. or greater, resulting from "aerodynamic heating." Hence, the designer can foresee a "thermal barrier" requiring a tremendous amount of internal cooling in this aircraft in order to keep the inhabitants, the aircraft, and the electronic equipment in safe operating condition. The problem of safe operation of electronic equipment is made even more difficult when it is realized that most of this equipment has been designed only for operation at low ambient temperatures and not for continuous operation at 1,000°F. or at greater temperatures.

The designers of supersonic aircraft require an extensive knowledge of friction coefficients, recovery factors, and heat-transfer coefficients over a wide range of Mach Numbers for both laminar and turbulent boundary layers. It is intended here to present a survey of available data and theory for supersonic velocities and then to discuss two research programs in this field now under way at M.I.T.

Because of the large number of papers published in this field in the last few years, only some of the latest

TABLE 1

SUMMARY OF ASSUMPTIONS USED IN THEORETICAL WORK ON LAMINAR BOUNDARY LAYER ON A FLAT PLATE

Author	Date	Density	Specific Heat	Thermal Conductivity	Viscosity	Prandtl No.	Pressure Gradient	Radiation	Dissociation	Mach No.	Friction Coefficients	Recovery Factor	Heat-Transfer Coefficient	Remarks
Blasius	1908	c	c	c	c	c	0	0	0	0	$c_f = 0.664 Re_L^{-1/2}$	-	-	
Pohlhausen	1921	c	c	c	c	c	0	0	0	0	$c_f = 0.664 Re_L^{-1/2}$	$r = Pr^{1/2}$	✓	
Busemann	1935	f(T)	c	$\sim T^{1/2}$	$\sim T^{1/2}$	1	0	0	0	8.8	✓	✓	-	
Von Karman and Tsien	1939	f(T)	c	$\sim T^{.77}$	$\sim T^{.77}$	1	0	0	0	0-10	✓	✓	-	
Crocco	1941	f(T)	c	$\sim T^{w}$ (for w = 0.5,.75,1.0,1.25)	$\sim T^{w}$	0.725	0	0	0	0-5	✓	✓	✓	
Brainerd and Emmons	1942	f(T)	c	$\sim T^{.768}$	$\sim T^{.768}$	0.733	0	0	0	0-3.2	✓	✓	-	
Crocco	1946	f(T)	c	$\sim T^{1}$	$\sim T^{1}$	c	0	0	0	>1	✓	✓	✓	
Cope and Hartree	1943	f(T)	c	$\sim T^{.89}$	$\sim T^{.89}$	0.78	0	0	0	>1	✓	✓	✓	
Chapman[18] and Rubesin	1949	f(T)	c	$\sim T^{1}$	$\sim T^{1}$	0.72	0	0	0	0-5	✓	✓	✓	Arbitrary surface temperature
Lighthill[28]	1950	f(T)	c	f(T)	f(T)	0.7	f(V)	✓	0	>1	✓	✓	✓	Arbitrary velocity of main stream and arbitrary surface temperature
Van Driest[3]	1951	f(T)	c	f(T)	Sutherland Rule	0.75	0	0	0	0-20	✓	✓	✓	
Klunker and McLean[29]	1951	f(T)	f(T)	f(T)	f(T)	f(T)	0	0	0	0-10	✓	✓	✓	
Young and Janssen[30]	1952	f(T)	f(T)	f(T)	f(T)	f(T)	0	0	0	0-5	✓	✓	✓	
Moore[2]	1952	f(T)	f(T)	f(T)	f(T)	f(T)	0	0	f(T,P)	0-20	✓	✓	✓	

c = constant
✓ = variable examined
- = variable not examined

ones are reviewed; no attempt is made to cover the field completely. In addition, although the problem of transition is closely associated with the above problems for laminar and turbulent boundary layers, it was decided to exclude the large number of papers treating this difficult problem.

Objectives

The objectives of the present discussion are threefold:

(1) To present a brief survey of the state of the art on theoretical and experimental work on friction coefficients, recovery factors, and heat-transfer coefficients for supersonic flow.

(2) To present a brief description of the program in supersonic flow of air in a tube at M.I.T. under the sponsorship of the Office of Naval Research.

(3) To present a brief description of the program on supersonic flow of air over a flat plate under way at M.I.T. under the sponsorship of the Office of Air Research.

Review

(A) *Theoretical Work on Laminar Boundary Layer*

The analytical investigation of the laminar boundary layer began in 1908 with the thesis of Blasius, who determined the velocity profiles for incompressible flow on a flat plate with zero pressure gradient. In 1921 Pohlhausen used these velocity profiles to calculate temperature profiles in the laminar boundary layer on a flat plate. Since then numerous papers have been published which extended and modified, first, the basic assumptions used in the analysis; second, the mathematical techniques of reduction of the partial differential equations; and third, the methods of obtaining numerical results. The variety of assumptions used in some of these papers is seen from the summary in Table 1. Most of the references before 1950 in Table 1 are given in detail in an excellent review by Kuerti,[1] which also contains the references to the earlier reviews of Lewis and of Rubesin and Johnson.

Since the papers listed in Table 1 represent only a fraction of the available papers, it is obviously possible to give here only a few samples of theoretical work. These will be selected from the most recent papers.

(*1*) *Skin-Friction Coefficient for Laminar Boundary Layer.*—The calculated values of local skin-friction coefficient, c_f, for flow of air over a flat plate are compared in Fig. A (Moore[2]—Fig. 10). These curves are for the insulated plate with all air properties evaluated at the free-stream temperature.

The effect of evaluating the air properties at the wall temperature is shown in Fig. B (Van Driest[3]—Fig. 3) by the curve marked $C_f'\sqrt{Re}$. The effect of heat transfer on the mean skin-friction coefficient for a flat plate is shown in Fig. B, in terms of the ratio of the wall temperature to free-stream temperature, T_w/T_∞.

(*2*) *Recovery Factors for Laminar Boundary Layer.*—The various theoretical analyses for recovery factors for both subsonic and supersonic flow over a flat insulated plate lead to the simple result,

$$r = \sqrt{Pr} \qquad (1)$$

This approximate rule for laminar boundary layers agrees within 1 per cent of the more exact and complicated function if the Prandtl Number lies between 1.2 and 0.7 and for Mach Numbers less than about 8.

For large values of the Mach Number, however, it is not clear what temperature should be used to evaluate the Prandtl Number. Note that this rule predicts that the recovery factor is independent of Mach Number and Reynolds Number.

If dissociation of the fluid at high Mach Numbers is taken into account, as Moore[2] has shown for air, the Prandtl Number varies strongly with the degree of dissociation, and the above rule does not hold. For this case, the temperature rise of the insulated plate over the free-stream temperature, rather than the recovery factor, is shown in Fig. C (Moore[2]—Fig. 13). For sea-level conditions, it is seen that dissociation begins to play an important role at a Mach Number greater than 8 if radiation effects are ignored. It is also evident that the effects of dissociation at these high Mach Numbers will be diminished if the cooling effect of radiation is considered at these high temperatures.

(3) Heat-Transfer Coefficient for Laminar Boundary Layer.—For incompressible flow, the local coefficient of heat transfer for a flat plate is given by

$$Nu_L = hL/k = 0.33 Re_L^{1/2} Pr^{1/3} \qquad (2a)$$

or by

$$St = h/c_p G = 0.33 Re_L^{-1/2} Pr^{-2/3} \qquad (2b)$$

where the coefficient, h, is defined by

$$h \equiv (q/A)/(t_w - t_\infty) \qquad (3)$$

For compressible flow in the boundary layer of a flat plate, the same form of theoretical result as Eqs. (2a) and (2b) is obtained for the case of isothermal plate, provided the "effective" heat-transfer coefficient is defined by

$$h_e \equiv (q/A)/(t_w - t_{aw}) \qquad (4)$$

and provided the values of the fluid properties are evaluated at the temperature just outside the boundary layer. The "constant" of Eqs. (2a) and (2b) changes with Mach Number for compressible flow.

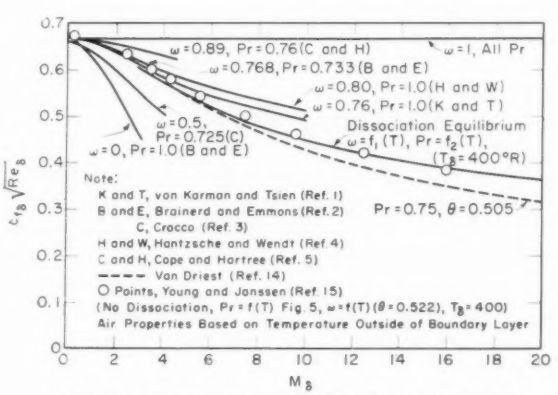
$c_{f_\delta}\sqrt{Re_\delta}$
M_δ
ω=0.89, Pr=0.76(C and H)
ω=1, All Pr
ω=0.768, Pr=0.733(B and E)
ω=0.80, Pr=1.0(H and W)
ω=0.76, Pr=1.0(K and T)
Dissociation Equilibrium
ω=0.5, Pr=0.725(C)
ω=0, Pr=1.0(B and E)
ω=f1(T), Pr=f2(T), (Tδ=400°R)
Note:
K and T, von Karman and Tsien (Ref. 1)
B and E, Brainerd and Emmons (Ref. 2)
C, Crocco (Ref. 3)
H and W, Hantzsche and Wendt (Ref. 4)
C and H, Cope and Hartree (Ref. 5)
Van Driest (Ref. 14)
O Points, Young and Janssen (Ref. 15)
(No Dissociation, Pr=f(T) Fig. 5, ω=f(T)(θ=0.522), Tδ=400)
Air Properties Based on Temperature Outside of Boundary Layer
Pr=0.75, θ=0.505

LOCAL SKIN FRICTION ON AN INSULATED FLAT PLATE WITH NO RADIATION

FIG. A–MOORE[2] –1952

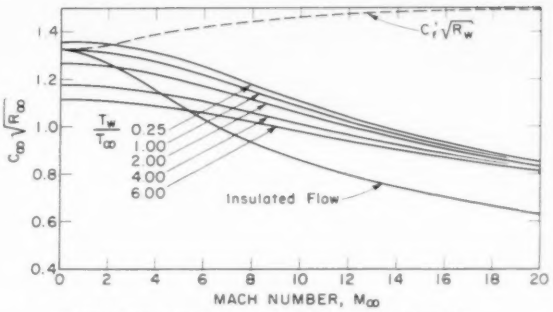

MEAN SKIN-FRICTION COEFFICIENT FOR LAMINAR BOUNDARY LAYER OF A COMPRESSIBLE FLUID FLOWING ALONG A FLAT PLATE. PRANDTL NUMBER, 0.75; θ=0.505

FIG. B–VAN DRIEST[3]–1952

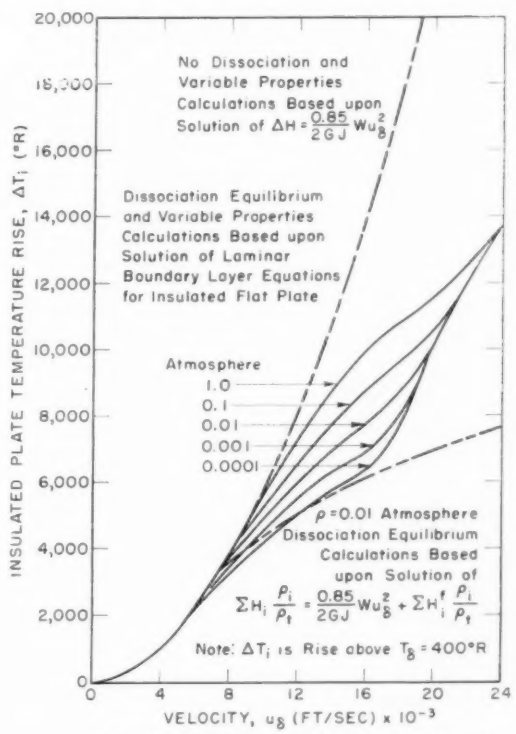
INSULATED PLATE TEMPERATURE RISE, ΔTi (°R)
No Dissociation and Variable Properties Calculations Based upon Solution of $\Delta H = \frac{0.85}{2GJ} Wu_\delta^2$
Dissociation Equilibrium and Variable Properties Calculations Based upon Solution of Laminar Boundary Layer Equations for Insulated Flat Plate
Atmosphere
1.0
0.1
0.01
0.001
0.0001
ρ=0.01 Atmosphere Dissociation Equilibrium Calculations Based upon Solution of $\Sigma H_i \frac{\rho_i}{\rho_1} = \frac{0.85}{2GJ} Wu_\delta^2 + \Sigma H_i' \frac{\rho_i}{\rho_1}$
Note: ΔTi is Rise above Tδ=400°R
VELOCITY, u_δ (FT/SEC) x 10^{-3}

INSULATED PLATE TEMPERATURE RISE VS VELOCITY OUTSIDE BOUNDARY LAYER

FIG. C–MOORE[2] –1952

Moore[2] has shown that the calculated value of the heat-transfer coefficient based on dissociation increases with increasing Mach Numbers and simultaneously decreasing absolute pressure to such an extent that these values can become double or triple the values of the corresponding heat-transfer coefficient without dissociation.

The variation of the product of Stanton Number and square root of length Reynolds Number versus Mach Number is shown in Fig. D (Van Driest[3]—Fig. 4) for several values of the ratio of wall to free-stream temperature. The effect of evaluating the air

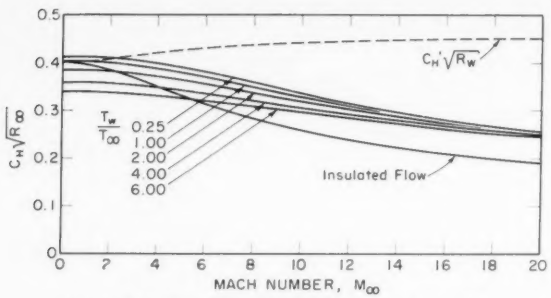

LOCAL HEAT-TRANSFER COEFFICIENT FOR LAMINAR BOUNDARY LAYER OF A COMPRESSIBLE FLUID FLOWING ALONG A FLAT PLATE. PRANDTL NUMBER, 0.75; $\theta = 0.505$

FIG. D-VAN DRIEST[3]-1952

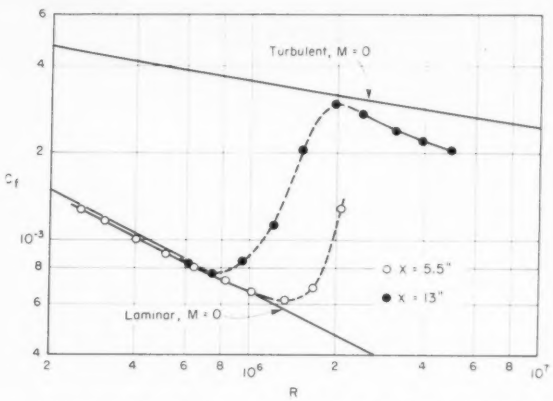

LOCAL FRICTION ON A SMOOTH FLAT PLATE AT A MACH NUMBER OF 26; NO TRIPPING DEVICE.

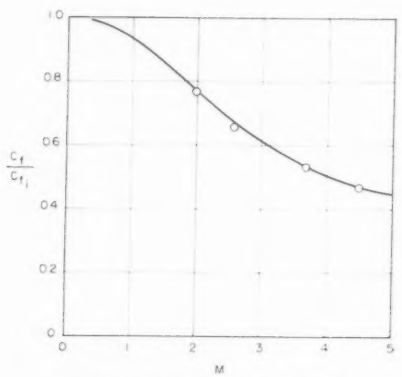

VARIATION OF TURBULENT LOCAL SKIN FRICTION COEFFICIENT WITH MACH NUMBER AT A REYNOLDS NUMBER OF 8,000,000

FIG. F-COLES[10] - 1952

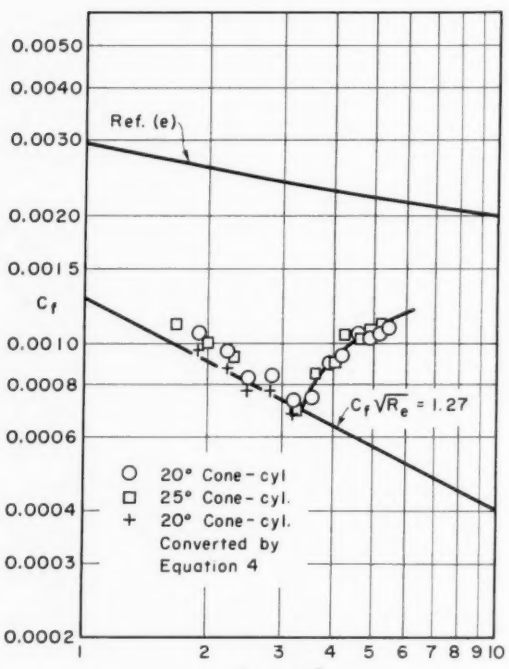

TOTAL SKIN FRICTION COEFFICIENTS AT M = 2.85 ($\bar{T}_w/T \simeq 2.58$)

FIG. E-POTTER[7]-1952

properties at the wall temperature is also shown by the curve labeled $C_H'\sqrt{Re}$.

(B) *Experimental Work on Laminar Boundary Layer*

(1) *Data on Friction Coefficients for Laminar Boundary Layer.*—The amount of experimental data available on skin-friction coefficient is limited in range of Mach Number and of length Reynolds Number.

The data of Blue[4] obtained by two methods (one an interferometer study and the other by a total-pressure probe), for a Mach Number of 2.0, showed that the measured average friction coefficients were from 7 to 39 per cent larger than the theoretical value of Crocco over the range of Reynolds Number from 0.3 to 1.1 × 10^6.

The data of Higgins and Pappas,[5] obtained by boundary-layer velocity profiles, agreed well with the independent work of Blue, although their Mach Number was 2.4. The average friction coefficients of Higgins and Pappas were from 32 to 48 per cent larger than the theoretical values.

Further work by Maydew and Pappas,[6] obtained by impact-pressure surveys of the boundary layer, showed average friction coefficients for the flat plate which were from 37 to 94 per cent larger than the theoretical values at a Mach Number of 2.4.

Potter,[7] at the Naval Ordnance Laboratory, found that average skin-friction coefficients for laminar boundary layers on cones and cone-cylinder combinations agreed with flat-plate values with a maximum deviation of about 20 per cent when appropriate conversion was made to a flat-plate geometry. These measurements covered the range of Mach Number from 1.86 to 4.24. A typical result is shown in Fig. E (Potter[7]—Fig. 7). Potter's friction coefficients are based on force measurements and not on interpretations of data on velocity profiles.

Liepmann and Dhawan,[8] Dhawan,[9] Coles,[10] and Coles and Goddard[11] presented data for local skin-friction coefficients on flat plates based on a sensitive force measuring element floating in the flat plate. The measurements covered the range up to a Mach Number of 4.5 and up to a Reynolds Number of 10^7. These data are probably the best local friction coefficients available at present and agree within a few per cent with the theoretical values predicted for a laminar boundary layer over a flat plate with zero pressure gradient. A typical result is shown in Fig. F (Coles[10]—Figs. 1 and 3).

From this group of experimental data it is evident that the available measurements of skin-friction coefficients extend to a Mach Number of 4 and that these data agree with the latest theories over this range of Mach Number probably within the experimental error inherent in the particular type of measurement.

(2) Data on Recovery Factors for Laminar Boundary Layer.—The experimental data on recovery factors for laminar boundary layers are summarized in Table 2.

The local recovery factors of Wimbrow[12] for one cone at a Mach Number of 2.0 and for one paraboloid at Mach Numbers of 1.5 and 2.0 agreed within 1 per cent of the theoretical value based on the square root of the Prandtl Number evaluated at the adiabatic wall temperature. These recovery factors were independent of Mach Number, Reynolds Number, and body shape but appeared to increase slightly with surface roughness.

The recovery factors of Stalder, Rubesin, and Tendeland[13] for a flat plate were independent of Reynolds Number and equal to 0.881 ± 0.007. This value is 4 per cent larger than the theoretical value evaluated at adiabatic wall temperature. The experimental data are shown in Fig. G (Stalder, Rubesin, and Tendeland[13]—Fig. 5).

Some typical results of the recent experimental values of Eber[14] for cones and cone-cylinders are shown in Fig. H (Eber[14]—Figs. 3, 4, 5, 7, 8, and 9). For the laminar boundary layer, Eber's recovery factors agreed with the square root of the Prandtl Number evaluated at the adiabatic wall temperature within 1 per cent.

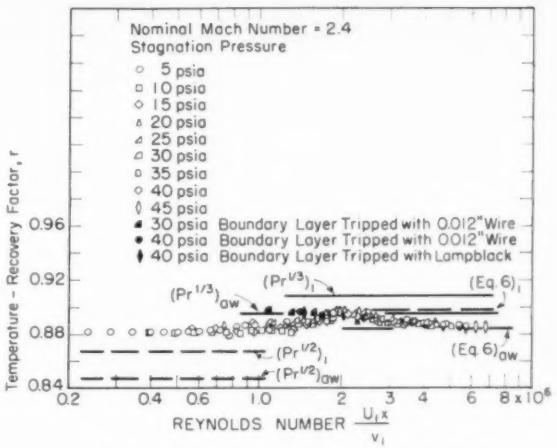

LOCAL TEMPERATURE - RECOVERY FACTOR ON FLAT PLATE

FIG. G - STALDER, RUBESIN, AND TENDELAND[13] - 1950

The recovery factors of des Clers and Sternberg,[15] of Slack,[16] and of Stine and Scherrer[17] are also shown in Table 2.

The M.I.T. recovery factors on a flat plate agreed with the cone values of 0.85 and not with the flat-plate values of 0.88 of references 13 and 16.

In summary, up to a Mach Number of 3, the experimental recovery factors agree within 1 per cent of the theoretical value given by the square root of the Prandtl Number evaluated at the adiabatic wall temperature. An unexplained discrepancy of about 4 per cent exists in some of the experiments made with flat plates. All evidence indicates the laminar recovery factors are independent of Mach Numbers up to 4 and of Reynolds Numbers up to the beginning of transition of the laminar boundary layer.

(3) Data on Heat-Transfer Coefficients for Laminar Boundary Layer.—Experimental data on heat-transfer coefficients for laminar boundary layers in supersonic flow are scarce. The following papers contain some results for supersonic flow.

The local heat-transfer coefficients of Slack,[16] for a flat plate at a Mach Number of 2.4, are shown in Fig. I (Slack[16]—Fig. 9). The uncorrected heat-transfer data (not shown in Fig. 1) scatter by a factor of 3, whereas

TABLE 2

Data on Recovery Factor for Laminar Boundary Layer

Author	Date	Model	Reynolds Number	Mach Number	Recovery Factor
Wimbrow[12]	1949	Cone	2.7×10^6	2.0	0.855 ± 0.008
		Paraboloid	4.8×10^6	1.5	0.845 ± 0.008
				2.0	0.855 ± 0.008
Stalder, Rubesin, and Tendeland[13]	1950	Flat plate	$0.2 - 1 \times 10^6$	2.4	0.881 ± 0.007
Eber[14]	1952	Cones (10°–80°)	6×10^3	0.88–4.65	0.845 ± 0.008
		Cone-cylinders	-5×10^6		
des Clers and Sternberg[15]	1952	Cone	$0.1 - 1.3 \times 10^6$	2.18	0.851 ± 0.007
Slack[16]	1952	Flat plate	$0.15 - 3 \times 10^6$	2.4	0.884 ± 0.006
Stine and Scherrer[17]	1952	Cone	$0.2 - 1.3 \times 10^6$	2.0	0.845

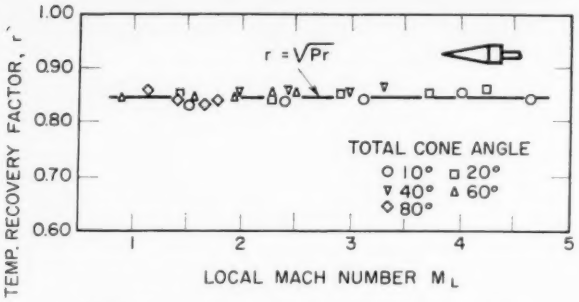

RECOVERY FACTOR FOR LAMINAR BOUNDARY LAYER FLOW VS. LOCAL MACH NUMBER.

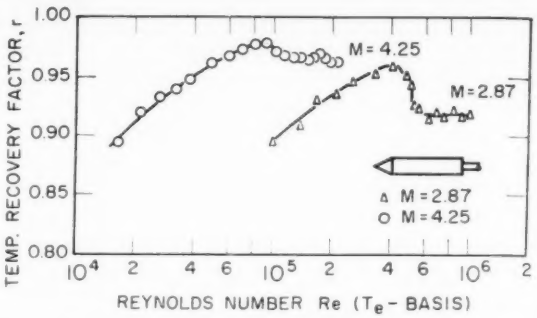

RECOVERY FACTOR FOR A CONE-CYLINDER MODEL VS. REYNOLDS. NUMBER.

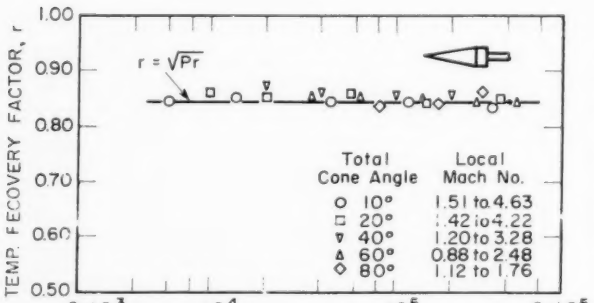

RECOVERY FACTOR FOR LAMINAR BOUNDARY LAYER FLOW VS. LOCAL MACH NUMBER.

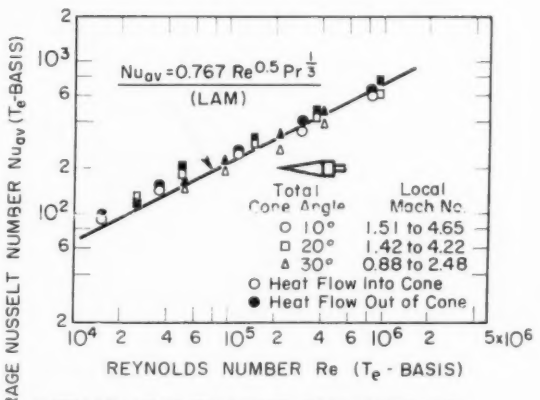
AVERAGE NUSSELT NUMBER Nu_{av} (T_e-BASIS)
$Nu_{av} = 0.767\ Re^{0.5}\ Pr^{\frac{1}{3}}$
(LAM)
Total Cone Angle
Local Mach No.
○ 10° 1.51 to 4.65
□ 20° 1.42 to 4.22
△ 30° 0.88 to 2.48
○ Heat Flow Into Cone
● Heat Flow Out of Cone
10^3
10^2
10^4 2 4 6 10^5 2 4 6 10^6 2 5×10^6
REYNOLDS NUMBER Re (T_e - BASIS)

AVERAGE HEAT TRANSFER FOR CONES WITH LAMINAR BOUNDARY LAYER VS. REYNOLDS NUMBER.

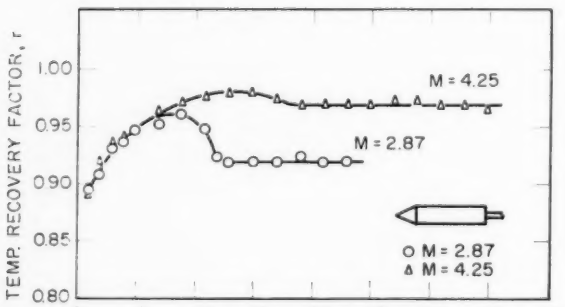

RECOVERY FACTOR ALONG A 40° CONE-CYLINDER.

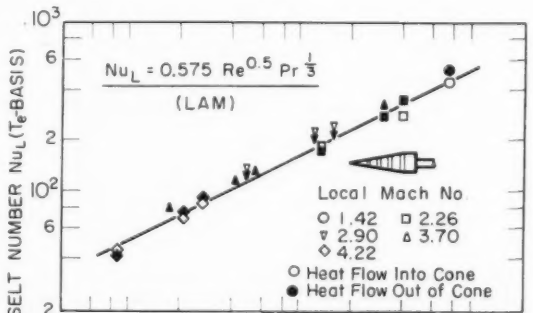
LOCAL NUSSELT NUMBER Nu_L (T_e-BASIS)
$Nu_L = 0.575\ Re^{0.5}\ Pr^{\frac{1}{3}}$
(LAM)
Local Mach No
○ 1.42 □ 2.26
▽ 2.90 △ 3.70
◇ 4.22
○ Heat Flow Into Cone
● Heat Flow Out of Cone
10^3
10^2
4 6 10^4 2 4 6 10^5 2 4 6 10^6 2
REYNOLDS NUMBER Re (T_e - BASIS)

LOCAL HEAT TRANSFER FOR CONES WITH LAMINAR BOUNDARY LAYER VS. REYNOLDS NUMBER.

FIG. H-EBER[14] - 1952

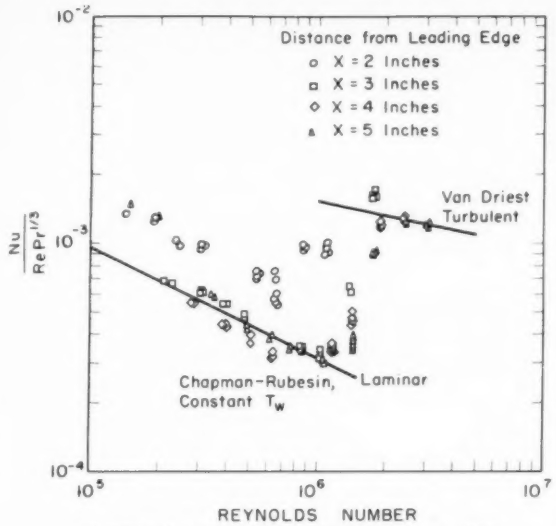

DIMENSIONLESS REPRESENTATION OF HEAT-TRANSFER DATA REFERRED TO THE CASE OF CONSTANT-SURFACE TEMPERATURE

FIG. I - SLACK[16] - 1952

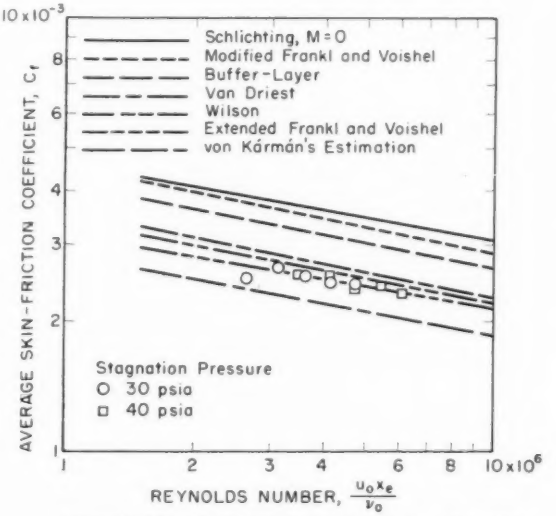

COMPARISON OF SEVERAL ANALYTICAL METHODS WITH EXPERIMENTAL SKIN-FRICTION COEFFICIENTS ALONG A FLAT PLATE, M=2.5

FIG. J - RUBESIN, MAYDEW, AND VARGA[20] - 1951

the data shown in Fig. I (Slack[16]—Fig. 9), corrected for variable surface temperature, scatter from −15 to +100 per cent relative to the theoretical line of Chapman and Rubesin[18] for constant wall temperature.

The heat-transfer coefficients of Eber,[14] some of which are shown in Fig. H, for cones with Mach Numbers ranging from 0.88 to 4.2, scatter from his correlation line by about ±20 per cent. His correlation for cones agreed well with the theoretical value for flat plates when the appropriate conversion was made from cone-type flow to flat-plate flow.

The local heat-transfer coefficients of Scherrer and Gowen[19] for a cone at a Mach Number of 2.0 indicated agreement within 10 per cent of the theoretical value at the base of the cone but showed a large difference of 50 per cent at the nose.

(C) *Theoretical Work on Turbulent Boundary Layer*

The problems of turbulence in general, of the turbulent boundary layer in particular, and of transition from a laminar to a turbulent boundary layer are probably the most important problems in fluid mechanics whose detailed nature and mechanism are not understood. Hence, all theoretical investigations on turbulent boundary layers are based on arbitrary and simplified models or sets of assumptions, which in turn permit the calculation of desired quantities to a first approximation. The extraordinary feature is that the results based on these arbitrary models agree fairly well with the available experimental data in many cases.

(*1*) *Skin-Friction Coefficient for Turbulent Boundary Layer.*—Several reviews have been presented of the many and various models used for the turbulent boundary layer in supersonic flow. In order to keep the size of this survey within bounds, the excellent review given by Rubesin, Maydew, and Varga[20] will be the only one discussed here. The basis of these models is to use one set of properties, velocity profiles, etc., for the laminar sublayer and another set of properties, eddy viscosity, velocity profiles, etc., for the turbulent portion of the boundary layer. Most of these models depend on slightly different methods of integration of

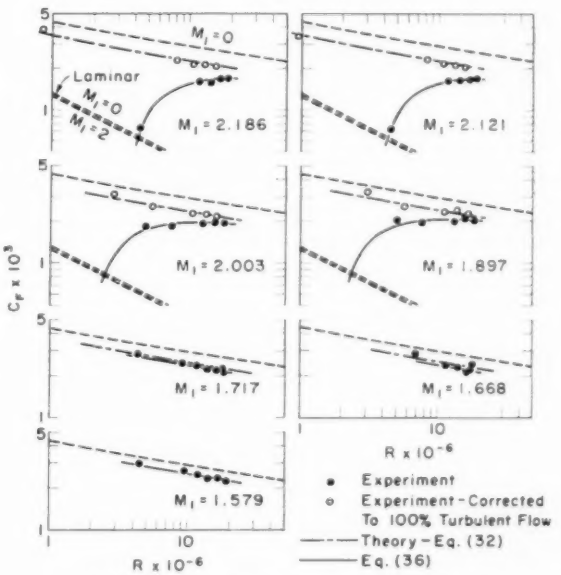

MEAN TURBULENT SKIN FRICTION COEFFICIENT—THEORY AND EXPERIMENT

FIG. K - WILSON[21] - 1950

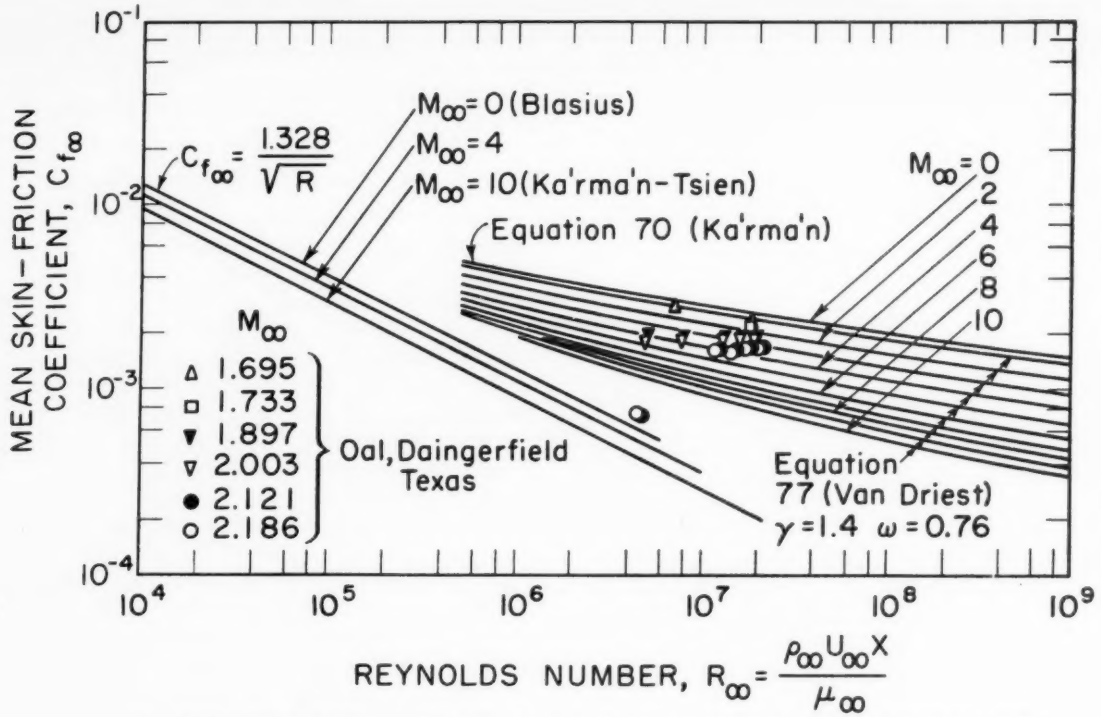

MEAN TURBULENT SKIN FRICTION AS A FUNCTION OF REYNOLDS NUMBER AND MACH NUMBER FOR ZERO HEAT TRANSFER

FIG. L—VAN DRIEST[22] —1951

the von Kármán momentum integral for the turbulent boundary layer. The resulting formulas for local and average skin-friction coefficients for a flat plate are not simple; for this reason the theoretical results are shown here only in chart form.

The friction coefficients of Rubesin, Maydew, and Varga,[20] obtained by extending the original analysis of Frankl and Voishel, are shown in Fig. J (Rubesin, Maydew, and Varga[20]—Fig. 9) for a Mach Number of 2.5. Wilson[21] extended von Kármán's analysis for incompressible flow to include the effects of compressibility. His results are shown in Fig. K (Wilson[21]—Fig. 6). Van Driest[22] derived the continuity, momentum, and energy equations for turbulent flow of a compressible fluid and used an eddy Prandtl Number of unity. He developed a general formula for skin friction including heat transfer. One of his charts for skin friction is shown in Fig. L (Van Driest[22]—Fig. 18).

Donaldson[23] rederived the form of the incompressible turbulent skin-friction law for a plate so as to extend it to compressible flow with an arbitrary set of velocity profiles. His theoretical values compare very well up to a Mach Number of 5 with those of Van Driest[22] and Rubesin, Maydew, and Varga[20] based on more complicated analyses.

(2) *Recovery Factors for Turbulent Boundary Layer.*—The theoretical work on recovery factors is limited to the assumption of constant properties in the turbulent portion of the boundary layer—i.e., to a constant value of eddy viscosity and eddy conductivity. The early

TABLE 3
Data on Skin Friction for Turbulent Boundary Layer

Author	Date	Model	Reynolds Number	Mach Number	Method
Wilson[21]	1950	Flat plate	-19×10^6	2.2	Velocity profiles
Rubesin, Maydew, and Varga[20]	1951	Flat plate	-6×10^6	2.5	Velocity profiles
Potter[7]	1952	Cones, cone-cylinders	-8×10^6	1.86–4.24	Drag forces
Bloom[25]	1952	Flat plate	-10×10^6	5.5	Velocity profiles
Brinich and Diaconis[26]	1952	Hollow cylinder	-14×10^6	3.05	Velocity profiles, Schlieren observations
Coles[10]	1952	Flat plate	-10×10^6	4.5	Floating element
Coles and Goddard[11]	1952	Flat plate	-10×10^6	4.5	Floating element

work of Ackermann, using a kinetic-theory model, showed the recovery factor to be equal to the cube root of the laminar Prandtl Number for Prandtl Numbers greater than 0.5 and less than 2. Other analyses gave similar results except that a decrease of recovery factor with increasing Mach Number was indicated.

The work of Tucker and Maslen[24] extended the incompressible analysis of Squire for a flat insulated plate to compressible flow. Their results can be represented by the following approximate rule within 1 per cent:

$$\ln r = \left[\frac{N + 1 + 0.528M_\infty^2}{3N + 1 + M_\infty^2}\right] \ln Pr$$

where Pr is the laminar Prandtl Number evaluated at the adiabatic wall temperature, M_∞ is the free-stream Mach Number, and N is the reciprocal of the exponent of the turbulent boundary-layer velocity profile approximated by the power law. This relation holds for Prandtl Numbers greater than 0.65 and less than 0.75. This relation reduces to the cube-root rule of Ackermann for zero Mach Number and large value of N or large Reynolds Numbers.

(3) Heat-Transfer Coefficients for Turbulent Boundary Layer.—The theoretical work on heat-transfer coefficients for a turbulent boundary layer is limited to the analysis by Van Driest[22] and to the use of the Reynolds analogy for the work on skin-friction coefficients by Rubesin, Maydew, and Varga.[20] The results of Van Driest's analysis are shown in a series of charts in Fig. M (Van Driest[22]—Figs. 1, 2, 3, and 5) covering a range of Mach Numbers from 0 to 6 and several values of the ratio of wall temperature to free-stream temperature.

(D) *Experimental Work on Turbulent Boundary Layer*

(1) Data on Skin-Friction Coefficient for Turbulent Boundary Layer.—Most of the experimental work on skin-friction coefficients for a turbulent boundary layer in supersonic flow is summarized in Table 3. Since none of the experimental models had a completely turbulent boundary layer from the leading edge, it was necessary to make a correction for the laminar portion of the total boundary layer. This correction altered the measured value of the local coefficient by 10 to 500 per cent.

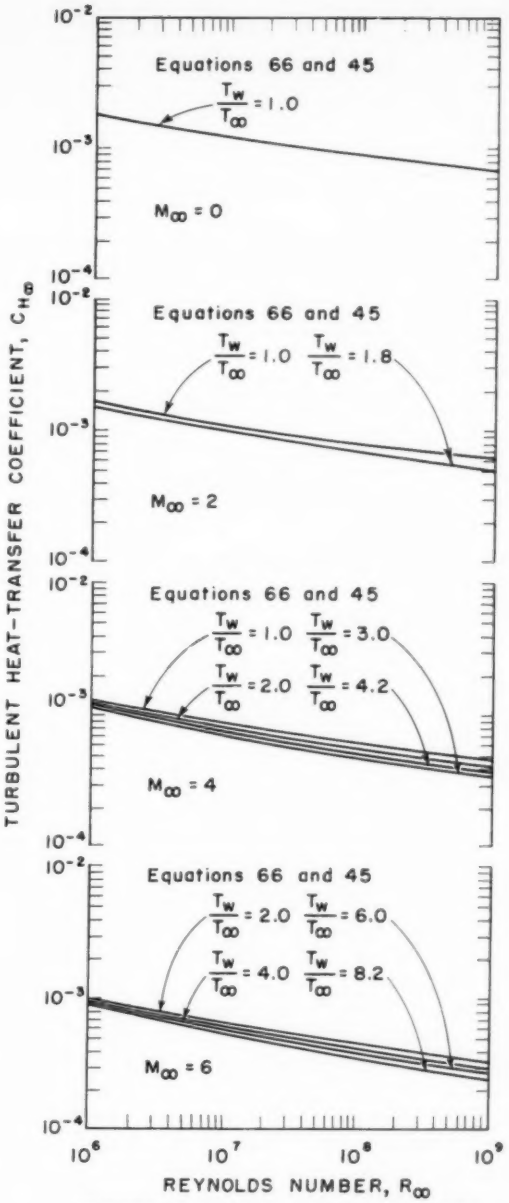

TURBULENT HEAT-TRANFER COEFFICIENT FOR AIR

FIG. M-VAN DRIEST[22]-1951

TABLE 4

Data on Recovery Factors for Turbulent Boundary Layer

Author	Date	Model	Reynolds Number	Mach Number	Recovery Factor
Wimbrow[12]	1949	Cone	-2.7×10^6	2.0	0.885 ± 0.008
		Paraboloid	-4.8×10^6	1.5	0.902 ± 0.005
				2.0	0.894 ± 0.008
Stalder, Rubesin, and Tendeland[13]	1950	Flat plate	-7×10^6	2.4	$0.884 - 0.897 \pm 0.007$
Hilton[27]	1951	Flat plate	-10×10^6	2.0	0.880 ± 0.004
Eber[14]	1952	Cone and cone-cylinder	-1×10^6	2.87	0.92
			-0.25×10^6	4.25	0.97
des Clers and Sternberg[15]	1952	Cone and cone-cylinder	-7×10^6	2-3.4	0.882 ± 0.007
Slack[16]	1952	Flat plate	-3×10^6	2.4	0.906
Stine and Scherrer[17]	1952	10° Cone	$0.4 - 4 \times 10^6$	1.97-3.77	0.882 ± 0.008
		40° Cone-cylinder	$0.3 - 1 \times 10^6$	3.10-3.77	0.885 ± 0.011

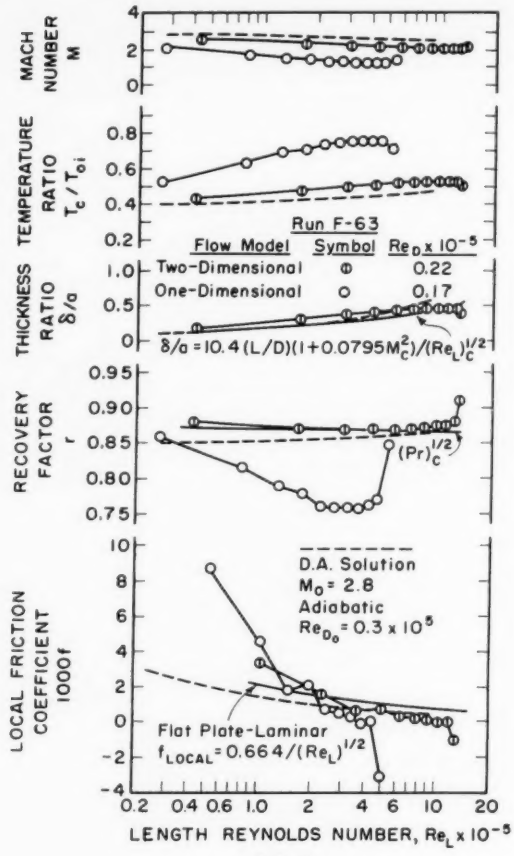

FIG. N

With the exception of the work of Potter[7] on cones, the experiments of the other investigators in Table 3, showed consistent values of turbulent skin-friction coefficients which agreed within about 10 per cent of the theories of Wilson,[21] of Rubesin, Maydew, and Varga,[20] and of Van Driest.[22] In order to test these theories to better than an error of 10 per cent, it appears necessary to measure turbulent skin-friction coefficients to a much smaller error. If, however, the variable effects of transition are considered, this requirement appears to be a difficult condition to achieve in tests.

(2) *Data on Recovery Factors for Turbulent Boundary Layer.*—It is evident from the data in Table 4 that, with the exception of Eber's data on cones and cone-cylinders and possibly Slack's data on a flat plate, the recovery factors for a fully turbulent boundary layer agree to within 1 per cent with the theoretical approximate rule—i.e., equal to the cube root of the Prandtl Number. Furthermore, the data indicate that these recovery factors are independent of Reynolds Number and Mach Number over the ranges tested. The theoretical work of Tucker and Maslen[24] does not agree with these experimental results.

(3) *Data on Heat-Transfer Coefficients for Turbulent Boundary Layer.*—Experimental data on heat-transfer coefficients for a turbulent boundary layer in supersonic flow are almost nonexistent. Eber[14] has measured a few heat-transfer coefficients on a cone at a Mach Number of 2.87 and over a limited range of Reynolds Numbers from 0.4 to 0.9 × 10^6; he found his values of the Nusselt Number to scatter from +10 to −40 per cent relative to the well-known Colburn equation for *subsonic* flow in a turbulent boundary layer—i.e.,

$$Nu = 0.029 Re^{0.8} Pr^{1/3} \tag{5}$$

Slack[16] has also measured some heat-transfer coefficients for a flat plate at a Mach Number of 2.4 and over a Reynolds Number from 1.8 to 3 × 10^6. The 20 odd points are shown in Fig. I (Slack[16]—Fig. 9).

M.I.T.-ONR PROGRAM

A research program, sponsored by the Office of Naval Research, has been under way for several years in the Department of Mechanical Engineering, with the objective of obtaining reliable data on the rate of heat transfer to air moving at supersonic speeds in a round tube. This program consists of two separate parts. In the first part, a well-insulated apparatus was used to measure the values of the local adiabatic wall temperature and local static pressure of a super-

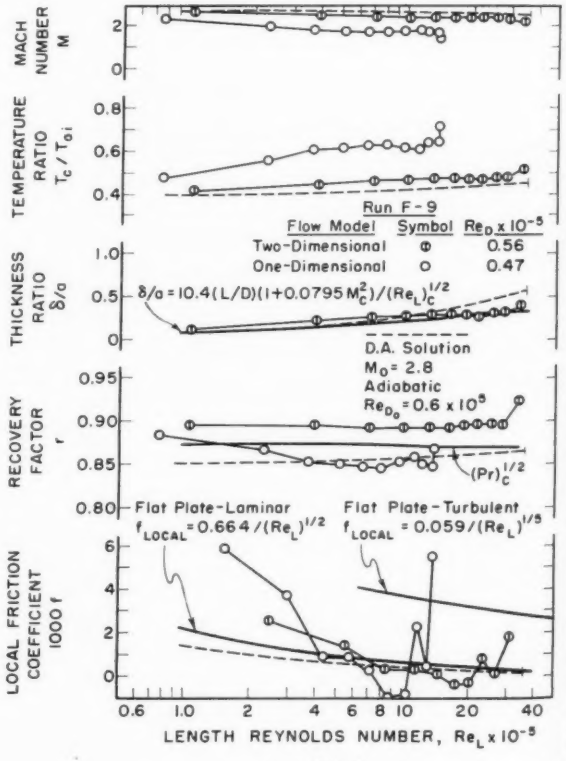

FIG. O

sonic stream of air in a tube with an entrance Mach Number of 2.8. In the second part, an apparatus using steam condensing outside a round brass tube was used to measure local coefficients of heat transfer to a similar supersonic stream of air from the same nozzle.

The results of the first part of this program are available in references 31, 32, and 33; hence, these data will not be discussed in detail. The results of some preliminary measurements of heat-transfer coefficients will be given. In addition, preliminary results will be given of some theoretical work for the compressible laminar boundary layer in the entrance region of a round tube.

(*1*) *Adiabatic Flow in Tube.*—Figs. N, O, and P present some typical results for supersonic flow of air in a round tube under adiabatic conditions for the case where a laminar boundary layer appears to exist in the tube. The calculated quantities are determined from two flow models: the first corresponding to the usual one-dimensional flow model based on constant properties at any cross section, and the second based on a two-dimensional flow model where the properties vary over the cross section of the tube. In addition, the preliminary calculations obtained from the M.I.T. Differential Analyzer in the solution of the theoretical problem, from the Doctoral Thesis of Toong,[34] are also shown.

The local coefficients of friction based on the two-dimensional flow model are in fair agreement with the values for a flat plate and the theoretical values for a tube, where it appears that a laminar boundary layer exists in the tube. In Fig. P, this agreement is excellent.

The recovery factors based on the two-dimensional flow model vary from 0.87 to 0.89 for that portion of the tube flow where it appears that a laminar boundary layer exists. These values are 2–3 per cent larger than the theoretical values for a laminar boundary layer on a flat plate with zero pressure gradient.

The calculated thickness of the laminar boundary layer in the tube, based on the two-dimensional flow model, is also shown in Figs. N, O, and P. The agreement between this quantity and the thickness determined from Howarth's flat-plate formula and from the Differential Analyzer solution is excellent for this type of calculation.

(*2*) *Heat-Transfer Measurements in the Tube.*—Preliminary heat-transfer data are shown in Fig. Q for the case where a laminar boundary layer appears to exist in the supersonic flow in the tube. The scatter present in these data is typical of most measurements of local heat-transfer coefficients. The data agree well with the theoretical value for a flat plate with zero pressure gradient and with the Differential Analyzer solution for tube flow.

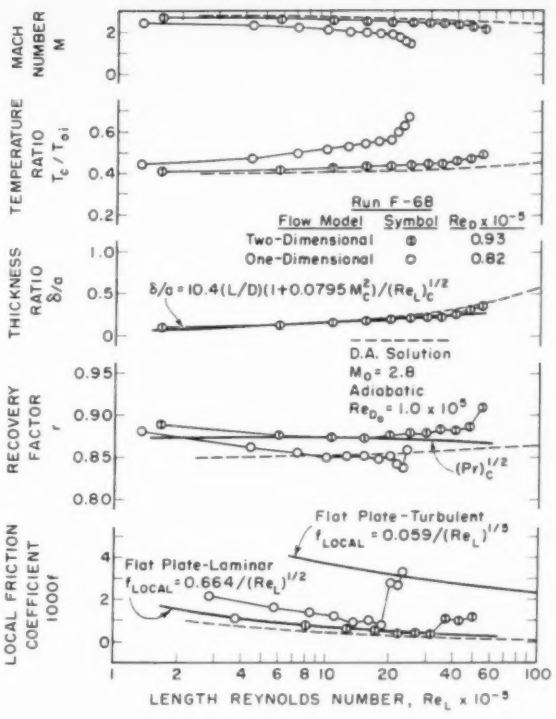

FIG. P

M.I.T.-OAR Program

A research program, sponsored by the Office of Air Research, was started about 1 year ago as a joint effort of the Departments of Aeronautical Engineering and Mechanical Engineering with the objective of obtaining reliable data on heat-transfer coefficients to air moving at supersonic speeds over a flat plate. The experimental program is being carried on at the M.I.T. Naval Supersonic Wind Tunnel over a range of Mach Numbers from 1.9 to 3.1 and up to a length Reynolds Number of 17×10^6.

This program has been divided in two parts. The first part consists of an attempt to secure a flat-plate model that corresponds as nearly as possible to an insulated flat plate. On this model the local recovery factors and velocity profiles in the boundary layer could be measured. Thus the type of boundary layer present on the plate could be identified. The second part of the program will be concerned with construction of a separate flat-plate model made of brass to secure local heat-transfer coefficients by use of condensing steam. Velocity profiles will be measured to determine the type of boundary layer present on the heated plate. The effects of turbulence promoters and of large temperature differences between the free stream and wall will be investigated.

To date the insulated plate tests have indicated that the recovery factor for a laminar boundary layer, properly corrected for the effect of the heated nose resulting from the shock at the nose is 0.850 ± 0.005 for Mach Numbers from 1.9 to 3.1. This value agrees within 1 per cent with the theoretical value based on the square root of the Prandtl Number evaluated at the adiabatic wall temperature and also agrees with similar data on cones.

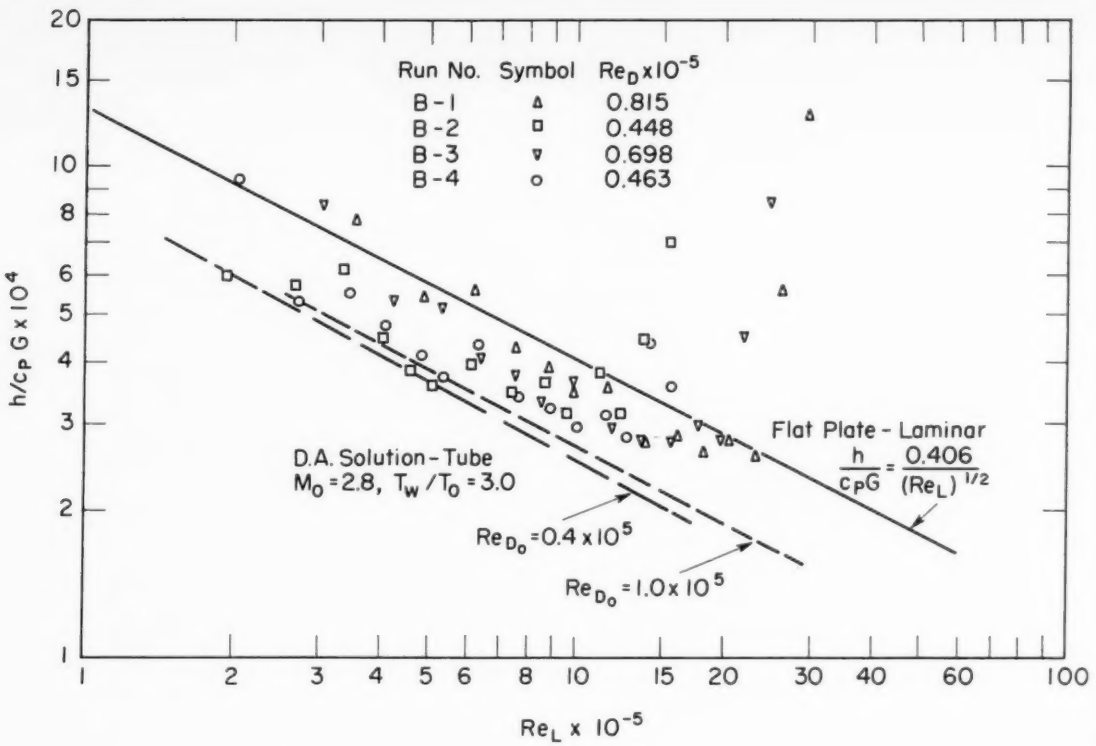

STANTON NUMBER VS. LENGTH REYNOLDS NUMBER

FIG. Q

The recovery factor for a turbulent boundary layer is 0.881 ± 0.003 for Mach Numbers of 1.9 to 3.1 and up to a Reynolds Number of 17 × 10^6. Within $^1/_2$ per cent, this recovery factor is independent of Mach Number and of Reynolds Number over the ranges measured.

Conclusions

In 1948, the author examined the problem of the transient temperature distribution in a wing moving at supersonic speeds; he found it necessary to review the state of the art relative to heat transfer at supersonic speeds. One conclusion reached at that time was that the state of the art was relatively undeveloped and that a considerable amount of theoretical and experimental work was required to improve it significantly.

In the past 4 years significant contributions have been made to both the theoretical and experimental work on laminar boundary layers up to about a Mach Number of 3. Small discrepancies between theory and experiment still exist in this range for friction coefficients and recovery factors. Additional experimental data are greatly needed for heat-transfer coefficients. The greatest need is to extend the experimental data beyond a Mach Number of 3 and to investigate problems such as the effect of a pressure gradient, the effect of radiation, the effect of transition, the properties of air at temperatures of the order 3,000°F, etc.

In the past 4 years several significant contributions have been made to the theory of the turbulent boundary layer for supersonic flow; these have been based on arbitrary models or assumptions because of the lack of knowledge of the details of turbulence. The experimental data on skin-friction coefficients and recovery factors for turbulent boundary layers have been extended to a Mach Number of about 3 and a length Reynolds Number of about 20 × 10^6. It is curious that for this case where the basis of the theory of the turbulent boundary layer is fairly uncertain, the agreement between the predicted and measured values of the skin-friction coefficient and recovery factor is the best of all available comparisons at the moment. There is a great need for reliable data on heat-transfer coefficients for turbulent boundary layers, since, practically speaking, none is available. The experimental work for the turbulent boundary layer should be extended to higher Mach Numbers and to larger Reynolds Numbers; the effects of pressure gradient, radiation, etc., should be investigated.

References

[1] Kuerti, G., *The Laminar Boundary Layer in Compressible Flow*, Advances in Applied Mechanics, Vol. II; Academic Press, Inc., New York, 1951.

[2] Moore, L. L., *A Solution of the Laminar Boundary-Layer Equations for a Compressible Fluid with Variable Properties, Including Dissociation*, Journal of the Aeronautical Sciences, Vol. 19, No. 8, pp. 505–518, August, 1952.

[3] Van Driest, E. R., *Investigation of Laminar Boundary Layer in Compressible Fluids Using the Crocco Method*, NACA TN No. 2597, January, 1952.

[4] Blue, R. E., *Interferometer Corrections and Measurements of Laminar Boundary Layers in Supersonic Stream*, NACA TN No. 2110, June, 1950.

[5] Higgins, R. W., and Pappas, C. C., *An Experimental Investigation of the Effect of Surface Heating on Boundary Layer Transition on a Flat Plate in Supersonic Flow*, NACA TN No. 2351, April, 1951.

[6] Maydew, R. C., and Pappas, C. C., *Experimental Investigation of the Local and Average Skin Friction in the Laminar Boundary Layer on a Flat Plate at a Mach Number of 2.4*, NACA TN No. 2740, July, 1952.

[7] Potter, J. L., *New Experimental Investigations of Friction Drag and Boundary Layer Transition on Bodies of Revolution at Supersonic Speeds*, NAVORD Report 2371, U.S. Naval Ordnance Laboratory, April 1952.

[8] Liepmann, H. W., and Dhawan, S., *Direct Measurements of Local Skin Friction in Low-Speed and High-Speed Flow*, 1st U.S. National Congress of Applied Mechanics, pp. 869–874, 1951.

[9] Dhawan, S., *Direct Measurements of Skin Friction*, NACA TN No. 2567, January, 1952.

[10] Coles, D., *Direct Measurements of Supersonic Skin Friction*, Readers' Forum, Journal of the Aeronautical Sciences, Vol. 19, No. 10, p. 717, October, 1952.

[11] Coles, D., and Goddard, F. E., Jr., *Direct Measurement of Skin Friction on a Smooth Flat Plate at Supersonic Speeds*, Eighth International Congress on Theoretical and Applied Mechanics, Istanbul, Turkey, August, 1952.

[12] Wimbrow, W. R., *Experimental Investigation of Temperature Recovery Factors on Bodies of Revolution*, NACA TN No. 1975, October, 1949.

[13] Stalder, J. R., Rubesin, M. W., and Tendeland, T., *A Determination of the Laminar-, Transitional-, and Turbulent-Boundary-Layer Temperature-Recovery Factors on a Flat Plate in Supersonic Flow*, NACA TN No. 2077, June, 1950.

[14] Eber, G. R., *Recent Investigation of Temperature Recovery and Heat Transmission on Cones and Cylinders in Axial Flow in the N.O.L. Aeroballistics Wind Tunnel*, Journal of the Aeronautical Sciences, Vol. 19, No. 1, pp. 1–6, January, 1952.

[15] des Clers, B., and Sternberg, J., *On Boundary-Layer Temperature Recovery Factors*, Readers' Forum, Journal of the Aeronautical Sciences, Vol. 19, No. 9, pp. 645–646, September, 1952.

[16] Slack, E. G., *Experimental Investigation of Heat Transfer Through Laminar and Turbulent Boundary Layers on a Cooled Flat Plate at a Mach Number of 2.4*, NACA TN No. 2686, April, 1952.

[17] Stine, H. A., and Scherrer, R., *Experimental Investigation of the Turbulent-Boundary-Layer Temperature-Recovery Factor on Bodies of Revolution at Mach Numbers from 2.0 to 3.8*, NACA TN No. 2664, March, 1952.

[18] Chapman, D. R., and Rubesin, M. W., *Temperature and Velocity Profiles in the Compressible Laminar Boundary with Arbitrary Distribution of Surface Temperature*, Journal of the Aeronautical Sciences, Vol. 16, No. 9, pp. 547–565, September 1949.

[19] Scherrer, R., and Gowen, F. E., *Comparison of Theoretical and Experimental Heat Transfer on a Cooled 20° Cone with a Laminar Boundary Layer at a Mach Number of 2.02*, NACA TN No. 2087, May, 1950.

[20] Rubesin, M. W., Maydew, R. C., and Varga, S. V., *An Analytical and Experimental Investigation of the Skin Friction of the Turbulent Boundary Layer on a Flat Plate at Supersonic Speeds*, NACA TN No. 2305, February, 1951.

[21] Wilson, R. E., *Turbulent Boundary-Layer Characteristics at Supersonic Speeds—Theory and Experiment*, Journal of the Aeronautical Sciences, Vol. 17, No. 9, pp. 585–594, September, 1950.

[22] Van Driest, E. R., *Turbulent Boundary Layer in Compressible Fluids*, Journal of the Aeronautical Sciences, Vol. 18, No. 3, pp. 145–160, March, 1951.

[23] Donaldson, C. du P., *On the Form of the Turbulent Skin-Friction Law and Its Extension to Compressible Flows*, NACA TN No. 2692, May, 1952.

[24] Tucker, M., and Maslen, S. H., *Turbulent Boundary-Layer Temperature Recovery Factors in Two-Dimensional Supersonic Flow*, NACA TN No. 2296, February, 1951.

[25] Bloom, H. L., *Preliminary Survey of Boundary-Layer Development at a Nominal Mach Number of 5.5*, NACA RM E52D03, June, 1952.

[26] Brinich, P. F., and Diaconis, N. S., *Boundary-Layer Development and Skin Friction at Mach Number 3.05*, NACA TN No. 2742, July, 1952.

[27] Hilton, W. F., *Wind-Tunnel Tests for Temperature Recovery Factors at Supersonic Velocities*, Journal of the Aeronautical Sciences, Vol. 18, No. 2, pp. 97–100, February, 1951.

[28] Lighthill, M. J., *Contributions to the Theory of Heat Transfer Through a Laminar Boundary Layer*, Proc. Royal Soc. A, Vol. 202, pp. 359–377, 1950.

[29] Klunker, E. B., and McLean, F. E., *Laminar Friction and Heat Transfer at Mach Numbers from 1 to 10*, NACA TN No. 2499, October, 1951.

[30] Young, G. B. W., and Janssen, E., *The Compressible Boundary Layer*, Journal of the Aeronautical Sciences, Vol. 19, No. 4, pp. 229–236, April, 1952.

[31] Kaye, J., Keenan, J. H., and McAdams, W. H., *Report of Progress on Measurements of Friction Coefficients for Supersonic Flow of Air in a Pipe*, Heat Transfer and Fluid Mechanics Institute, pp. 147–164, June, 1949.

[32] Kaye, J., Keenan, J. H., Klingensmith, K. K., Ketchum, G. M., and Toong, T. Y., *Measurement of Recovery Factors and Friction Coefficients for Supersonic Flow of Air in a Tube; Part I—Apparatus, Data and Results Based on a Simple One-Dimensional Flow Model*, J. Applied Mech., Vol. 19, No. 1, pp. 77–96, March, 1952.

[33] Kaye, J., Toong, T. Y., and Shoulberg, R. H., *Measurement of Recovery Factors and Friction Coefficients for Supersonic Flow of Air in a Tube; Part II—Results Based on a Two-Dimensional Flow Model for Entrance Region*, J. Applied Mech., Vol. 19, No. 2, pp. 185–194, June, 1952.

[34] Toong, T. Y., *The Laminar Boundary Layer of a Steady Compressible Flow in the Entrance Region of a Tube*, Sc.D. Thesis, M.I.T., January, 1952.

Readers' Forum

BRIEF REPORTS of investigations in the aeronautical sciences and discussions of papers published in the JOURNAL are presented in this special department. The publication will be completed as soon as possible after receipt of the material. The Editorial Committee does not hold itself responsible for the opinions expressed by the correspondents. Contributions should not exceed 800 words in length.

Note on an Interaction Between the Boundary Layer and the Inviscid Flow

Antonio Ferri and Paul A. Libby
Department of Aeronautical Engineering and Applied Mechanics, Polytechnic Institute of Brooklyn, Brooklyn, N.Y.
November 2, 1953

ACCORDING TO THE CLASSICAL boundary-layer theory the flow about bodies at Reynolds Numbers of aeronautical interest can be considered as composed of two régimes: an outside inviscid flow and a thin boundary-layer region adjacent to the body. This point of view leads to the approximation that, on a slightly curved surface, $\partial p/\partial y$ throughout the layer is negligibly small. The additional assumption that the inviscid flow is irrotational leads to the requirement that $\partial u/\partial y$ is zero at the outer edge of the boundary layer. In this theory any interaction between the two régimes is accountable by a simple correction to the body shape based on the boundary-layer displacement thickness.

Recently, in connection with hypersonic laminar boundary layers, this classical point of view has been modified; an interaction between the two flow régimes leading to a self-induced axial pressure gradient has been considered. It is the purpose of the present note to point out another type of interaction which may be of practical importance and of fundamental interest even at Mach Numbers below those considered in the hypersonic boundary-layer theory and which may have to be considered in that theory.

This interaction may be discussed from the following point of view: It is evident that the division of the flow field into the aforementioned two régimes is somewhat arbitrary but well defined for low-speed flow. However, in what would correspond to the inviscid régime for supersonic flow, it is possible to generate, by means of upstream highly curved shock waves, a flow region adjacent to the surface with large entropy gradients and large vorticity. In such regions the pressure and velocity are not uniquely related, and thus for slightly curved surfaces $\partial p/\partial y$ can still be small, although $\partial u/\partial y$ can be on the same order of magnitude as exists in classical laminar boundary layers. This possibility seems to require a modification of the classical approach when highly curved shock waves exist at the leading edge.

In order to indicate the practical importance of this interaction, consider two slender bodies of revolution. The first is sharp-nosed and has the usual almost conical shock wave. The second has the identical shape except for a rounded nose that fairs rapidly into the same contour as the first body. It is pointed out that the ogive of minimum pressure drag is just such a rounded nose body. At the nose of this second body will be a highly curved shock that generates a layer of large entropy gradients and high vorticity close to the surface of the body. Somewhat downstream of the nose of this second body the pressure, as determined by inviscid flow theory, will be essentially uniform through this vorticity layer and will be equal to that at the corresponding point of the first body. However, the velocity at the wall will be less in the second body.

If, now, boundary-layer calculations are made for the two bodies, it is clear that this vorticity layer has two effects: The velocity at the "outer edge" of the boundary layer in the classical sense is reduced, and $\partial u/\partial y$ there is not zero. Both alterations are functions of the local displacement thickness and of the vorticity distribution, are interdependent, and tend to reduce the skin friction and heat transfer if the boundary layer remains laminar. It is not evident what the influence of the outside vorticity on the transition would be. If the boundary layer is turbulent on both bodies, the outside vorticity would probably have a marked influence on the turbulent skin friction and heat transfer.

The fundamental significance of this type of interaction between the essentially inviscid and the boundary-layer flows appears to be that the division of the flow into separate régimes is not well defined for this case. The boundary between the regions in which shear stresses are and are not important is not well defined.

To develop some feeling for this interaction, the following analysis was carried out: An incompressible, constant pressure, laminar boundary layer was superposed on an inviscid vorticity layer of a given thickness. The velocity in the vortex layer was assumed to vary from a value at the wall of 90 per cent of free stream to the free-stream value within the thickness of the vorticity layer. The boundary layer was required to be thin compared with the vorticity layer so that displacement effects were small. Consequently, the values of $\partial u/\partial y$ at the outer edge were small although included in the analysis. As in the usual integral approach, the boundary-layer equation was integrated from the wall to a boundary-layer thickness $\delta = \delta(x)$. Within this layer, the viscous stresses were thus taken to be significant. At $y = \delta$, the velocity and velocity gradient $\partial u/\partial y$ were matched to the corresponding values in the inviscid flow at $y = \delta$. At the wall, the usual no-slip conditions were imposed. The skin friction was thus found as a function of Reynolds Numbers based on vorticity-layer thickness and on distance from the leading edge and of the per cent deficiency in the inviscid wall velocity. The results of this simple analysis indicate a reduction in skin friction of about 15 per cent. It is pointed out that this deficiency is on the order of what can be expected in high supersonic flow. These results appear to be insensitive to the thickness of the vorticity layer probably because the boundary-layer thickness was required to be small compared to the same.

These considerations seem to indicate that the influence of upstream highly curved shock waves on boundary-layer characteristics warrants further investigation.

Aerodynamic Flutter Coefficients for an Airfoil with Leading- and Trailing-Edge Flaps in Two-Dimensional Supersonic Flow

Hermann J. Hassig
Dynamics Engineer, Lockheed Aircraft Corporation, Burbank, Calif.

November 9, 1953

SUPERSONIC TWO-DIMENSIONAL AERODYNAMIC FLUTTER COEFFICIENTS for a wing with leading- and trailing-edge flaps are presented in terms of the coefficients for a wing without flaps.

With the help of the results in reference 1, the coefficients, describing the aerodynamic forces and moments on a harmonically oscillating wing with leading- and trailing-edge flap in a two-dimensional supersonic flow, can be expressed in terms of quantities tabulated in references 2 and 3. If these coefficients are used for a strip-type flutter analysis of a wing with arbitrary ratios of leading- and trailing-edge flap chord to wing chord, numerous rather inaccurate interpolations are required. Because interpolations for hinge axes position and for the value of k are necessary, they are not amenable to high-speed digital computers.

The purpose of the present note is to express all the required coefficients in terms of the coefficients for the harmonic oscillation of a wing without flaps, thus avoiding the coefficients that depend on the location of the hinge axes as well as their interpolation. An indication that this should be possible for a wing-aileron combination is found in reference 2, where it is stated that $f_0(M, \tilde{\omega})$ is the only quantity that needs evaluation. It can be shown from reference 2 that L_{56}, M_{56}, N_{12}, N_{34}, and N_{56},* all depending on the location of the hinge axis, can be expressed in terms of L_{12}, L_{34}', M_{12}', and M_{34}', which determine the force and moment due to h and α motion for $x_0 = 0$ (Fig. 1). With the help of reference 1, this can be extended to include the leading-edge flap.

However, the required coefficients can be obtained in a much simpler way by taking advantage of the characteristic of supersonic flow that a downstream element cannot have any effect on an upstream element and by using a simple technique of superposition of displacements and loads.

When P, M_α, M_β, and M_γ are, respectively, the complex amplitude of the downward force, the tail-down moment about a reference axis, the tail-down hinge moment of the trailing-edge flap and the nose-up hinge moment of the leading-edge flap due to the complex amplitudes h, α, β, and γ of the displacements (Fig. 1), the following matrix equations can be written

$$\begin{Bmatrix} P \cdot b \\ M_\alpha \\ M_\beta \\ M_\gamma \end{Bmatrix} = -4\rho b^2 v^2 k^2 \begin{bmatrix} A_{hh} & A_{h\alpha} & A_{h\beta} & A_{h\gamma} \\ A_{\alpha h} & A_{\alpha\alpha} & A_{\alpha\beta} & A_{\alpha\gamma} \\ A_{\beta h} & A_{\beta\alpha} & A_{\beta\beta} & A_{\beta\gamma} \\ A_{\gamma h} & A_{\gamma\alpha} & A_{\gamma\beta} & A_{\gamma\gamma} \end{bmatrix} \cdot \begin{Bmatrix} h/b \\ \alpha \\ \beta \\ \gamma \end{Bmatrix} \tag{1}$$

where ρ is the air density, v is the forward speed, k is the reduced frequency $\omega b/v$, and b is the semichord.

In order to demonstrate the method two examples are given.

EXAMPLE (1) DERIVATION OF $A_{h\beta}$

The force on the airfoil due to trailing-edge flap deflection is equal to the force on the flap itself, since a downstream element cannot have any effect on an upstream element. From reference 2, the expression for the force due to α is

$$(P)_\alpha = -4\rho b v^2 k^2 L_{34}'(k)\alpha \tag{2}$$

Replacing b by $(1 - x_1)b$, the semichord of the flap, and α by β, the flap deflection, leads to the following expression for the force on the flap due to β:

$$(P)_\beta = -4\rho(1 - x_1)b v^2(1 - x_1)^2 k^2 L_{34}'[(1 - x_1)k]\beta \tag{3}$$

[It will be noted that L_{34}' is now evaluated at $(1 - x_1)k$ rather than at k.]

Comparison of Eq. (3) with its equivalent term in Eq. (1) leads to

$$A_{h\beta}(k) = (1 - x_1)^2 L_{34}'[(1 - x_1)k] \tag{4}$$

EXAMPLE (2) DERIVATION OF $A_{h\gamma}$

Leading-edge flap deflection γ can be obtained from superposition of the three displacements shown in Fig. 2.

The force on the entire section is determined by the following coefficients:

$$\left.\begin{array}{ll} \text{Due to I:} & L_{34}'(k) \\ \text{Due to II:} & -(1 - x_2)^2 L_{34}'[(1 - x_2)k] \\ \text{Due to III:} & -2x_2 A_{hh}(k) \end{array}\right\} \tag{5}$$

It follows that

$$A_{h\gamma}(k) = L_{34}'(k) - (1 - x_2)^2 L_{34}'[(1 - x_2)k] - 2x_2 A_{hh}(k) \tag{6}$$

Using the technique shown in the above examples, the remaining coefficients in Eq. (1) can be determined. The results are as follows:

* $L_{12} = L_5 + iL_6$, etc.; L_5, L_6, etc., are defined in reference 2.

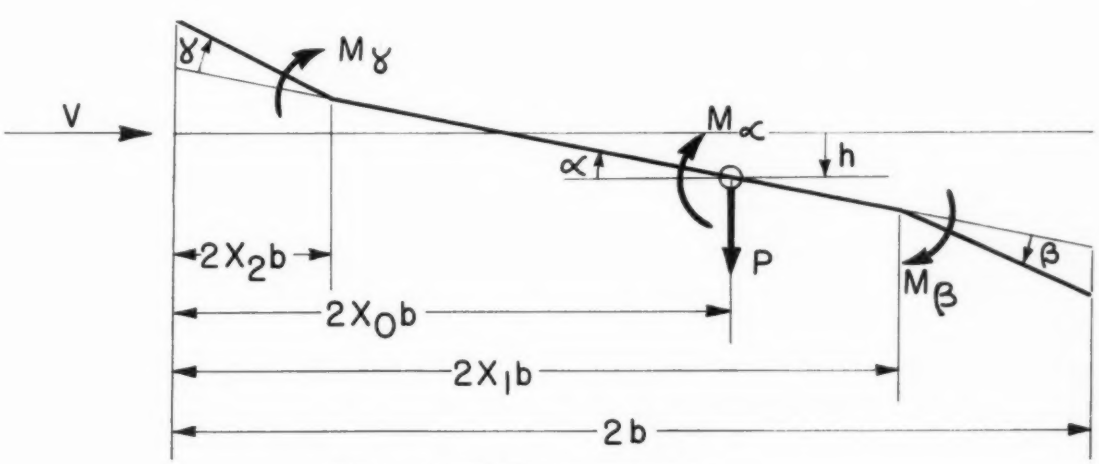

FIG. 1 DEFINITION OF SYMBOLS

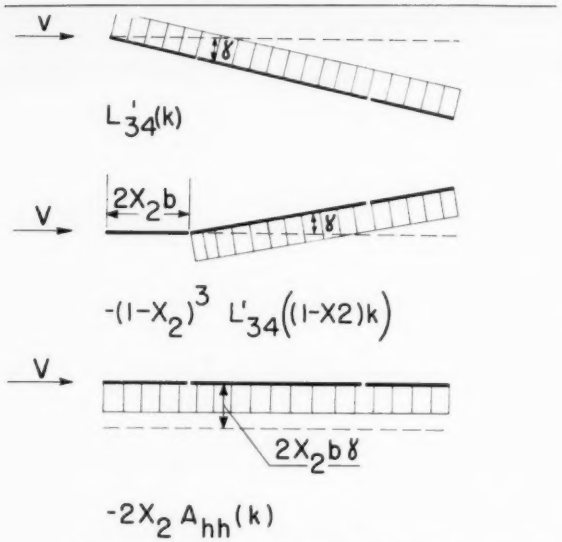

FIG. 2 ILLUSTRATION OF THE DERIVATION OF $A_{h\gamma}(k)$

$$
\begin{aligned}
A_{hh}(k) &= L_{12}(k) \\
A_{h\alpha}(k) &= L_{34}'(k) - 2x_0 A_{hh}(k) \\
A_{h\beta}(k) &= (1 - x_1)^3 L_{34}'[(1 - x_1)k] \\
A_{h\gamma}(k) &= L_{34}'(k) - (1 - x_2)^3 L_{34}'[(1 - x_2)k] - 2x_2 A_{hh}(k) \\
A_{\alpha h}(k) &= M_{12}'(k) - 2x_0 A_{hh}(k) \\
A_{\alpha\alpha}(k) &= M_{34}'(k) - 2x_0\{L_{34}'(k) + A_{\alpha h}(k)\} \\
A_{\alpha\beta}(k) &= A_{\beta\beta}(k) + 2(x_1 - x_0)A_{h\beta}(k) \\
A_{\alpha\gamma}(k) &= M_{34}'(k) - 2x_0 L_{34}'(k) - (1 - x_2)^4 M_{34}'[(1 - x_2)k] + 2(x_0 - x_2)(1 - x_2)^3 L_{34}'[(1 - x_2)k] - 2x_2 A_{\alpha h}(k) \\
A_{\beta h}(k) &= M_{12}'(k) - 2x_1 L_{12}(k) - x_1^3\{M_{12}'(x_1 k) - 2L_{12}(x_1 k)\} \\
A_{\beta\alpha}(k) &= M_{34}'(k) - 2x_1 L_{34}'(k) - x_1^3\{M_{34}'(x_1 k) - 2L_{34}'(x_1 k)\} - 2x_0 A_{\beta h}(k) \\
A_{\beta\beta}(k) &= (1 - x_1)^4 M_{34}'[(1 - x_1)k] \\
A_{\beta\gamma}(k) &= A_{\beta\alpha}(k) + 2x_0 A_{\beta h}(k) - (1 - x_2)^4 M_{34}'[(1 - x_2)k] - 2x_2 A_{\beta h}(k) + 2(x_1 - x_2)(1 - x_2)^3 L_{34}'[(1 - x_2)k] + (x_1 - x_2)^4\{M_{34}'[(x_1 - x_2)k] - 2L_{34}'[(x_1 - x_2)k]\} \\
A_{\gamma h}(k) &= x_2^3\{M_{12}'(x_2 k) - 2L_{12}(x_2 k)\} \\
A_{\gamma\alpha}(k) &= x_2^4\{M_{34}'(x_2 k) - 2L_{34}'(x_2 k)\} - 2x_0 A_{\gamma h}(k) \\
A_{\gamma\beta}(k) &= 0 \\
A_{\gamma\gamma}(k) &= 2(x_0 - x_2)A_{\gamma h}(k) + A_{\gamma\alpha}(k)
\end{aligned}
\qquad (7)
$$

The coefficients L_{12}, L_{34}', M_{12}' and M_{34}' in the above equations are tabulated in reference 2 for several Mach Numbers and for a large range of the argument k. The lowest k value listed is of the order of $k = 0.01$. If a 10 per cent flap chord is used, the lowest k value, based on the semichord b for which the A_{ij} coefficients can be obtained from these tables, is of the order $k = 0.1$. Thus if lower values of k are needed, the tables have to be extended to lower values of the argument k if Eqs. (7) are used.

Although the presented method involves interpolation of L_{12}, L_{34}', M_{12}' and M_{34}' for nontabulated values of the arguments k, it seems, however, that the amount of work involved is much less than when interpolations for hinge axes location, as well as reduced frequency k, are necessary, as is the case when the coefficients in reference 3 are used. This is especially true if Eqs. (7) are used in combination with high-speed digital computers that can do the interpolation. In addition, more significant figures can be obtained. In view of these advantages it appears that the tables for the plain wing given in reference 2 should be extended to very low values of reduced frequency k in preference to extending the tables in reference 3 for additional hinge axis locations and reduced frequencies.

It is also worth noting that the same principles can also be applied for determining the associated indicial functions for a wing with leading- and trailing-edge flaps in terms of the indicial functions for a plain wing. The required indicial functions for a plain wing have been evaluated in closed form in reference 4.

References

[1] Baird, Eugene F., et. al, *Theoretical Aerodynamic Coefficients for an Oscillating Airfoil with Both Leading and Trailing Edge Flaps in a Two-Dimensional Supersonic Flow*, Grumman Aircraft Engineering Corporation, Report No. RE 31.

[2] Garrick, I. E., and Rubinow S. I., *Flutter and Oscillating Air-Force Calculations for an Airfoil in Two Dimensional Supersonic Flow*, NACA Report No. 846. 1946.

[3] Huckel, Vera, and Durling, Barbara J., *Tables of Wing-Aileron Coefficients of Oscillating Air-Forces for Two-Dimensional Supersonic Flow*, NACA TN No. 2055, March, 1950.

[4] Lomax, Harvard, Heaslet, Max. A., and Sluder, Loma, *The Indicial Lift and Pitching Moment for a Sinking or Pitching Two-Dimensional Wing Flying at Subsonic or Supersonic Speeds*, NACA TN No. 2403. July, 1951.

On a Differential Equation Occurring in the Theory of Heat Flow in Boundary Layers with Hartree's Velocity Profiles

Henry E. Fettis

Aeronautical Research Laboratory, Wright-Patterson Air Force Base, Dayton, Ohio

October 30, 1953

In a recent note in this Journal, Schuh[1] derives the equation

$$\frac{d^2\theta}{d\xi^2} + \frac{\xi^2}{2}\frac{d\theta}{d\xi} - \epsilon\xi\theta = 0 \qquad (1)$$

for the temperature variation in the boundary-layer flow about a body. In this equation, θ represents the variation of temperature normal to the body when the variation along the body contour is assumed proportional to a power of the distance. The variable ξ is defined as

$$\xi = \sigma^{1/3} b^{1/3} (2 - \beta)\,(U_1/\nu x)^{1/2} y$$

with

- σ = Prandtl Number
- U_1 = speed of laminar flow = x^m
- β = $2m/2m + 1$
- ν = kinematic viscosity
- ϵ = $n(2 - \beta)$
- x = distance parallel to wall
- y = distance normal to wall
- b = parameter defined by Schuh;[1] (proportional to velocity gradient at wall)

The purpose of this note is to present the solution of Eq. (1) in closed form, subject to the conditions

$$\theta(0) = 1, \qquad \theta(\infty) = 0 \qquad (2)$$

It is first convenient to change the independent variables from ξ to t, where $t = \xi^3/6$. The new equation becomes

$$\frac{d^2\theta}{dt^2} + \left(1 + \frac{2}{3t}\right)\frac{d\theta}{dt} - \frac{2\epsilon}{3t}\theta = 0 \qquad (3)$$

Introducing a new dependent variable defined by

$$\varphi = t^{1/3} e^{t/2}\theta \qquad (4)$$

Eq. (3) is transformed to

$$\frac{d^2\varphi}{dt^2} + \varphi\left[-\frac{1}{4} - \frac{1+2\epsilon}{3t} + \frac{2}{9t^2}\right] = 0 \tag{5}$$

which is the standard form for the Whittaker confluent Hypergeometric Equation (reference 2, Chapter VI, Paragraph 2),

$$\frac{d^2\varphi}{dt^2} + \varphi\left[-\frac{1}{4} + \frac{k}{t} + \frac{(1/4) - m^2}{t^2}\right] = 0 \tag{6}$$

Comparison of (5) and (6) indicates that

$$m = 1/6, \qquad k = -(1 + 2\epsilon)/3$$

A solution to Eq. (6) which satisfies the conditions at infinity is the Whittaker function $W_{k,m}(t)$. Thus

$$\varphi = AW_{k,m}(t) \tag{7}$$

where A is a multiplicative constant. From Eq. (4) it then follows that

$$\theta = 6^{1/3}A\xi^{-\epsilon}e^{1-\xi^3/12}\,W_{-(1+2\epsilon)/3,1/6}\,(\xi^3/6) \tag{8}$$

To determine the constant A, it is convenient to resort to the integral representation of $W_{k,m}(z)$ (*loc. cit.*)

$$W_{k,m}(z) = \frac{z^{(1/2)-m}}{\Gamma[m - k + (1/2)]}\int_0^\infty s^{m-k-(1/2)}(z+s)^{m+k-(1/2)}e^{-s}\,ds \tag{9}$$

so that Eq. (8) may be written

$$\theta(\xi) = \frac{6^{1/3}Ae^{-\epsilon^3/6}}{\Gamma[(3+2\epsilon)/3]}\int_0^\infty s^{2\epsilon/3}\left(\frac{\xi^3}{6}+s\right)^{-(2/3)(1+\epsilon)}e^{-s}\,ds \tag{10}$$

For $\xi = 0$, this reduces to

$$\theta(0) = \frac{6^{1/3}A}{\Gamma[(3+2\epsilon)/3]}\int_0^\infty s^{-2/3}e^{-s}\,ds = 6^{1/3}A\Gamma(1/3)/\Gamma[(3+2\epsilon/3)] \tag{11}$$

Hence,

$$A = \Gamma[(3+2\epsilon)/3]/6^{1/3}\Gamma(1/3) \tag{12}$$

$$\theta = \frac{\Gamma[(3+2\epsilon/3]}{\Gamma(1/3)}\,\xi^{-\epsilon}\,e^{-\xi^3/12}\,W_{-(1+2\epsilon)/3,\,1/6}\,(\xi^3/6) \tag{13}$$

or

$$\theta = \frac{e^{-\xi^3/6}}{\Gamma(1/3)}\int_0^\infty s^{2\epsilon/3}\,(\xi^3/6)+s]^{-(2/3)(1+\epsilon)}\,e^{-s}\,ds \tag{14}$$

Eq. (14) is suitable for numerical calculation when ξ is small. For large values of ξ, the change of variable

$$s = (\xi^3/6)u$$

gives

$$\theta = \frac{6^{1/3}\,\xi e^{-\xi^3/6}}{\Gamma(1/3)}\int_0^\infty u^{2\epsilon/3}\,(1+u)^{-(2/3)(1+\epsilon)}\,e^{-(\xi^3/6)u}\,du \tag{15}$$

The temperature gradient at $\xi = 0$ is best evaluated by expanding $W_{k,m}(z)$ in the vicinity of $z = 0$. We obtain (see reference 2, Chapter VI—2)

$$W_{k,m}(z) = \frac{\Gamma(-2m)}{\Gamma[(1/2) - k - m]}\,M_{k,m}(z) + \frac{\Gamma(2m)}{\Gamma[(1/2) - k + m]}\,M_{k,-m}(z) = e^{-z/2}z^{1/2}\times$$
$$\left\{\frac{\Gamma(-2m)}{\Gamma[(1/2) - k - m]}\,z^m\left[1 + \frac{m - k + (1/2)}{2m+1}\,z + \ldots\right] + \frac{\Gamma(2m)z^{-m}}{\Gamma[(1/2) - k + m]}\left[1 + \frac{m + k - (1/2)}{2m-1}\,z + \ldots\right]\right\} \tag{16}$$

and with $k = -(1 + 2\epsilon)/3$, $m = 1/6$, and $z = \xi^3/6$, this gives

$$\theta = e^{-\xi^3/6}\left\{1 + \frac{\Gamma\left(1+\frac{2\epsilon}{3}\right)\Gamma(-1/3)}{\Gamma\left(\frac{2+2\epsilon}{3}\right)\Gamma(1/3)}\,\frac{\xi}{6^{1/3}} + \ldots\right\} \tag{17}$$

so that

$$\left[\frac{d\theta}{d\xi}\right]_{\xi=0} = \frac{\Gamma[1 + (2\epsilon/3)]\Gamma(-1/3)}{6^{1/3}\Gamma[(2+2\epsilon)/3]\Gamma(1/3)} \tag{18}$$

The resulting value of the heat transfer coefficient is

$$\frac{h}{k\sqrt{U_1/\nu x}} = -\frac{(ab/6)^{1/3}}{\sqrt{2-\beta}}\,\frac{\Gamma\left(1+\frac{2\epsilon}{3}\right)\Gamma(-1/3)}{\Gamma\left(\frac{2+2\epsilon}{3}\right)\Gamma(1/3)} \tag{19}$$

The comparison between this value and that given by Schuh depends on the closeness of the approximation

$$\frac{\Gamma[1 + (2\epsilon/3)]}{\Gamma[(2+2\epsilon)/3]} \simeq \left(\frac{2\epsilon}{3}\right)^{1/3} \tag{20}$$

which may be shown to be asymptotically correct for large values of ϵ.

References

[1] Schuh, H., *On Asymptotic Solutions for the Heat Transfer at Varying Wall Temperatures in a Laminar Boundary Layer with Hartree's Velocity Profiles*, Journal of the Aeronautical Sciences, Vol. 20, No. 2, pp. 146–147, February, 1953.

[2] Magnus, W., and Oberhettinger, F., *Formulae and Theorems for the Special Functions of Mathematical Physics*, English Ed.; Chelsea Publishing Company, New York, 1949.

On a Result of Nikolskii and Taganov Concerning Transonic Flow

Marvin Stern
Republic Aviation Corporation, Farmingdale, L.I., N.Y.

November 24, 1953

BY ELEMENTARY CONSIDERATIONS we can strengthen the basic theorem derived in the paper of Nikolskii and Taganov[1] and thereby immediately conclude their important result: "It is impossible to have potential transonic flow if a straight portion of the physical contour lies in the local supersonic region."

We strengthen their basic theorem to read: "In potential transonic flow, moving along the sonic line in a clockwise direction, the angle that the velocity vector makes with the horizontal steadily decreases." This differs from the original by omitting the equality sign in their statement of the theorem—viz., $\theta_s \leq 0$.

We consider potential transonic flow over a convex contour. It is assumed that both the contour, K, and the sonic line, $q = c_*$, are continuous curves that intersect at two points. The sonic line then separates the flow field into two regions, $q < c_*$ and $q > c_*$ (Fig. 1).

Consider a point P within the supersonic region. Through this point there pass two characteristics making an angle with each other. At their intersections with the sonic line, A and B, the velocity magnitudes are equal, while the velocity angles must satisfy one of the three possibilities:

$$\theta_A < \theta_B \tag{1}$$
$$\theta_A = \theta_B \tag{2}$$
$$\theta_A > \theta_B \tag{3}$$

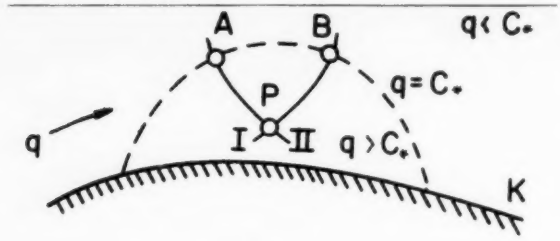

FIG. 1.

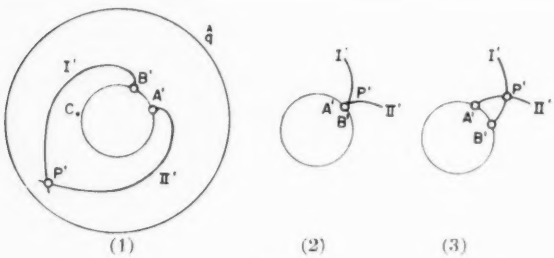

FIG. 2.

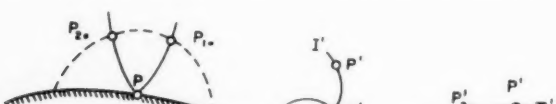

FIG. 3.

The three possible image systems on the hodograph plane are shown in Fig. 2. The directions of I' and II' are set by their orthogonality with II and I, respectively.[2]

Without any assumption on the functional determinant, $j = \partial(q, \theta)/\partial(x, y)$, we will be able to exclude two of the above three possibilities. We can state that characteristics I and II must map in some manner onto at least portions of the epicycloid characteristics I' and II' on the hodograph plane. Further, merely the assumption of potential transonic flow guarantees that the point P of the physical plane maps onto one point P' on the hodograph, this point necessarily being on the intersection of the I' and II' characteristics.

Case 1.—We assume only that q and θ are continuous. For point P on the sonic line, the angle between the characteristics is zero. It follows that, as we bring point P close to the sonic line, the angle between the characteristics becomes arbitrarily small.

As the angle between the characteristics becomes small, the intersection points A and B come arbitrarily close together.

From the continuity of θ, as the distance between A and B becomes small, the difference between θ_A and θ_B becomes arbitrarily small, and consequently the distance between the images A' and B' becomes sufficiently small.

But as A' and B' approach each other, the intersection point P' must approach the limit circle $\hat{q}$. This is a contradiction and Case 1 must be excluded.

Case 2.—From the exclusion of Case 1, it follows that Case 2 cannot allow for θ to take on the same value at the end points of the finite interval AB without being constant throughout this interval. The validity of this statement is evident, since, if θ were not constant throughout an interval, it would be decreasing strictly monotonically and could not therefore take on the same value at isolated points.

We will now show that the assumption of θ being constant along a finite segment of the sonic line also leads to a contradiction.

It is evident that the image point P', which falls on the intersection of epicycloids I' and II', would in this case map coincidentally with A' and B' on the sonic circle. Point P then has sonic velocity.

Similarly, the two characteristics drawn from any other point within the characteristic triangle APB will intersect the sonic line between A and B (the segment along which θ is assumed constant). It follows that all points within the characteristic triangle APB have sonic velocity.

This extension of a sonic region into the assumed supersonic domain represents a contradiction, and Case 2 must therefore be excluded.

It follows that Case 3 is the only possibility, and therefore the theorem has been proved.

It now remains to show that: "It is impossible to have potential transonic flow if a straight portion of the physical contour lies in the local supersonic region."

Consider a point P on a straight segment of contour in a locally supersonic region. The two characteristics emanating from P terminate on the sonic curve. Their images on the hodograph plane are as shown in Fig. 3.

On either epicycloid, the magnitude of the velocity at point P can be represented as an increasing function of its argument.

$$q_P = f(\theta_P - \theta_{P_{1*}})$$
$$q_P = f(\theta_{P_{2*}} - \theta_P)$$

If P were to move along this flat portion of the physical contour, then θ_P would remain constant. But if $\theta_s < 0$, then $\theta_{P_{1*}}$ and $\theta_{P_{2*}}$ would both decrease. The first equation above would show q_P to be increasing, while the second shows q_P decreasing. Here is the contradiction, and therefore the theorem proved on strict monotonicity of angle variation cannot hold. It follows that potential flow for this case is impossible.

REFERENCES

[1] Nikolskii and Taganov, *Gas Motion in a Local Supersonic Region and Conditions of Potential Flow Breakdown*, NACA TM No. 1213, 1949 (translated from the Russian).

[2] Courant and Friedrichs, *Supersonic Flow and Shock Waves;* Interscience Publishers, N. Y., 1948.

Leading-Edge Separation from Delta Wings

R. H. Edwards
Hughes Aircraft Company, Research and Development Laboratories, Culver City, Calif.
November 10, 1953

RECENTLY, LEGENDRE[1] AND ADAMS[2] have presented approximate analyses of the problem of leading-edge separation from delta wings at supersonic speeds. In both cases the slender body or low aspect ratio approximation is made, the flow is considered to be conical, a Kutta condition is applied at the leading edge, and the vortex sheet that separates from the leading edge is replaced by a concentrated vortex.

Since the flow is conical, the strength of this vortex is proportional to the downstream distance from the vertex of the wing, and a multivaluedness of the pressure in the fluid results. This multivaluedness can be removed only by the introduction of a branch cut that connects the separated vortex to the leading edge of the wing. Along this branch cut, however, a discontinuity in pressure appears. In effect, then, the branch cut represents a sheet of bound vorticity which feeds the concentrated vortex, and

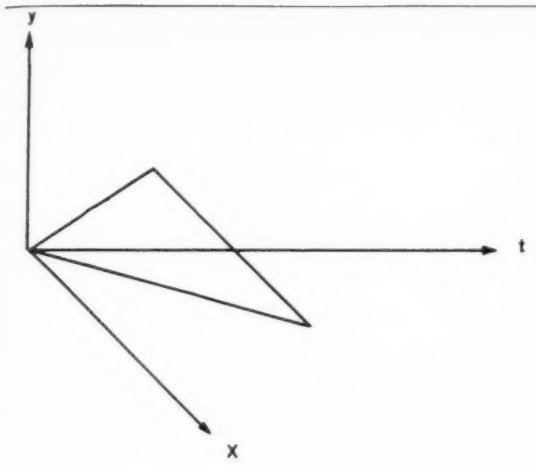

FIGURE 1

the true vortex sheet has been replaced by this fictitious arrangement in which the pressure continuity condition has been relaxed.

Some selection principle is then necessary in order that the strength and position of the concentrated vortices may be determined. The Kutta condition yields one of the determining equations. A further assumption used by both Legendre and Adams is that the concentrated vortex should move with the fluid. Since the configuration is conical, this assumption prescribes the local mean velocity at the vortex, and the problem is then completely defined. This procedure leads to an ambiguity in the determination of the lift.[2]

A different assumption is suggested here. Since there is no net force on the true vortex sheet, the first mean value condition on the simplified representation would seem to be that there should be no net force on the vortex and branch cut. In contrast, the condition of Legendre and Adams is equivalent to the stipulation that there should be no net force on the vortex alone. One advantage of the method suggested here is that the ambiguity in the determination of the lift is removed.

In order to formulate the foregoing assumptions analytically, let the xyt coordinate system be introduced as in Fig. 1, and let us suppose that Fig. 2 represents the plane $t = 1$. Let $z \equiv x + iy$.

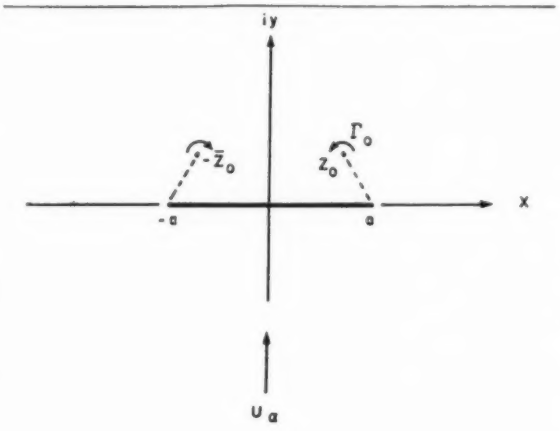

FIGURE 2

The condition of Adams and Legendre is expressible in the form: $V(z_0) = Uz_0$. Here $V(z_0)$ is the mean velocity vector in the cross-flow plane $t = 1$ at $z = z_0$.

The condition proposed here may be formulated readily. The force on the branch cut is given by: $\rho U\Gamma(z_0 - a)i$. The force on the vortex has the form: $-\rho[V(z_0) - Uz_0]\Gamma i$. The required condition is, then,

$$V(z_0) = U(2z_0 - a)$$

A different way of looking at this assumption is the following: At each cross section, the cross flow due to a vortex sheet has been replaced by the cross flow due to a single vortex. Asymptotically, such a replacement is achieved with a single vortex of strength equal to the total vorticity, located at the center of gravity of the vorticity of the sheet. Now, for the problem at hand, the center of gravity of vorticity of the true sheet moves conically, but vorticity is being fed continuously into the sheet from the leading edge of the wing. Consider then the velocity of the center of gravity of the vorticity that has been shed forward of $t = 1$, evaluated at the plane $t = 1$.

Let (Γ_0, z^*), (Γ_1, z_1), and (Γ_2, z_2) represent the strengths and centers of gravity of the vorticity at $t = t_1$ of the vorticity that was shed prior to $t = 1$, after $t = 1$ but prior to $t = t_1$, and prior to $t = t_1$, respectively.

From conical considerations, the following relations are found to be true:

$$z_2 = t_1 z_0, \quad \Gamma_2 = t_1\Gamma_0, \quad \Gamma_1 = (t_1 - 1)\Gamma_0$$

Then

$$z_2 = t_1 z_0 = \frac{\Gamma_0 z^* + (t_1 - 1)\Gamma_0 z_1}{\Gamma_0 t_1}$$

$$\frac{dz^*}{dt_1} = 2t_1 z_0 - z_1 - (t_1 - 1)\frac{dz_1}{dt_1}$$

Now as $t_1 \to 1$, $z_1 \to a$, since the vorticity is shed from the leading edge. Hence,

$$V(z^*)\,|_{t_1=1} = U\frac{dz^*}{dt_1}\,|_{t_1=1} = U(2z_0 - a)$$

This form is, of course, identical to that given previously for $V(z_0)$ and would indicate that the assumption given here is equivalent to making the vortex motion similar to that of the c.g. of the vorticity.

For his assumption, Adams gives two values for the lift coefficient for small angles of attack. They are

$$C_L = \frac{\pi}{2}(\text{A.R.})\,\alpha + \pi\left(1 + \frac{1}{2\sqrt{2}}\right)(4\ \text{A.R.})^{1/3}\,\alpha^{4/3}$$

$$C_L = \frac{\pi}{2}(\text{A.R.})\,\alpha + \pi(4\text{A.R.})^{1/3}\,\alpha^{4/3}$$

For the hypothesis indicated here, the ambiguity is removed, and the single value obtained for the lift coefficient has the form

$$C_L = \frac{\pi}{2}(\text{A.R.})\alpha + \pi(\text{A.R.})^{1/3}\,\alpha^{4/3}$$

The general form of the lift coefficient is similar to those given by Adams, but the coefficient of the $\alpha^{4/3}$ term is smaller than either of his values.

References

[1] Legendre, Robert, *Écoulement au voisinage de la pointe avant d'une aile a forte flèche aux incidences moyennes*, La Recherche Aéronautique, Bulletin Bimestriel, de l'Office National d'Études et de Recherches Aéronautiques, Novembre-Decembre, 1952.

[2] Adams, Mac C., *Leading-Edge Separation from Delta Wings at Supersonic Speeds*, Readers' Forum, Journal of the Aeronautical Sciences, Vol 20, No. 6, p. 430, June, 1953.

Transport of the Boundary Layer in Secondary Flow

F. F. Ehrich and R. W. Detra
Aviation Gas Turbine Division, Westinghouse Electric Corporation
November 6, 1953

NOMENCLATURE

- A = area = $\int\int d\sigma\, dn$
- A.R. = passage aspect ratio
- c = blade chord
- C_e = secondary flow energy loss coefficient
- n = length measured normal to the secondary flow stream lines
- q = perturbation velocity normal to the main flow direction
- R = passage radius of curvature
- s = pitch
- t = time
- U = main flow velocity
- U_0 = maximum value of the main flow velocity
- x = coordinate in pitch direction
- y = coordinate along the blade height
- ϵ = turning angle
- ϵ_0 = total turning angle
- σ = length measured along the secondary flow stream line
- ψ = perturbation stream function

SQUIRE AND WINTER[1] have effectively described the perturbation velocity pattern in secondary flow through a bend in a rectangular channel or cascade blade passage. In terms of a perturbation stream function in the plane perpendicular to the direction of flow (in normalized form),

$$\frac{\partial^2(\psi/U_0 s)}{\partial(x/s)^2} + \frac{\partial^2(\psi/U_0 s)}{\partial(y/s)^2} = 2\epsilon_0 \frac{\partial(U/U_0)}{\partial(y/s)} \tag{1}$$

where ϵ_0 is the total turning angle. A first-order estimate of the transport of the boundary layer may be had by considering the movement of the boundary layer due to this velocity pattern and neglecting the cross effect that the distortion of the boundary layer has on the perturbation velocities.

Actually, Eq. (1) is pertinent only to the stream function in the exit plane. But, if the assumption is made that the secondary velocities (and, hence, the stream function) build up linearly through the cascade, then,

$$\frac{\partial^2(\psi/U_0 s)}{\partial(x/s)^2} + \frac{\partial^2(\psi/U_0 s)}{\partial(y/s)^2} = 2\epsilon \frac{\partial(U/U_0)}{\partial(y/s)} \tag{2}$$

where ϵ is the turning in the cascade. Then the quantity

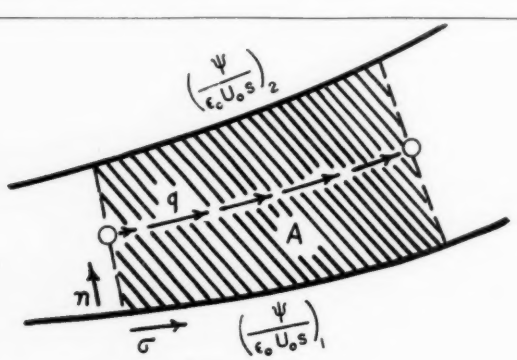

FIG. 1.

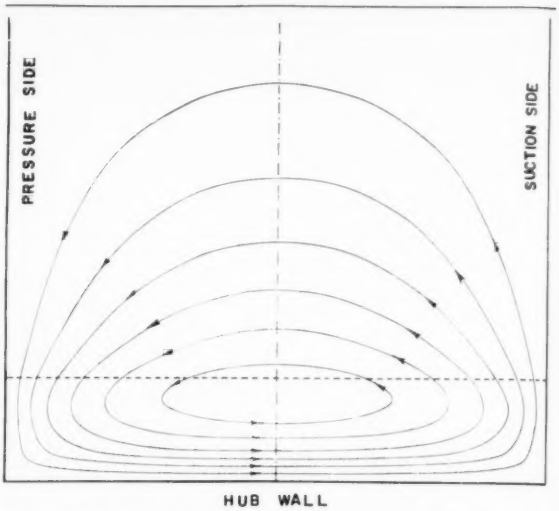

FIG. 2. Calculated streamlines of the secondary flow $\Delta(\psi/\epsilon_0 U_0 s) = 0.02$.

$$\psi/\epsilon U_0 s = f(x/s, y/s) \tag{3}$$

is invariant in the direction of flow.

Considering a particle of fluid in the cascade, its movement in the plane perpendicular to the direction of flow as it progresses through the passage is given by

$$d\sigma = q\, dt \tag{4}$$

where q is the perturbation velocity normal to the main direction of flow. Then

$$q = d\psi/dn = \epsilon U_0 s\,|d(\psi/\epsilon U_0 s)/dn| \tag{5}$$

where n is the direction normal to secondary stream line in the plane normal to the main flow. The time element can be expressed in terms of the radius of curvature of the passage,

$$dt = (R/U)d\epsilon \tag{6}$$

Thus,

$$d\sigma = sR(U_0/U)\,|d(\psi/\epsilon U_0 s)/dn|\,\epsilon\, d\epsilon \tag{7}$$

Considering a short fluid filament in the plane perpendicular to the main flow:

$$\int\int d(\sigma/s)d(n/s) = A/s^2 = \int\int (U_0/U)\,(R/s)\,|d(\psi/\epsilon U_0 s)|\,\epsilon\, d\epsilon \tag{8}$$

where A is the area swept by the stream filament in the normal plane.

Assuming that the filament maintains its mean velocity through the cascade, we find

$$A/s^2 = (R/s)\,(U_0/U)\,[\Delta(\psi/\epsilon U_0 s)]\,(\epsilon^2/2) \tag{9}$$

In the exit plane ($\epsilon = \epsilon_0$) we get, finally,

$$A/s^2 = (c/s)\,(U_0/U)\,[\Delta(\psi/\epsilon_0 U_0 s)]\,(\epsilon_0/2) \tag{10}$$

A very straight-forward graphical procedure is implied by Eq. (10). Taking a short stream filament between two stream lines of the secondary flow calculated from Eq. (1), the position of the filament in the exit plane may be located by positioning it such that the swept area is equal to the amount given in Eq. (10) as in Fig. 1. Fig. 2 gives the stream line picture in a semi-infinite (i.e., pitch/height ratio $\ll 1$) passage for an inlet boundary layer whose thickness is equal to 0.2 times the pitch with a linear variation in velocity.

The stream function was calculated by using an electrical analog for a coarse solution and refining the data by relaxation

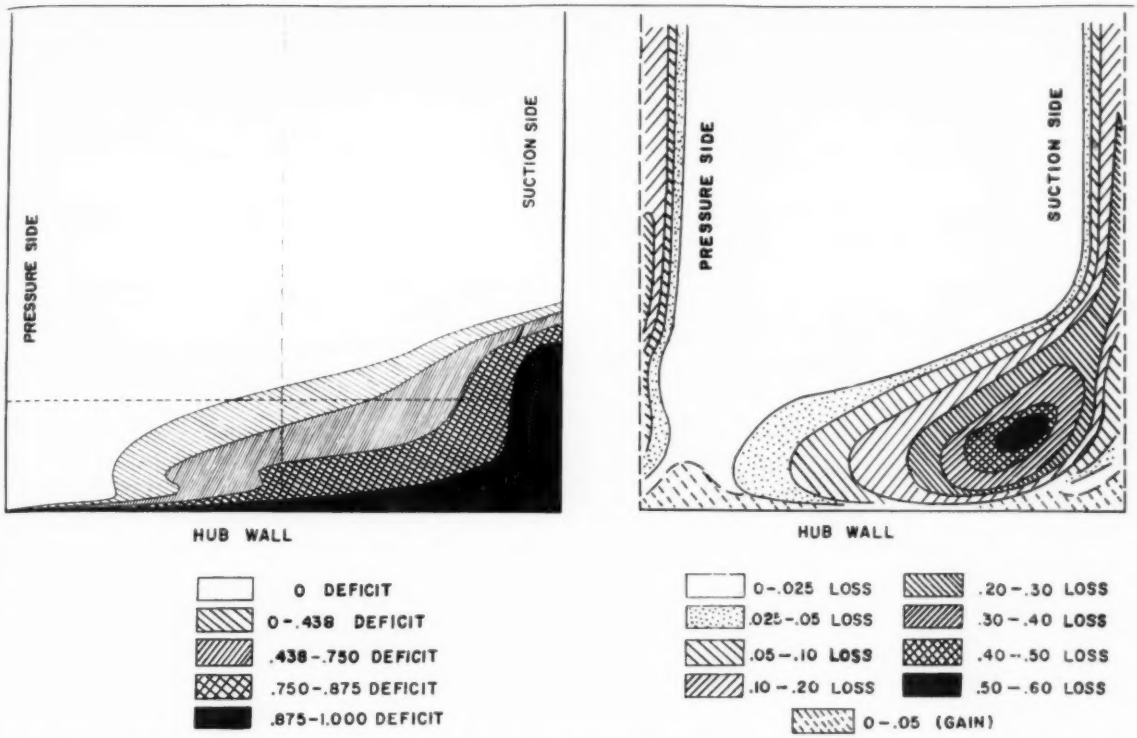

FIG. 3a (*left*). Calculated transport of the inlet boundary layer total pressure contours. FIG. 3b (*right*). Measured total pressure loss contour (reference 2).

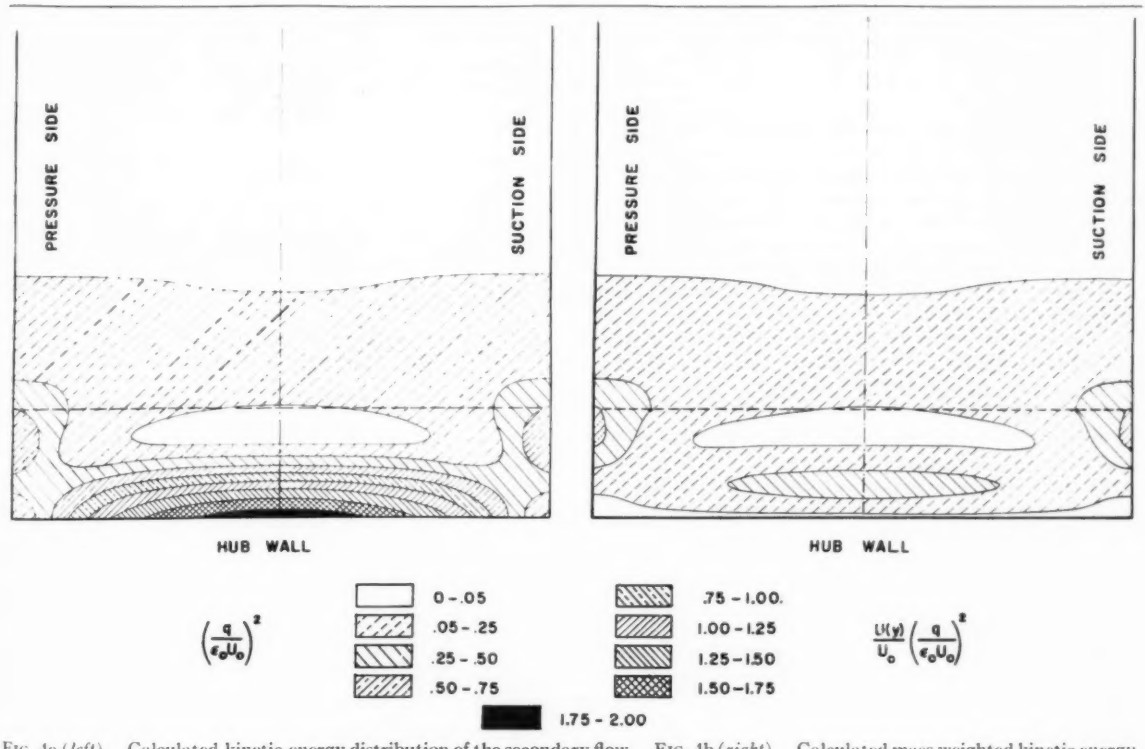

FIG. 4a (*left*). Calculated kinetic energy distribution of the secondary flow. FIG. 4b (*right*). Calculated mass weighted kinetic energy distribution of the secondary flow.

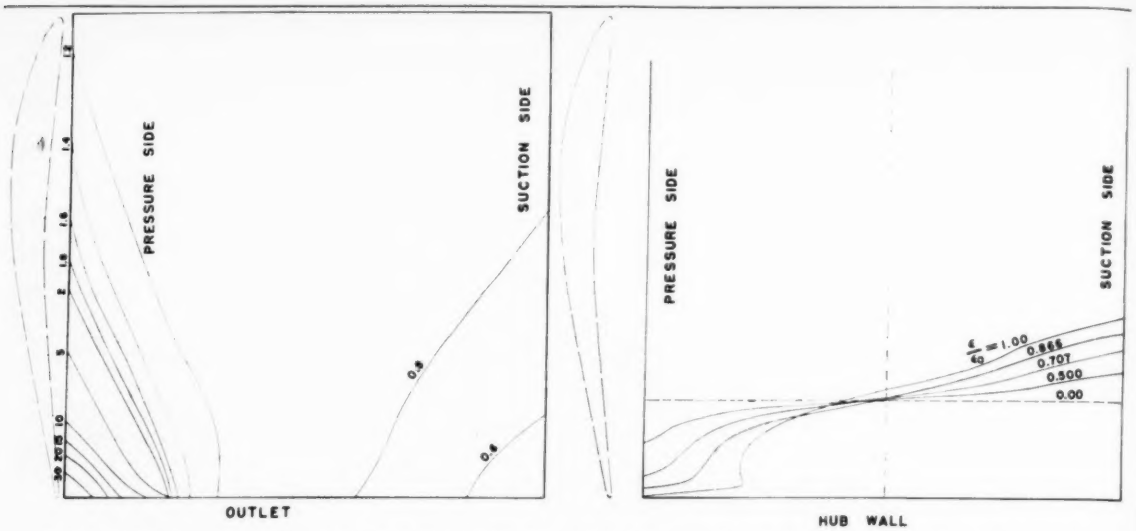

FIG. 5a (*left*). Contour map of δ_c/δ. FIG. 5b (*right*). Distortion of the boundary-layer edge through the blade passage.

methods. Taking

$$(c/s)\,(\epsilon_0/2) = 0.375 \tag{11}$$

and plotting stream function at increments of

$$\Delta(\psi/\epsilon_0 U_0 s) = 0.02 \tag{12}$$

it was found that Bernoulli surfaces would be calculated to cross one another, because the Bernoulli surfaces traveling at low velocities are presumed to remain in the cascade for excessive amounts of time and, hence, are subject to excessive distortions. In order to obtain a reasonable picture of the outlet flow then, we take

$$U/U_0 \approx 1 \tag{13}$$

for purposes of Eq. (10).

Fig. 3a gives the results of tracing the position of a large number of points associated with various Bernoulli surfaces of the inlet plane by the graphical technique. An interesting but somewhat deceptive comparison is given by the experimental results of Carter and Cohen[2] given in Fig. 3b. While Fig. 3a incorporates no loss phenomena and is merely the inlet boundary layer transported, Fig. 3b is an actual loss survey with the losses at each point being reported as the *difference* between inlet and outlet total pressures (normalized on mean dynamic head). Hence the comparison in Fig. 3 is not quantitative but merely verifies the equivalent regions of secondary flow phenomena.

Eq. (9) allows the graphical procedure to be applied to regions within the cascade and, hence, to trace the gradual development of the distortion of the boundary layer as it starts to turn as in Fig. 4b.

A possible origin of secondary losses might be the high-velocity gradients associated with sweeping high energy fluid onto the hub wall near the pressure side.

If a measure of the shear stress is taken to be the vertical height of the boundary layer at any station, Fig. 4a gives a contour map on the floor of the cascade of the shear stress. The effect is apparently negligible on this basis of computation since the mean value of this shear figure on the floor of the cascade is practically equal to that of the undistorted boundary layer. Fig. 5 describes another possible mechanism of the secondary flow. Fig. 5a shows a map of the kinetic energy of the secondary flow and Fig. 5b shows the map of the kinetic energy mass weighted with the axial flow.

The energy loss coefficient resulting from the integrated mass weighted kinetic energy of the secondary flow (Fig. 5b) and nondimensionalized on the kinetic energy of the inlet flow is

$$C_e = 0.1178\epsilon_0^2/\text{A.R.}[1 - (0.2/\text{A.R.})]^3 \tag{14}$$

where A.R., the passage aspect ratio, = blade height/pitch.

This secondary loss coefficient is small for typical values of aspect ratio and turning angle.

REFERENCES

[1] Squire and Winter, *The Secondary Flow in a Cascade of Airfoils in a Nonuniform Stream*, Journal of the Aeronautical Sciences, Vol. 18, No. 4, p. 271, April, 1951.

[2] Carter and Cohen, *Preliminary Investigations into the Three-Dimensional Flow Through a Cascade of Aerofoils*, Aero. Res. Council, R. & M. 2339, 1946.

Remarks on "Interactions Between Wholly Laminar or Wholly Turbulent Boundary Layers and Shock Waves Strong Enough to Cause Separation"*, [1]

Seymour M. Bogdonoff
Associate Professor, Gas Dynamics Laboratory, James Forrestal Research Center, Princeton University
November 17, 1953

IN REFERENCE 1, Gadd presents experimental results and a theoretical analysis of interactions between laminar or turbulent boundary layers and shock waves strong enough to cause separation. For the turbulent boundary interaction, the prime justification for the theory is its approximate verification by his experimental studies. The writer would like to point out several relatively new sets of data obtained at the Gas Dynamics Laboratory which deviate considerably from Gadd's experimental results. References 2 and 3 present studies of the separation of a turbulent layer as caused by shock waves of varying strengths and steps of varying height. These investigations were carried

* This research was sponsored jointly by Office of Naval Research, Mechanics Branch and Office of Scientific Research, under Contract No. N6-onr-270.

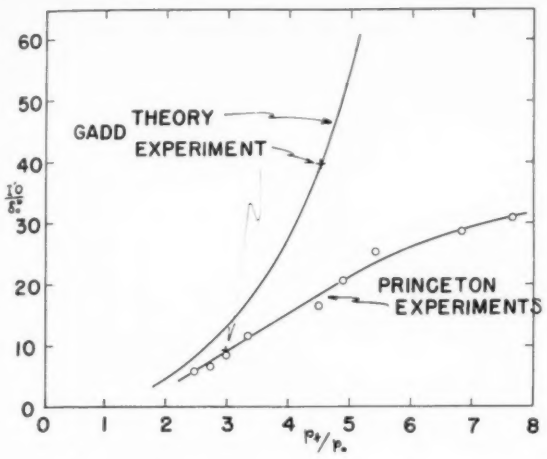

FIGURE 1

out in some detail at $M \sim 3$ and both show separation occurring at a wall static pressure ratio between 2.0 and 2.1, as compared with 2.5 predicted by Gadd. Of even greater importance are comparisons of the effect of pressure ratio on the "influence regions," Fig. 1. The vertical scale, the influence region (using the nomenclature of Gadd), is defined as the distance from the theoretical point of impingement of the incident shock to the beginning of the interaction divided by the displacement thickness of the boundary layer ahead of the interaction. The horizontal scale is the overall pressure ratio across the interaction.

A likely cause of the discrepancy may be the use by Gadd of shock generators that did not completely span the tunnel. This has been shown to have large effects on the phenomena under investigation.[2] Other results in reference 2 show that the assumption of the basic velocity profile at the reattachment point is also questionable. The above results throw considerable doubt on the results of the analysis as applied to the prediction of the interaction of a turbulent boundary layer with a shock wave.

References

[1] Gadd, G. E., *Interactions Between Wholly Laminar or Wholly Turbulent Boundary Layers and Shock Waves Strong Enough to Cause Separation*, Journal of the Aeronautical Sciences, Vol. 20, No. 11, p. 729, November, 1953.

[2] Bogdonoff, S. M., Kepler, C. E., and Sanlorenzo, E., *A Study of Shock Wave Turbulent Boundary Layer Interaction at $M = 3$*, Princeton University Aeronautical Engineering Department Report No. 222, July, 1953.

[3] Kepler, C. E., and Bogdonoff, S. M., *Interaction of a Turbulent Boundary Layer with a Step at $M = 3$*, Princeton University Aeronautical Engineering Department Report No. 238, September 1, 1953.

Aerodynamic Determination of Flame Speed

Robert A. Gross
Harvard University, Cambridge, Mass.
November 6, 1953

THE FUNDAMENTAL PROBLEM in combustion studies is the determination of flame speed. Intensive efforts in the theoretical analysis of this problem and the experimental determination of flame speeds have been carried out. Important fundamental and practical difficulties still plague the theorist and the experimenter.

Rather than review here the extensive and rapidly growing literature on this subject, I refer the interested reader to two recent reviews of the subject.[1, 2] Here you can read of some of the problems involved and various attempts to overcome them. It was from reading these reviews that I decided to make more widely known an entirely different method of measuring flame speed. This method, based upon aerodynamic pressure measurements, has been employed at the Harvard University Combustion Aerodynamics Research Laboratory since mid-1951. Although there are, of course, difficulties in this technique, it has several distinct advantages. It is a point-type measurement permitting the determination of local flame speed. The physical quantities measured are different from those of other existing methods, permitting further checks on existing data.

In addition, information has been obtained on the total pressure variation through the entire flame front.

It is first necessary to define what is meant by flame speed. Here we restrict ourselves to a laminar flow of a homogeneous gaseous mixture of combustible material. The flame speed S is defined as the dot product,

$$S = \vec{q} \cdot \hat{n} \tag{1}$$

where $\vec{q}$ is the velocity vector immediately prior (upstream) to the flame front and $\hat{n}$ is the unit normal vector to the flame-front surface. Now, what surface do we mean? We shall define this surface as that area where, upon approaching the flame front, we are first able to physically detect a change from the free-stream temperature, pressure, or composition. (See Fig. 1.) In the temperature data that can be found in the literature and in our pressure measurements, this point is well defined. Let us designate the properties at this point by the subscript 1. The element of gas thus proceeds from the free stream to the point 1, whereupon its properties start to change because of significant heat transfer, mass transfer, and chemical reaction. Finally, thermodynamic equilibrium is established. Let us call this point of thermodynamic equilibrium point 2. The gas then flows away from the reaction zone. At atmospheric pressure, for common combustible mixtures, the distance from point 1 to point 2 is of the order of 1 mm. The volume enclosed between the surfaces 1 and 2 constitute the flame front.

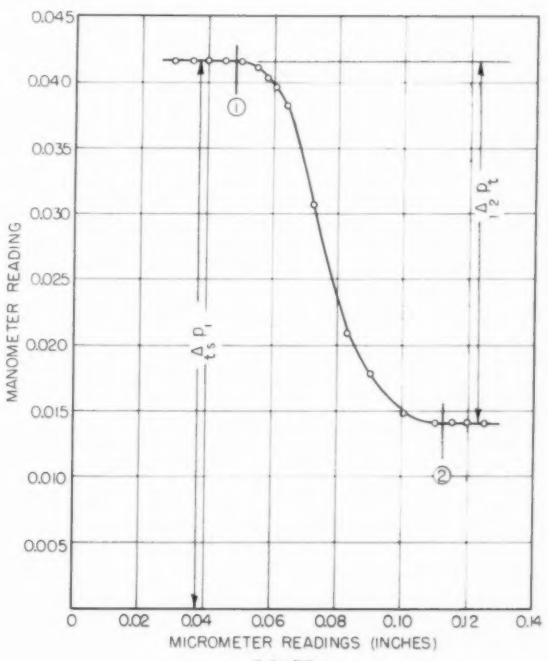

FIGURE 1

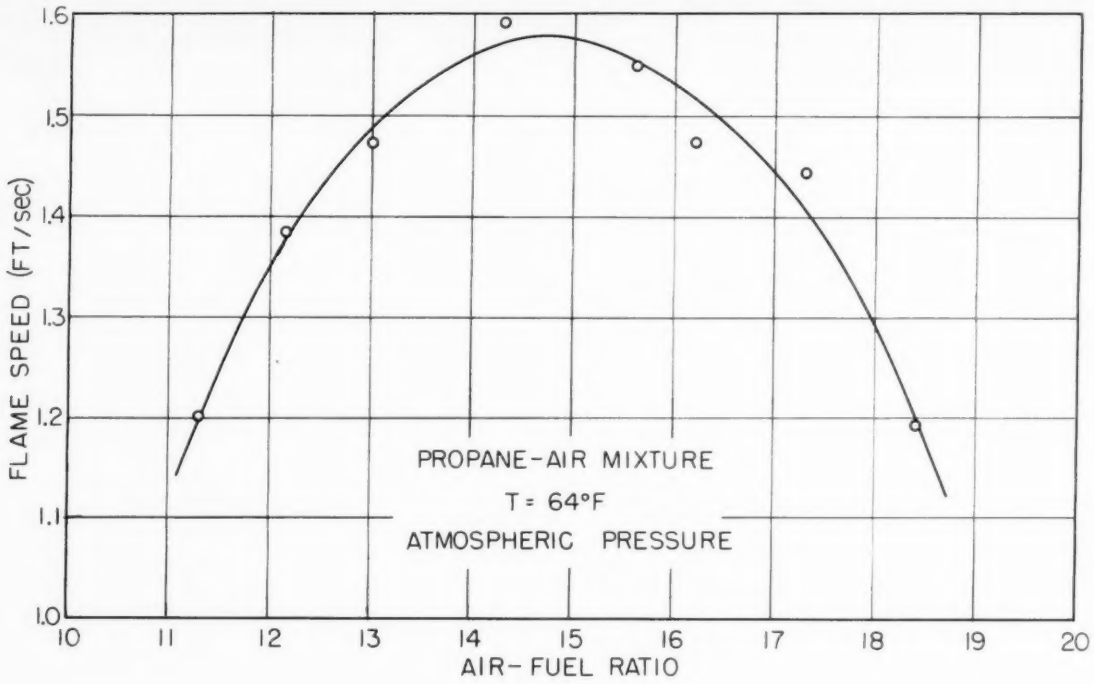

FIGURE 2

Since the flame front is so thin, it is reasonable to assume that it behaves as a discontinuity. We can therefore write mass and momentum conservation equations for a stream tube that passes through this flame front. Thus, mass conservation gives us

$$q_{2n} = \lambda S \tag{2}$$

where q_{2n} is the normal (to the surface 2) component of the velocity vector leaving point 2, and λ is the density ratio

$$\lambda = \rho_1/\rho_2$$

Momentum conservation normal to the flame front is given by

$$p_1 + \rho_1 S^2 = p_2 + \rho_2 q_{2n}^2 \tag{3}$$

where p is the static pressure. The tangential velocity remains unchanged;

$$q_{1\alpha} = q_{2\alpha} = q_\alpha \tag{4}$$

We now introduce the total pressure p_t, defined as

$$p_t = p + (\rho q^2/2) \tag{5}$$

Equations (2), (3), and (4), together with the definition of total pressure, permit the determination of the total pressure change across a flame front.

$$p_{t_2} - p_{t_1} = -\frac{(\lambda - 1)\rho_1 S^2}{2}\left[1 + \frac{1}{\lambda}\left(\frac{q_\alpha}{S}\right)^2\right] \tag{6}$$

The flame speed may be solved for in terms of measurable quantities using Eq. (6). Thus,

$$S = \frac{1}{\lambda - 1}\sqrt{\frac{2}{\rho_1}\left[\lambda_1 \Delta_2 p_t - (\lambda - 1)_t \Delta_s p_1\right]} \tag{7}$$

where ${}_1\Delta_2 p_t$ is the total pressure change between points 1 and 2 and ${}_t\Delta_s p_1$ is the difference between total and static pressure (dynamic pressure) at point 1.

Eq. (7) is the basis of the flame-speed measurements to be presented. It is based upon momentum and mass conservation across the flame front, and these appear to be reasonable assumptions.

Measurements have been carried out on propane-air flames in the Combustion Tunnel at Harvard University. A flat two-dimensional V flame was employed. A small pitot-static probe was used to measure ${}_t\Delta_s p_1$. Radiation to the surrounding room was the chief agent that kept the probes from melting. The probes were rotated to obtain maximum readings at both points 1 and 2 to eliminate errors because of yaw. A typical traverse through the flame front is shown in Fig. 1. A sensitive micromanometer, accurate to ±0.0002-in. manometer fluid, was used to obtain pressure magnitudes. Values of the density ratio λ were computed from the best thermodynamic data available. Using Eq. (7), values for the flame speed of a propane-air flame at atmospheric pressure are presented in Fig. 2.

Flame speed is a function of the initial thermodynamic state of the combustible mixture and the radius of curvature of the flame front.[3] The initial state of our combustible is defined by the air-fuel ratio, the temperature, and the pressure. A flat V flame was used to eliminate the problem of flame front curvature.

The experimental difficulties are primarily those encountered in accurate pressure measurements. Eq. (7) is extremely sensitive to small errors in either pressure measurement and herein lies the most serious problem of using this technique. Great care must be exercised in making all measurements. Primarily because of the nature of Eq. (7) and the limit of the resolution of our measuring instruments, this technique is insufficient to differentiate among flame-speed values given by other investigators.[2] It does, however, give additional flame-speed data obtained by an entirely new technique. Further information of pressure measurements within the flame front itself can be read in a report by Quinn.[4] This work has been supported by the Office of Ordnance Research.

References

[1] Summerfield, M., *Recent Advances and Current Problems in the Theory of Flame Propagation*, 1953 Semi-Annual Meeting, ASME, Los Angeles, Calif.

[2] Linnett, J. W., *Methods of Measuring Burning Velocities*, Fourth International Symposium on Combustion, pp. 20–35; Williams and Wilkins Company, 1953.

[3] Markstein, G. H., *Experimental and Theoretical Studies of Flame-Front Stability*, Journal of the Aeronautical Sciences, Vol. 18, No. 3, pp. 199–209, March, 1951.

[4] Quinn, J. C., *Measurement of Laminar Flame-Front Thickness at Atmospheric Pressure as Function of Air-Propane Ratio*, Combustion Aerodynamics Laboratory Interim Technical Report No. 5, Harvard University, May, 1953.

Errata to "The Aerodynamic Forces on Low Aspect Ratio Wings Oscillating in an Incompressible Flow"[1]

H. R. Lawrence and E. H. Gerber
Cornell Aeronautical Laboratory, Inc., Buffalo, N.Y.
December 1, 1953

THE HEADING: "Imaginary Part" in Table VI should read "Negative Imaginary Part."

The heading of Table VII should read

"Values of the Integral $P^*(p, q)$"

and the second equation should be:

$$P(x, b, k) = bP^*(p, q) = \frac{e^{ip}}{k} \int_p^\infty dt\, e^{-it} \left\{ 1 - \frac{\sqrt{t^2 + q^2}}{t} \right\}$$

The writers wish to thank H. M. Voss for pointing out the corrections presented herein.

REFERENCE

[1] Lawrence, H. R., and Gerber, E. H., Journal of the Aeronautical Sciences, Vol. 19, No. 11, p. 769, November, 1952.

Note on "Calculation Method for Three-Dimensional Rotationally Symmetrical Laminar Boundary Layers with Arbitrary Free-Stream Velocity . . ."

J. C. Cooke
Professor of Applied Mathematics, University of Malaya, Singapore
November 17, 1953

IN THE SUBJECT PAPER, Drake[1] gives a method for rapid prediction of the important coefficients in this case, based on Mangler's transformation[2] and the two-dimensional Hartree[3] profiles. Seban[4] has deduced from these profiles that it is approximately true that

$$(U_1/\nu)\,(d\theta^2/ds) = B - A(U_1'\theta^2/\nu)$$

in Drake's and indeed the usual notation, and Drake gives $B = 0.44$ and $A = 5.23$ for $0 > m > -0.09$ and $A = 5.32$ for $0.068 > m > 0$. Here we have written $m = -U_1'\theta^2/\nu$ following Thwaites, to whose paper we now wish to refer.[5] By analyzing a large number of two-dimensional flows, Thwaites arrived at the conclusion that the coefficients A and B could be written $A = 6$, $B = 0.45$. These formed the best linear approximation to cover all the flows whose solutions were known. Thwaites also stated that the work of Young and Winterbottom led to values $A = 6.28$, $B = 0.47$ but did not consider these to fit the known flows so well as his own. It should be noted that the Hartree flows were, of course, included in the investigations of Thwaites. It would probably therefore be better to take the values of Thwaites in preference to those given by Drake in his approximate method. The value of m at separation is 0.068 for the Hartree profiles. Thwaites, pointing out that this can be taken arbitrarily in his approximate method, chose 0.082 for various reasons. Although, of course, Seban's approximation fits the Hartree profiles better than that of Thwaites, the latter fits all known solutions better and should be used in the approximate method under consideration.

Drake then proceeds to make a test by comparison with Homann's exact solution for flow at a stagnation point.[6] It is surprisingly evident that it still does not seem to be generally known that Homann's solution is in error, though this was pointed out by Mangler.[7] Again, Schlichting[8] pointed out that the Homann differential equation

$$\phi''' + 2\phi\phi'' - \phi'^2 + 1 = 0$$

(primes denoting differentiation with respect to the independent variable y) could, by putting

$$\eta = \sqrt{2}y, \qquad f(\eta) = \sqrt{2\phi(y)}$$

be transformed into the Hartree differential equation

$$f''' + ff'' = \beta(f'^2 - 1)$$

(primes denoting differentiation with respect to η) with $\beta = 1/2$. Schlichting also refers to some work on the subject by Frössling. As a matter of fact Miss Hannah[9] solved Homann's equation directly and obtained results different from those of Homann. Cooke[10] pointed out the transformation and gave results substantially the same as Miss Hannah's by interpolation from Hartree's results. The possibility of the transformation is indeed implied in Drake's work, and he actually gives the value $\beta = 1/2$ in the course of his work. As a result of all this, we know that the coefficient in Drake's Eq. (25) should be 1.312 (and not 1.3172), comparing closely with his approximate result 1.311.

However the closeness of this agreement cannot be considered as a test of Drake's approximation because Homann's problem can be *exactly* reduced to Hartree's problem. Since Seban's approximation was taken from Hartree's solutions, we should expect the agreement to be close. It would indeed be exact but for the fact that Seban's approximation aimed to fit *all* the Hartree profiles as closely as possible and not merely that for $\beta = 1/2$. Still the approximation is bound to be close if Seban's approximation is close, and the test is in fact a test of Seban's work and not Drake's.

It may well be pointed out here that two errors have been detected in Hartree's table for y' in his notation. They were found by differencing. They are as follows:

$\beta = 1/2$, $x = 1.6$, *for* 0.8860 *read* 0.8760
$\beta = 2$, $x = 0.8$, *for* 0.7858 *read* 0.7958

These corrections are made on the assumption that one digit only is in error in the values given.

REFERENCES

[1] Drake, R. M., *Calculation Method for Three-Dimensional Rotationally Symmetrical Laminar Boundary Layers with Arbitrary Free-Stream Velocity and Arbitrary Wall-Temperature Variation*, Journal of the Aeronautical Sciences, Vol. 20, No. 5, pp. 309–316, May, 1953.

[2] Mangler, W., *Zusammenhang zwischen ebenen und rotations-symmetrischen Grenzschichten in kompressiblen Flussigkeiten*, ZAMM, Vol. 28, 1948.

[3] Hartree, D. R., *On an Equation Occurring in Falkner and Skan's Approximate Treatment of the Equation of the Boundary Layer*, Proc. Camb. Phil. Soc., Vol. 33, pp. 223–239, 1937.

[4] Seban, R. A., *Calculation Method for Two-Dimensional Laminar Boundary Layers with Arbitrary Free Stream Velocity Variation and Arbitrary Wall Temperature Variation*, University of California, Institute of Engineering Research Report, 2-12,1950.

[5] Thwaites, B., *Approximate Calculation of the Laminar Boundary Layer*, Aeronautical Quarterly, Vol. 1, pp. 245–280, 1949.

[6] Homann, F., *Der Einfluss grosser Zähigkeit bei der Strömung um den Zylinder und die Kugel*, ZAMM, Vol. 16, pp. 153–164, 1936.

[7] Mangler, W., M.A.P. Volkenrode, AVA Monographs, Reports and Translations No. 1001, p. 65, 1948.

[8] Schlichting, H., *Grenzschicht-Theorie*, G. Braun, 1951.

[9] Hannah, Miss, Rep. Aero. Res. Council, R. & M. No. 2772, 1947.

[10] Cooke, J. C., *Note on the Boundary Layer near a Stagnation Point* Rep. Aero. Res. Council, No. 15,016, 1952.

Errata—"Quadruple Velocity Correlations and Pressure Fluctuations in Isotropic Turbulence"

M. S. Uberoi
Department of Aeronautical Engineering, University of Michigan, Ann Arbor, Mich.
November 23, 1953

SOME MISTAKES were overlooked in the original manuscript of my paper.[1] The correct formulas are:

In the "Introduction,"

$$\frac{1}{\rho^2}\left(\frac{\partial p}{\partial x_1}\right)^2 \cong \overline{U_1^2}\left(\frac{\overline{\partial U_1}}{\partial x_1}\right)^2 \Big/ (0.13)^2 R_\lambda$$

Below Eq. (20),

$$\overline{(\Delta V)^2} = \frac{35}{3}\left[\frac{\partial^4 R_l^{\,l}(r)}{\partial r^4}\right]_{\lambda=0}$$

Eq. (21) should be

$$\overline{(\Delta V)^2} = \frac{35}{3}\frac{V'^2}{\lambda^4}\left(\frac{30}{7} + 0.2R_\lambda\right)$$

Eq. (22) should be

$$(\lambda^2/V'^4)\,(dV'/dt)^2 = 25/R_\lambda{}^2$$

Eq. (23) should be

$$\frac{\rho^2 V'^4}{\lambda^2(\overline{\partial p/\partial y})^2} = \left(\frac{2\lambda^2}{\lambda_\eta{}^2} - \frac{25}{R_\lambda{}^2} - \frac{2.3}{R_\lambda}\right)^{-1}$$

Changes in Eq. (23) have negligible effect on the final calculations.

REFERENCE

[1] Uberoi, Mahinder S., *Quadruple Velocity Correlations and Pressure Fluctuations in Isotropic Turbulence*, Journal of the Aeronautical Sciences, Vol. 20, No. 3, p. 197, March, 1953.

Further Remarks Concerning Integral Transforms of the Wave Equation

Max. A. Heaslet and Harvard Lomax
Aeronautical Research Scientists, Ames Aeronautical Laboratory, NACA, Moffett Field, Calif.
November 19, 1953

FRAENKEL[1] HAS INVESTIGATED auxiliary terms that appear in an operational form of the potential equation of supersonic flow. The purpose of the present note is to supply a physical meaning to these terms and to indicate a similar case that has occurred previously.

Consider the normal form of the linearized equation of steady-state supersonic flow

$$(\partial^2\varphi/\partial x^2) - (\partial^2\varphi/\partial y^2) - (\partial^2\varphi/\partial z^2) = 0 \qquad (1)$$

where $\varphi(x, y, z)$ is the perturbation velocity potential and the x axis is aligned with the direction of the free stream. The Laplace transform of any function $F(x, y, z)$ is

$$\bar{F}(s; y, z) = \int_{f_0(y,z)}^{\infty} e^{-sx} F(x, y, z)\, dx \qquad (2)$$

The transform of Eq. (1) is, after straightforward calculation,

$$s^2\bar{\varphi} - \frac{\partial^2\bar{\varphi}}{\partial y^2} - \frac{\partial^2\bar{\varphi}}{\partial z^2} = \sum_{i=0}^{n} e^{-sf_i}\left[\Delta\frac{\partial\varphi}{\partial x} + \frac{\partial f_i}{\partial y}\Delta\frac{\partial\varphi}{\partial y} + \frac{\partial f_i}{\partial z}\Delta\frac{\partial\varphi}{\partial z}\right]_{x=f_i} \qquad (3)$$

where discontinuity surfaces $x = f_i(y, z)$ $(i = 0, 1, \ldots, n)$ exist in the flow field and the delta notation indicates the jump in the value of the function at a discontinuity surface, the value $\Delta\varphi$ being assumed equal to zero. Considering, in particular, surfaces of discontinuity which are envelopes of Mach waves or characteristics of Eq. (1), it follows that the bracketed terms in the right member of Eq. (3) are directional derivatives of $\Delta\varphi(x, y, z)$ along these surfaces. This direction, usually termed the conormal, lies in a plane determined by the free-stream velocity vector and the normal to the surface. The directional derivatives represent increments in tangential velocity and vanish from physical considerations. The same condition follows formally in linear theory from the assumed continuity of φ, and the right-hand side of Eq. (3) can thus be suppressed.

We originally encountered this effect in the study[2] of unsteady motion based upon the equation

$$\frac{\partial^2\varphi}{\partial x^2} + \frac{\partial^2\varphi}{\partial y^2} + \frac{\partial^2\varphi}{\partial z^2} - \frac{\partial^2\varphi}{\partial t^2} = 0 \qquad (4)$$

Lagerstrom had suggested in his lectures at the California Institute of Technology that certain simplifications could be achieved in the study of wing plan forms with supersonic edges through the introduction of a transformed variable $\bar{\varphi}$, where

$$\bar{\varphi}(x, z, t) = \int_{-\infty}^{\infty} \varphi(x, y, z, t)\, dy \qquad (5)$$

Let $y = g_1(x, z, t)$ and $y = g_2(x, z, t)$ be envelopes of the foremost discontinuity surfaces induced to the left and right sides of the wing. Since φ is continuous across these surfaces, Eq. (4) becomes

$$\frac{\partial^2\bar{\varphi}}{\partial x^2} + \frac{\partial^2\bar{\varphi}}{\partial z^2} - \frac{\partial^2\bar{\varphi}}{\partial t^2} = \sum_{i=1}^{2}(-1)^i\left[\Delta\frac{\partial\varphi}{\partial x}\frac{\partial g_i}{\partial x} - \Delta\frac{\partial\varphi}{\partial y} + \Delta\frac{\partial\varphi}{\partial z}\frac{\partial g_i}{\partial z} - \Delta\frac{\partial\varphi}{\partial t}\frac{\partial g_i}{\partial t}\right]_{y=g_i} \qquad (6)$$

The bracketed terms again are directional derivatives along the conormals to characteristic surfaces in four dimensions, and the continuity of φ on these surfaces leads to the fact that the right side of the equation is zero.

REFERENCES

[1] Fraenkel, L. E., *On the Operational Form of the Linearized Equation of Supersonic Flow*, Readers' Forum, Journal of the Aeronautical Sciences, Vol. 20, No. 9, pp. 647–648, September, 1953.

[2] Lomax, Harvard, Heaslet, Max. A., and Fuller, F. B., *Three-Dimensional Unsteady-Lift Problems in High-Speed Flight*, NACA Rep. No. 1077, 1952.

Approximate Solutions for Heat Transfer with Convection Flows

M. Herbeck
Max Planck-Institut fur Strᵒmungsforschung, Göttingen, Germany
November 19, 1953

NOTATION

T = temperature
λ = thermal conductivity

c_p = specific heat
ρ = density
ν = kinematic viscosity
μ = absolute viscosity
σ = Prandtl Number
x = coordinate parallel to the wall
y = coordinate normal to the wall
ψ = stream function
u = velocity of flow in x-direction: $\psi_y = \rho \cdot u$
v = velocity of flow in y-direction: $-\psi_x = \rho \cdot v$
$A, A'', B, D, a, \alpha, p, r$ = arbitrary constants

(1) Introduction

For certain boundary conditions, Lighthill,[1] Schuh,[2] and Punnis[3] have given solutions of the differential equation

$$(\mu/\sigma) \cdot T_{yy} = \psi_y \cdot T_x - \psi_x \cdot T_y \tag{1.1}$$

with

$$\psi = y^2 \cdot f(x) \tag{1.2}$$

especially

$$\psi = \text{const} \cdot y^2 \cdot x^{\alpha+1} \tag{1.3}$$

Eq. (1.1) holds for the two-dimensional temperature field over a heated wall if the simplifying assumptions exist: (a) constant fluid properties, (b) negligible heat of friction and compression, and (c) heat conduction in x-direction negligible against heat convection. The application of the stream function, Eq. (1.2) or (1.3), respectively, presupposes that the temperature decreases essentially in that part of the flow field where the velocity profile may be approximated by the tangent at $y = 0$.

Now we will briefly demonstrate that the methods of solutions for Eqs. (1.1) and (1.2) proposed in references 1 and 2 may be extended without any difficulties for the case that instead of Eq. (1.2) the more general function

$$\psi = y^{r-1} \cdot f(x) \tag{1.4}$$

with $r > 2$ is used. (The special solutions for $\psi = B \cdot y^{r-1} \cdot x^{\alpha+1}$ will be given in brackets below the more general solution.) Thus the heat transfer for separation flows, where $r = 4$, is included.

(2) Solutions of the Differential Equation (1.1) for $\psi = y^{r-1} \cdot f(x)$

(2.1) *Proposition of Solution with Exponential Function*

Introducing into Eq. (1.1) the new variables

$$t = t(x) = \frac{\mu}{\sigma}(r-1) \cdot \int_0^x f(x)^{1/(r-1)} \cdot dx \tag{2.11}$$

$$\left[t = \frac{\mu}{\sigma}(r-1)^2 \cdot (\alpha + r)^{-1} \cdot B^{1/(r-1)} \cdot x^{(\alpha+r)/(r-1)} \right]$$

$$z = z(x,y) = (r-1)^{2/r} \cdot \psi^{1/(r-1)} \tag{2.12}$$

$$[z = (r-1)^{2/r} \cdot B^{1/(r-1)} \cdot y \cdot x^{(\alpha+1)/(r-1)}]$$

leads to

$$T_t = z^{2-r} \cdot T_{zz} \tag{2.13}$$

with the particular solution

$$T = \text{const} \cdot e^{-a^2 t} \cdot z^{1/2} \cdot Z_{1/r}\left(\frac{2a}{r} \cdot z^{r/2}\right) \tag{2.14}$$

$$[Z = \text{Bessel function of the order } \pm 1/r]$$

The application of integral transformations to Eq. (2.14) yields additional solutions of Eq. (2.13) which are not to be discussed here.

(2.2) *Solutions with Confluent Hypergeometric Functions*

Solutions in the first quadrant which fulfill the following conditions are of practical importance:

$$y = 0, x > 0: \quad T(x,0) \equiv T_0(x) = A'' \cdot t^p \tag{2.21}$$
$$[T_0(x) = A \cdot x^\gamma \text{ for } f(x) = B \cdot x^{\alpha+1}]$$

$$y \to \infty, x > 0: \quad T(x,y) \to 0 \tag{2.22}$$

$$x = \text{const.}: \quad T(x,y) \tag{2.23}$$

decreases monotonously with y. Using the proposition

$$T = A'' \cdot t^p \cdot g(\zeta) \tag{2.24}$$
$$[T = A \cdot x^\gamma \cdot g(\zeta)]$$

with

$$\zeta = z/(r^2 \cdot t)^{1/r}$$

$$\left[\zeta = \left(\frac{\sigma}{\mu} B \frac{\alpha + r}{r^2}\right)^{1/r} \cdot y \cdot x^{\alpha/r} \right] \tag{2.25}$$

yields

$$T = A'' \cdot t^p \cdot e^{-\zeta^r} = [C_1 \cdot g_1(\zeta) + C_2 \cdot g_2(\zeta)] \tag{2.26}$$

where

$$g_1 = {}_1F_1\left(p + \frac{r-1}{r}; \frac{r-1}{r}; \zeta^r\right) \tag{2.27}$$

$$g_2 = \zeta \cdot {}_1F_1\left(p+1; \frac{r+1}{r}; \zeta^r\right) \tag{2.28}$$

$$\left[p = \frac{\gamma(r-1)}{\alpha + r} \text{ for } T_0 = Ax^\gamma \right]$$

The boundary condition, Eq. (2.21), requires that $C_1 = 1$. In order to satisfy Eq. (2.22), we apply the asymptotic expansions of Eq. (2.27) and (2.28), see reference 4, page 113, which yield that

$$C_2 = C(p) = -\frac{(-1/r)!\,p!}{(1/r)!\,(p - 1/r)!} \tag{2.29}$$

is required if $rp \geq 0$.

Furthermore, Eq. (2.23), too, is satisfied according to the theory of confluent hypergeometric functions, see integral representation in reference 4, page 115.

If $0 > r \cdot p \geq 1 - r$, the conditions of Eqs. (2.21), (2.22), and (2.23) are satisfied according to reference 4, pages 113–115 by

$$C_p \leq C_2 \leq 0 \tag{2.210}$$

However, $C_2 = C_p$ yields the solutions that are physically plausible: If $0 > r \cdot p \geq -1$, only $C_2 = C_p$ gives a finite thermal boundary layer

$$\delta_T = \frac{1}{T_0} \int_0^\infty T \cdot dy$$

if $-1 > r \cdot p \geqq 1 - r$, $C_2 = C_p$ yields the temperature field with the minimum δ_T among the one-parametric family of solutions with Eq. (2.210), which fulfills Eqs. (2.21), (2.22), and (2.23) together with a finite δ_T. If $r \cdot p = 1 - r$, the region of Eq. (2.210) is reduced to $C_2 = 0$. For this interpretation, see reference 7, page 243.

If $r \cdot p < 1 - r$, the theorems for the zeros of confluent hypergeometric functions (reference 5, page 179) and the theorems for the zeros of solutions of differential equations of second order (reference 2, page 211) yield that no solutions of the form of Eq. (2.24) exist which satisfy Eqs. (2.21)–(2.23).

When $r \cdot p \geq 1 - r$, we get, with Eq. (2.29), for the temperature gradient at the wall

$$(T_y)_{y=0} = A'' \cdot C(p) \cdot \frac{(r-1)^{-1+(2/r)}}{r^{2/r}} \cdot \frac{\sigma}{\mu} \cdot t^{p-(1/r)} \cdot \frac{dt}{dx} \tag{2.211}$$

$$\left[(T_y)_{y=0} = A \cdot C(p) \cdot \left(B \cdot \frac{\alpha + r}{r^2}\right)^{1/r} \cdot \left(\frac{\sigma}{\mu}\right)^{1/r} \cdot x^{\gamma + (\alpha/r)}\right]$$

We get a constant $(T_y)_{y=0}$, independent of x, if

$$t^{p-1/r} \cdot (dt/dx) = \text{const.}$$

$$[\gamma + (\alpha/r) = 0] \tag{2.212}$$

(3) Application

In addition to references 1 and 2, which investigate solutions with $r = 3$ for the conditions (2.21)–(2.23), we calculate as example with $r = 4$, the temperature field of a heated wall which is cooled by a flow with the stream function

$$\psi = \frac{0.0375}{2 - \beta} \cdot \frac{\rho}{\nu} \cdot D^2 \cdot x^{-1,18} \cdot y^3 \tag{3.1}$$

Eq. (3.1) is the first approximation for the stream function of the boundary-layer profile with separation where $U_\infty = D \cdot x^{-0.09}$. (reference 6, page 60). Applying Eq. (3.1) to Eqs. (2.26)–(2.29), we get

$$T = A \cdot x^\gamma \cdot e^{-\zeta^4} \cdot [{}_1F_1(1.65\gamma + 0.75); (0.75; \zeta^4) + C(p) \cdot \zeta \cdot {}_1F_1(1.65\gamma + 1; 1.25; \zeta^4)] \tag{3.2}$$

with

$$\zeta = 0.311 \cdot \sigma^{1/4} \cdot \left(\frac{D}{\nu(2 - \beta)}\right)^{1/2} \cdot x^{-0.545} \cdot y \tag{3.3}$$

$$C(p) = -\frac{(-1/4)!(1.65\gamma)!}{(1/4)![1.65\gamma - (1/4)]!} \tag{3.4}$$

Furthermore

$$(T_y)_{y=0} = A \cdot C(p) \cdot 0.311 \cdot \sigma^{1/4} \cdot \left(\frac{D}{\nu(2 - \beta)}\right)^{1/2} \cdot x^{-0.545} \tag{3.5}$$

$(T_y)_{y=0}$ is independent of x for $\gamma = 0.545$.

We compare the above approximation with computations of Levy,[7] who has given solutions for Eq. (1.1) by means of numerical integration where, instead of Eq. (3.1), the stream function of the exact solution of the boundary layer equation for separation is applied. Levy calculates, instead of Eq. (3.5), the "reduced" temperature gradient $(\theta_\eta)_{\eta=0}$, which is defined by

$$T(x, y) = A \cdot x^\gamma \cdot \theta(\eta) \tag{3.6}$$

with

$$\eta = \left(\frac{D}{\nu(2 - \beta)}\right)^{1/2} \cdot x^{-0.545} \cdot y \quad \text{with } \beta = -0.198 \tag{3.7}$$

Applying Eq. (3.1) yields

$$(\theta_\eta)_{\eta=0} = C(p) \cdot 0.311 \cdot \sigma^{1/4} \tag{3.8}$$

Values according to Eq. (3.8) and "improved" solutions of reference 7 are represented in Table 1. They indicate only few per cents of difference. Thus the application of the approximation Eq. (3.1) into Eq. (1.1), which allows a simple computation of the heat transfer, seems to be as useful as corresponding calculations for $r = 3$ in references 1 and 2, if $\sigma > 1/2$ is chosen according to the simplifying assumptions.

Table 1
Values of $(\theta_\eta)_{\eta=0}$ for $\sigma = 1$

γ	Eq. (3.8)	Calculation[7]
$-1/2.198$	0	0
-0.25	-0.242	-0.217
0	-0.344	-0.323
$+0.25$	-0.401	-0.383
0.50	-0.443	-0.424
1	-0.503	-0.484
2	-0.583	-0.562
3	-0.638	-0.617
4	-0.685	-0.661

References

[1] Lighthill, M. J., Proc. Roy. Soc. A, Vol. 202, No. 1070, pp. 359–377, 1950.

[2] Schuh, H., Journal of the Aeronautical Sciences, Vol. 20, p. 146, 1953.

[3] Punnis, B., Journal of the Aeronautical Sciences, Vol. 20, p. 505, 1953.

[4] Magnus-Oberhettinger, *Formeln und Sätze für die speziellen Funktionen der mathematischen Physik;* 2. Aufl., Springer-Verlag, 1948.

[5] Buchholtz, H., *Die konfluente hypergeometrische Funktion;* 1. Aufl., Springer-Verlag, 1953.

[6] Pretsch, J., Jahrbuch der Deutschen Luftfahrtforschung, 1942, S.54.

[7] Levy, S., Journal of the Aeronautical Sciences, Vol. 19, p. 341, 1952.

Skin Friction in Slip Flow

(*Concluded from page 90*)

[18] Kuhlthau, A. R., *Air Friction on Rapidly Moving Surfaces*, Jour. Appl. Phys., Vol. 20, pp. 217–223, February, 1949.

[19] Schaaf, S. A., Horning, D. O., and Kane, E. D., *Design and Initial Operation of a Low Density Supersonic Wind Tunnel*, published by the ASME, June, 1949.

[20] Kane, E. D., and Maslach, G. J., *Impact-Pressure Interpretation in a Rarefied Gas at Supersonic Speeds*, NACA TN No. 2210, October, 1950.

[21] Talbot, L., *Viscosity Corrections to Cone Probes in Rarefied Supersonic Flow at a Nominal Mach Number of 4*, NACA TN (in press).

[22] Kopal, Z., *Tables of Supersonic Flow of Air Around Cones*, M.I.T., Cambridge, 1947.

[23] Maslach, G. J., *A Precision Manometer for Low Pressures*, Rev. Sci. Instruments, Vol. 23, pp. 367–369, July, 1952.

[24] Howarth, L., *Raleigh's Problem for a Semi-Infinite Plate*, Proc. of the Cambridge Phil. Soc., Vol. 46, January, 1950.

[25] Janour, Zbydnek, *Resistance of a Plate in Parallel Flow at Low Reynolds Numbers*, NACA TM No. 1316, November, 1951.

[26] Young, A. D., *Skin Friction in the Laminar Boundary Layer in Compressible Flow*, Report No. 20, College of Aeronautics, Cranfield, England, 1948.

[27] Lamb, H., *Hydrodynamics*, 6th Ed., p. 576; Dover Publications, New York, 1945.

[28] Grad, H., *On the Kinetic Theory of Rarefied Gases*, Communications on Pure and Applied Mathematics, New York Univ. Vol. II, pp. 331–407, December, 1949.

[29] Alden, H. L., *Second Approximation to the Laminar Boundary Layer Flow over a Flat Plate*, Jour. Math. & Phys., p. 91, April, 1948.

[30] Lees, L., and Probstein, R. F., *Hypersonic Viscous Flow over a Flat Plate*, Princeton Univ., Aero. Eng. Lab., Rep. No. 195, April, 1952.

[31] Lees, L., *On the Boundary Layer Equations in Hypersonic Flow and Their Approximate Solutions*, Princeton Univ., Aero. Eng. Lab., Rep. No. 212, September, 1952.

[32] Truesdell, G., *On the Differential Equations of Slip Flow*, Proc. Nat. Academy Sci., pp. 342–347, July, 1948.

[33] Lewis, J. A., and Carrier, G. F., *Some Remarks on the Flat Plate Boundary Layer*, Quarterly of Applied Math., p. 228, July 1949.

[34] Rayleigh, Lord, *On the Flow of Compressible Fluid Past an Obstacle*, Phil. Mag., Ser. 6, Vol. 32, pp. 1–6, July, 1916.